JAERI-Review
96-011

JAERI TANDEM & V.D.G. ANNUAL REPORT 1995

(April 1, 1995 - March 31, 1996)

August 1996

Depertment of Reactor Engineering

日本原子力研究所
Japan Atomic Energy Research Institute

本レポートは，日本原子力研究所が不定期に公刊している研究報告書です。
入手の問合わせは，日本原子力研究所研究情報部研究情報課（〒319-11 茨城県那珂郡東海村）あて，お申し越しください。なお，このほかに財団法人原子力弘済会資料センター（〒319-11 茨城県那珂郡東海村日本原子力研究所内）で複写による実費領布をおこなっております。

This report is issued irregularly.
Inquiries about availability of the reports should be addressed to Research Information Division, Department of Intellectual Resources, Japan Atomic Energy Research Institute, Tokai-mura, Naka-gun, Ibarakiken 319-11, Japan.

編集兼発行　日本原子力研究所
印　　刷　ニッセイエブロ株式会社

JAERI-Review 96-011

JAERI TANDEM & V.D.G.
Annual Report
1995
April 1, 1995 - March 31, 1996

Department of Reactor Engineering

Tokai Research Establishment
Japan Atomic Energy Research Institute
Tokai-mura, Naka-gun, Ibaraki-ken

(Received July 16, 1996)

This annual report describes research activities which have been performed with the JAERI Tandem accelerator and the Van de Graaff accelerator from April 1, 1995 to March 31, 1996. Summary reports of 59 papers, and list of publications, personnel and cooperative researches with universities are contained.

Keywords: JAERI TANDEM, V.D.G., Nuclear Structure, Nuclear Reaction, Nuclear Theory, Atomic Physics, Solid State Physics, Radiation Effects in Materials, Progress Report

---

Editors: Suehiro TAKEUCHI, Hiroshi IKEZOE, Akira IWAMOTO, Masao SATAKA, Yuichiro NAGAME, Tokio SHOJI, Takashi OKABE and Hiroshi MAEKAWA

原研タンデム，バンデグラフ加速器
1995年度年次報告

日本原子力研究所東海研究所
原子炉工学部

（1996年７月16日受理）

本年次報告は，原研タンデム及びバンデグラフ加速器で，1995年４月１日から1996年３月31日までの間に東海研で行われた研究活動をとりまとめたものである。

(1)加速器の運転と開発研究　(2)核構造　(3)核反応　(4)核理論　(5)原子物理・固体物理及び材料の放射線効果の５部門にまたがる59編の研究報告，公表された文献，関与した職員及び大学等との協力研究のリストを収録している。

東海研究所：〒319-11　茨城県那珂郡東海村白方白根2-4
（編集者）竹内末広，池添　博，岩本　昭，左高正雄，永目諭一郎，荘司時雄，岡部　隆，
前川　洋

PREFACE

This report covers research and development activities using the tandem, superconducting tandem-booster and Van de Graaff accelerators at JAERI, Tokai, during the period from April 1, 1995 to March 31, 1996. During this period, the tandem accelerator was operated over 4500 hours and supplied stable beams to the experiments in the fields of accelerator development, nuclear structures, nuclear reactions, atomic physics, solid state physics and radiation effects in materials. Twenty-four research programs have been carried out in collaboration with a hundred researchers from universities and national research institutes.

The 30MV superconducting booster was put in use. A recoil mass separator installed in the target room was completed. Research for exotic nuclei has begun. A new isotope of ^{209}Th was successfully synthesized for the first time by using the recoil mass separator. A gamma-ray detector array was assembled and used for nuclear structure studies in cooperation with several universities. The booster was stably running during the experiments and has been established as a reliable accelerator.

Hiroshi Maekawa
Deputy Director
Department of Reactor Engineering

Contents

1. Accelerator Operation and Development

1.1 TANDEM AND VAN DE GRAAFF ACCELERATOR OPERATION

Accelerators operation group

Tandem accelerator and Booster; The scheduled operations of the tandem accelerator for experiments were performed through the past one year. There were two short periods of scheduled maintenance. The running time was 4525.8 hours. The summary of the operation from April 1, 1995 to March 31, 1996 is as follows.

1) Time distribution by terminal voltage

>16MV	58 days	26.7 %
15-16	66	30.4
14-15	22	10.1
13-14	21	9.7
12-13	16	7.4
11-12	18	8.3
10-11	11	5.1
9-10	2	1.0
8-9	3	1.4
<8	0	

2) Time distribution by projectile

^{1}H (2H,3H)	35 days		^{45}Sc		1 day
^{6,7}Li	11		^{54,56}Fe		6
^{11}B	3		^{59}Co		7
^{12,13}C	11		^{58,60}Ni		11
^{16,18}O	22		^{63}Cu		8
^{19}F	1		^{74}Ge		2
^{27}Al	2		^{79,81}Br		2
^{28}Si	27		^{90}Zr		18
^{31}P	5		^{107}Ag		4
^{32,33}S	10		^{127}I		17
^{35,37}Cl	7		^{197}Au		7

3) Time distribution by activity

Operation for research		217 days
Atomic and solid state physics	(44)	
Radiation effects in materials	(18.5)	
Nuclear chemistry	(32)	
Nuclear physics	(101)	
Fast neutron physics	(2)	
Radiation chemistry	(6)	
Detector development	(6)	
Nuclear fusion	(1)	
Accelerator test operation	(6)	
Voltage conditioning		2
Scheduled maintenance(2 tank opening)		77

Unexpected repair with tank opening	0
Holidays	65
Training of the operation	4

The tandem booster and the helium refrigeration system were operated 2 times during 2 scheduled machine times. On November 20, one of the two refrigerators had a failure in the heater control circuit which controlled the liquid level in the cold box. The helium refrigeration systems were in operation between November 15 and December 21, 1995 and between February 19 and March 27, 1996. During these times, the super-conductin g booster was utilized for 18 days for 4 experimental subjects.
In every machine time, the booster ran steadily. The accelerating field gradients in the super-conducting resonators were between 2.8MV/m and 4.6MV/m.

The recoil mass separator as the main experimental apparatus was completed in April, and experiments started from June. The research for nuclear structure also started in collaboration between JAERI and universities researchers using a small crystal ball. These experiments will be reported in other chapters.

2MV Van de Graaff accelerator; The 2MV Van de Graaff accelerator was operated for 285.3 hours from April 1,1995 to March 31,1996. The main research subjects are solid state physics, atomic and molecular physics and material physics. Most of the Van de Graaff accelerator users made experiments with the tandem accelerator in the compliment of their researches.

1.2 STATUS OF THE SUPERCONDUCTING BOOSTER

S. TAKEUCHI

In FY1994, acceleration tests were carried out by using heavy ion beams of $^{35}Cl^{10+}$, $^{35}Cl^{14+}$, $^{58}Ni^{20+}$, $^{107}Ag^{25+}$, $^{127}I^{27+}$ and $^{197}Au^{25+}$ from the tandem accelerator. Installation of an experimental apparatus, a recoil mass separator was carried out in the period from December 1994 to April 1995. Beam acceleration tests resumed with Si beams in June and experiments using the booster and the new experimental apparatus started.

Ion beams of $^{28}Si^{10+}$ and $^{74}Ge^{11+}$ were accelerated by the booster from 180 MeV to about 327MeV for both as an additional acceleration test in order to examine the consistency between beam dynamics calculations and accelerated beams as well as the beam transmission. The consistency with respect to the beam energy was found to be very good with an accuracy of 0.3-0.5%[1]. Beam transmission through the booster linac and the transport line was often as low as 30% and sometimes close to 100%. There was no clear dependence on ion species or operating parameters such as synchronous phases. It hinted that we should make the resonators, apertures and quadrupole magnets aligned well.

Boosted beams of $^{74}Ge^{11+}$ were used by a user on July 13 for the first time. Beams of $^{90}Zr^{12+}$and $^{127}I^{28+}$ were boosted for experiments on nuclear structure in many days from December . The booster was found to be very stable for a long period of operation. Weekend experiments could be done without on-duty assistance of booster operators. The accelerating field gradients in the superconducting linac resonators were mostly between 2.8 and 4.6 MV/m. The load to the cryogenic system was moderate enough at these field gradients.

Design work of low-β superconducting resonators proceeded by using a 3-dimensional code, MAFIA and full scale copper models. The value of β (=v/c) we considered was 0.06 to 0.07. Among some structures investigated, a quarter wave resonator structure was studied by an exchange program visitor, Y. Zhang, for the project of superconducting booster at the China Institute of Atomic Energy. Two different structures of quarter wave type and half wave type were investigated for the replacement project of the initial part of the JAERI tandem booster with low-β resonators(by the replacement, very heavy ions like lead can be accelerated up to the energy necessary for nuclear reactions without using additional stripper foils in the tandem accelerator). As a result, a quarter wave resonator structure was chosen because we can expect higher performance(accelerating field gradient) from the simpler structure(a quarter wave resonator structure is much simpler than a half wave one). The basic design and field profile measurements with a copper model were done enough to start fabricating a prototype superconducting resonators made of niobium and copper.

A serious problem to our superconducting resonators is the Q-degradation due to hydrogen absorption during chemical surface treatments and slow cool-down at about 120K. Initial 16 resonators have the disease of the Q-degradation and their field gradients were limited below 5 MV/m. The cool-down rate was found in the previous year to be increased about 50% by cooling two halves of the resonators one after another from 140K to 80K. This year, we obtained another increase of about 30% by closing the valve through which 300K helium gas was mixed into the cooled gas in the refrigeration system. No problem was found, although the gas mixing was controlled by the automatic control program. A combination of these two cooling methods is promising.

We have another problem. The two spare resonators for the booster was found to have low Q and to be infected with the disease of Q degradation. Chemical polishing was carried out with one of the resonators in stead of electropolishing, which had been used for all the

resonators installed in the booster, in order to improve the Q and to prevent additional hydrogen absorption as much as possible. The polishing was successfully done and the Q was improved up to about 50% of a good resonator's Q. More improvement is necessary for its use in the booster. For finding a cure method of the Q disease, we kept trying any possibilities. For example, one month long rinsing with highly de-ionized water was tried but had no effect. We, however, found an interesting fact that the rf power mainly dissipated on the surface of the center conductor or the shorting end plate rather than on the outer conductor niobium surface which was backed by thick copper layer. It is considered as a hint for solving the Q disease problem.

An important further improvement of the booster performace is to increase the beam intensity. Development of electron cyclotron resonance(ECR) ion sources has been proceeded well and a small ECR ion source with high performances has become commercially available. If one is installed in the tandem terminal, highly charged and intense heavy ion beams like Ar^{12+} can be accelerated directly from the tandem terminal and boosted by the booster. We purchased one this fiscal year in order to start the development of the interminal ECR ion source. We are planning to install it in a few year.

Reference

[1] Y. Zhang and S. Takeuchi, JAERI-memo 07-205(1995)

1.3 CONTROL SYSTEM FOR THE JAERI TANDEM ACCELERATOR

S.HANASHIMA

In the second half of the financial year, we met many failures of the control system. They were the events without any permanent damages, and we could restart the operation through normal reinitialization processes. We are using CAMAC serial highway system. The front ends of the computer system are serial highway drivers using transputers as control processors[1,2]. Almost all of the troubles were the events that one or more of the serial highway drivers had stopped transmissions of data to serial highways. Several crash events were analyzed by a postmortem debugger. These analyses showed that processes in the transputers were working and waiting for acknowledges. In the serial highway driver, a transputer sends data bytes to a CAMAC serial highway through a serial link and a C011 link adapter. It seems that there is a problem in the data path.

On the other hand, We found that failure was rare with reset lines disconnected from serial highway drivers. We analyzed hardware circuit diagrams and actual circuits. We found the following defects.

1) At outputs of photo-couplers receiving reset and analyze signals, connections to the pull-up resisters were missing.
2) Sensitivities of the photo-couplers were very high, and the design had no noise margin when the input is in an inactive state
3) Shields of signal cords were insufficient.

These remarkable defects had been fixed. In the results, the rate of system down had decreased, but it had not completely disappeared. We had decided to run the system in the state of the control line disconnected, for the present accelerator operation.

The serial highway drivers have been working since 1992. They had worked without such a trouble before. We suppose that the origins of the trouble were electrostatic discharge and weakness of the serial highway drivers against electromagnetic disturbance.

References

1)S.Hanashima, JAERI TANDEM & V.D.G. Annual Report 1993 pp7-8.
2)S.Hanashima et al., Transputer/Occam Japan 5 IOS Press, 1993 pp69-81.

2. Nuclear Structures

2.1 NUCLEAR g-FACTORS OF THE HIGH-SPIN STATES IN ^{181}Ta

N. HASHIMOTO[1], T. SAITOH[1], J. LU[1], T. KOMATSUBARA[1], K. FURUNO[1]
M. OSHIMA, Y. HATSUKAWA, T. HAYAKAWA, K. FURUTAKA,
M. MATSUDA, T. ISHII and M. KIDERA[2]

The nucleus ^{181}Ta is a well deformed nucleus and exhibits a typical rotational band structure. Inamura *et al.* observed the ground-state rotational band up to the state with $I^\pi = 21/2^+$ using multiple Coulomb excitation with ^{84}Kr ions at 348 MeV[1]. The lower part of the level scheme is shown in Fig. 1. In addition to the excitation energies, they deduced transition probabilities from lifetimes which were extracted by means of Doppler-broadened line-shape analysis. Nuclear g-factors are measured for the ground and the first excited state by NMR and IPAC method[2,3]. From these experimental data, the ground-state rotational band of ^{181}Ta can be described by a model in which a proton is coupled to an axially symmetric core with prolate deformation. The present measurement of nuclear g-factors for high-spin states has been performed to investigate to what extent the model is applicable at the high-spin region.

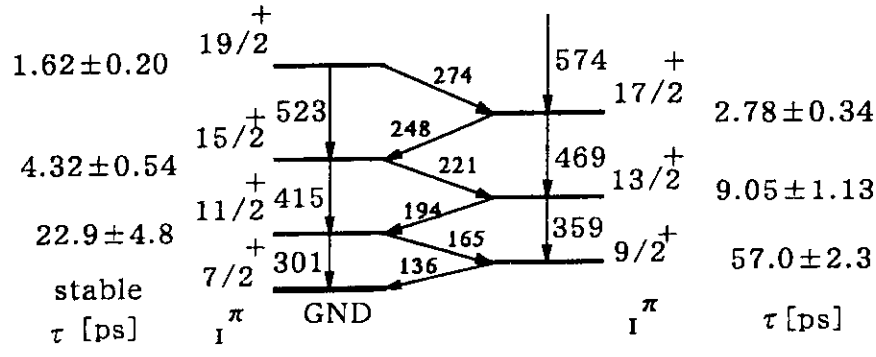

Fig. 1. The level scheme of the lower part of of ^{181}Ta. The ground state with $I^\pi = 7/2^+$ is stable. Lifetimes are given in pico seconds.

The experimental method was based on time-integrated perturbed angular distribution measurements. Because of short lifetimes of the states of interest, the transient magnetic field(TMF) applied to fast ions during the passage through a magnetized iron foil was utilized to obtain an observable Larmor precession angle. The magnitude of TMF was calculated from an empirical formula proposed by Andrews *et al*[4]. Denoting the velocity of ions and light by v and c, the field strength is given by $B_{\rm TMF} = aZ \cdot (v/v_0)$ for ion velocities in the range of $0.03 \leq (v/c) \leq 0.06$. The symbol Z is the atomic number of fast ions, and v_0 is defined by $c/137$. The factor a is an empirical parameter. A value of $a \simeq 12$[T] is used in many cases[5].

The excited states were populated through the Coulomb excitation with a ^{90}Zr beam at a bombarding energy of 385 MeV. The beam has been provided by the accelerator complex consisting of the 20UR tandem accelerator and a superconducting linear accelerator which has recently been constructed in JAERI.

1 Institute of Physics and Tandem Accelerator Center, University of Tsukuba 305 Ibaraki, JAPAN
2 On leave from Kyushu University, Hakozaki, Fukuoka, Japan

The target consisted of three layers. The thicknesses of Ta, iron and copper were 1.9, 6.0 and 5.7 mg/cm^2, respectively. The ^{90}Zr beam was introduced from the tantalum side. The target was placed in an external magnetic field(0.15 T) generated by rare-earth permanent magnets. An assembly of the target and permanent magnets was positioned at the center of an array of 9 Compton-suppressed Ge detectors which was constructed in the Tsukuba-JAERI tandem collaboration. The yields of de-excitation γ rays were measured by changing the direction of the external magnetic field periodically.

Mean Larmor presession angles were extracted from the ratios of γ-ray intensities at angles of 31.7° and 58.3° with respect to the beam direction for external magnetic fields up and down. In order to minimize spurious ratios, which were mainly ascribed to different efficiencies of the γ-ray detectors, the so-called double ratio method was employed. From the double ratios and the results of angular distribution, g-factors were derived by the prescription described in ref. [6].

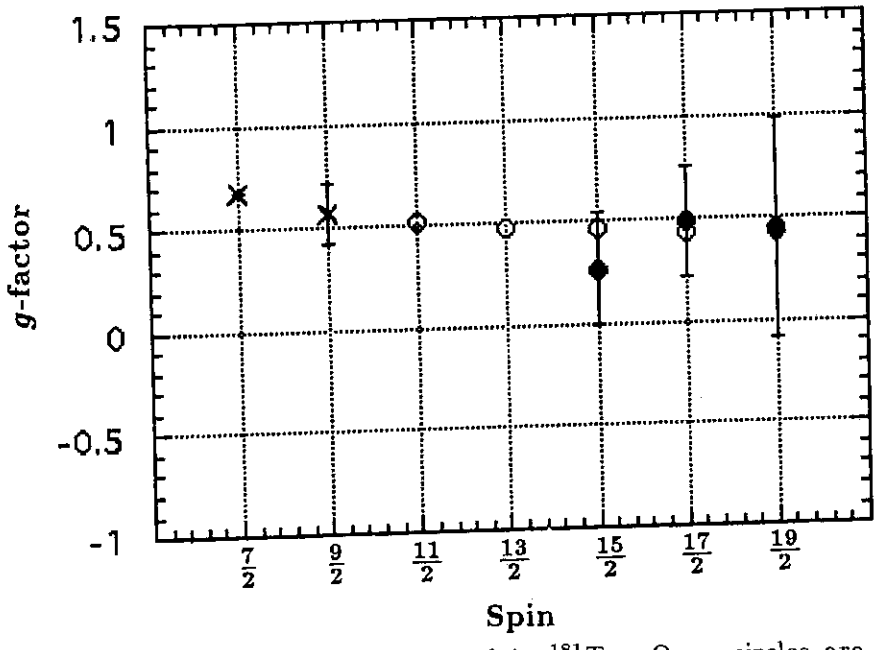

Fig. 2. g-factors of the ground-state band in ^{181}Ta. Open circles are the calculated g-factors(see text).

The g-factors obtained in the present experiment are presented in Fig. 2. The g-factors reported in refs. [2] and [3] are represented by crosses. In the framework of the rotational model, g-factors are given by $g = g_R + (g_K - g_R)K^2/\{I(I+1)\}$. From the two g-values for the $7/2^+$ and $9/2^+$ states, one can estimate g-factors of $g_K = 0.761$ and $g_R = 0.385$. The open circles in Fig. 2 are the calculated g-factors for higher states in terms of the above formula, g_K and g_R. The present result is consistent with the interpretation that the ground-state rotational band in ^{181}Ta involves the $\pi[404]7/2$ configuration as a main component.

References

1) T. Inamura *et al*, Nucl. Phys. **A 270**(1976)255.
2) C.M. Lederer *et al*, Table of Isotopes, 7th edition.
3) Z.Z. Aksel'rod *et al*, Izv. Akad. Nauk. SSSR, **47**(1983)31.
4) H.R. Andrews *et al*, Nucl. Phys. **A 383**(1982)509.
5) D. Ward *et al*, Nucl. Phys. **A330**(1979)225.
6) O. Höusser and I.S. Towner, Hyperfine Interactions of Radioactive Nuclei, Springer Verlag, 1983.

2.2 SEARCH FOR M1 BANDS IN ^{142}Gd

M.SUGAWARA[1], H.KUSAKARI[2], Y.IGARI[2], K.TERUI[2], K.MYOJIN[2], D.NISHIMIYA[2],S.MITARAI[3], M.OSHIMA, T.HAYAKAWA, M.KIDERA, K.FURUTAKA and Y.HATSUKAWA

Recently the interesting sequences of $\Delta I=1$ dipole transitions(M1 bands) were found in the light Pb region and discussed extensively on the basis of tilted-axis cranking approach[1]. S.Frauendorf suggested that those M1 bands would appear in case high spin proton particle states were combined with high spin neutron hole states [2]. Similar M1 bands had been reported in A≈130 region a few years before the discovery in the light Pb region[3]. In particular M1 bands were found in every N=78 isotone from ^{135}La to ^{141}Eu[3,4,5]. In ^{142}Gd four $\Delta I=2$ sequences were found, however no M1 bands have been reported so far. One of those four $\Delta I=2$ sequences starts from the $(\pi h_{11/2}^{2})10^{+}$ isomeric state and another starts from the $(\nu h_{11/2}^{-2})10^{+}$ isomeric state. These two isomeric states are almost degenerate at about 3.1 MeV in excitation energy[6]. Therefore M1 bands can be simply expected at around 6 MeV in excitation energy if the mechanism Frauendorf pointed out will work.

We made an in-beam spectroscopic study on high spin states of ^{142}Gd by the reaction of ^{111}Cd(^{35}Cl,1p3n)^{142}Gd. A 7 mg/cm^2 thick Cd foil, enriched in ^{111}Cd to 96.30 %, was bombarded with the 170 MeV ^{35}Cl beam provided by the JAERI tandem accelerator. Gamma-rays from the excited states populated after the fusion reaction were measured by the JAERI-TSUKUBA crystal ball[7] consisting of 11 BGO anti Compton spectrometers in coincidence with the charged particles detected by the silicon ball[8] made up of 21 detector segments. Approximately 450 million two- or higher fold Ge-Ge events were collected. A total projection spectrum of γ-rays in coincidence with 1 proton detected by the silicon ball is shown in Fig. 1. 514.4 and 693.5 keV are the lowest two transitions in ^{142}Gd. Detailed analysis is now in progress, while two new γ-rays of 789 and 680 keV are found on top of the $(\pi h_{11/2}^{2})$ band and four new γ-rays of 892, 604, 470 and 342 keV are found on top of the $(\nu h_{11/2}^{-2})$ band so far.

References

1) M.A.Deleplanque, Nucl. Phys. A557(1993)39c
2) S.Frauendorf, Nucl. Phys. A557(1993)259c
3) D.B.Fossan et al., Nucl. Phys. A520(1990)241c
4) G.de Angelis et al., Phys. Rev. C49(1994)2990
5) S.Lunardi et al., Phys. Rev. C42(1990)174
6) W.Starzecki et al., Phys. Lett. B200(1988)419
7) K.Furuno et al., JAERI-Review 95-017(1995)22
8) T.Kuroyanagi et al., Nucl. Instrum. Methods A316(1992)289

---

[1]Chiba Institute of Technology
[2]Faculty of Education, Chiba University
[3]Faculty of Science, Kyushu University

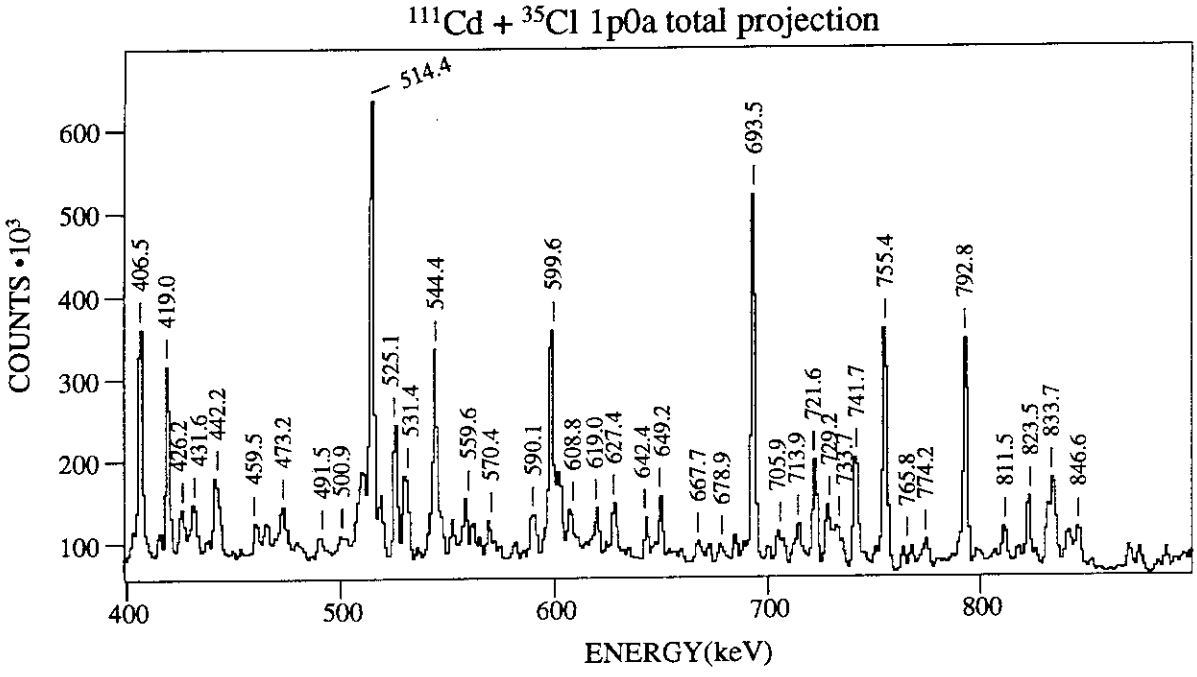

Fig. 1. A total projection spectrum of γ-rays in coincidence with 1 proton detected by the silicon ball

2.3 HIGH SPIN STATES OF ^{61}Cu

Y. HATSUKAWA, T. HAYAKAWA, K. FURUTAKA, M. KIDERA, T. ISHII, M. OSHIMA, T. SHIZUMA[1)], S. MITARAI[1)], T. MORIKAWA[1)], Y. GONO[1)], H. KUSAKARI[2)], and M. SUGAWARA[3)]

High spin states of ^{61}Cu nucleus excited through the ^{40}Ca(^{28}Si,3p1α) reaction at 120 MeV beam energy of the Tandem accelerator of JAERI were studied utilizing the JAERI Compton suppression spectrometer system. A thick Au-Ca(natural)-Au target was used. γ-γ Coincidence events were measured with 10 Compton-suppressed HP-Ge detectors and a charged particle detectors system (Si ball). The 5 x10^8 two fold events were collected, when at least two Ge detectors and at least one charged particle detector fired. The γ–γ coincidences were analyzed in a coincidence matrix gated by 3-proton and 1-α particle channel. The high spin states of ^{61}Cu were observed extending up to excitation energies about 9 MeV. Tentative level scheme is shown in Fig.1.

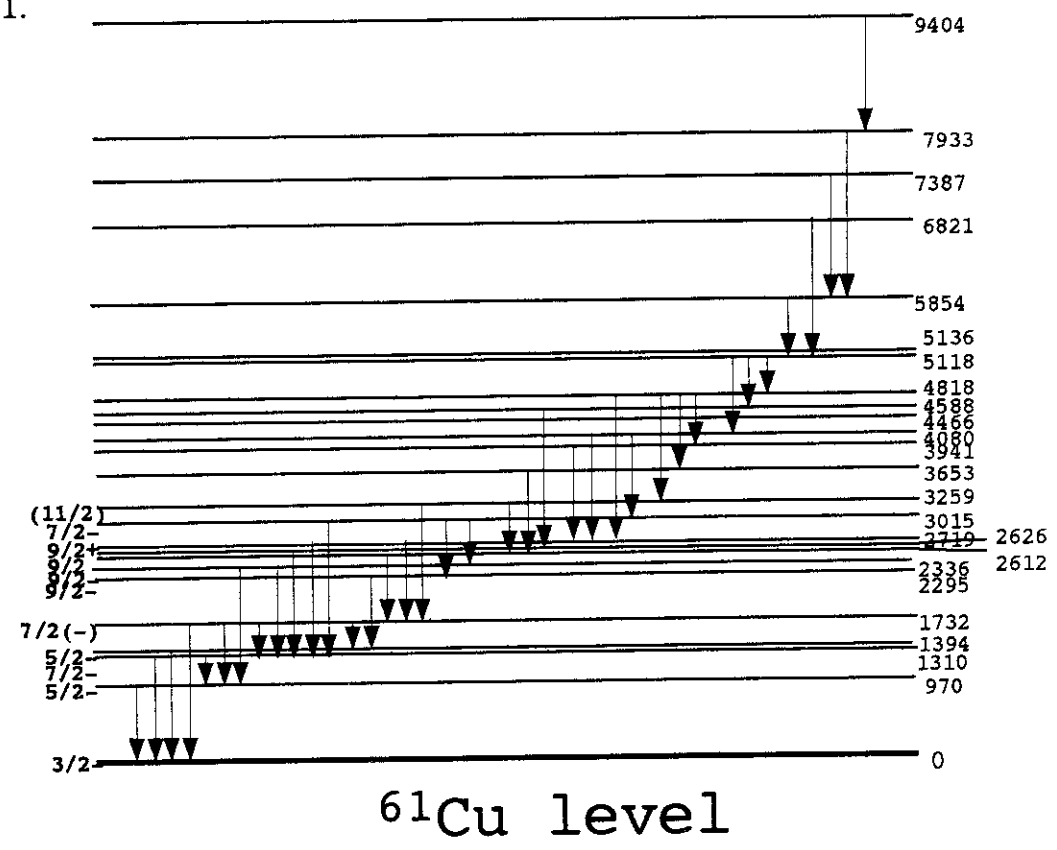

Fig. 1
Tentative level scheme of ^{61}Cu

1 Department of Physics, Kyushu University, Hakozaki, Fukuoka 812, Japan
2 Faculty of Education, Chiba University, Chiba-shi, Chiba 260, Japan
3 Faculty of Natural Science, Chiba Institute of Technology, Narashino-shi, Chiba 275, Japan

2.4 LIFETIMES OF THE $17/2^+$ STATES IN ^{103,105,107}In

T. ISHII, A. MAKISHIMA[1], M. OGAWA[2] and M. ISHII

We have measured the lifetimes of the $17/2^+$ states in ^{103,105,107}In by the recoil distance method. These nuclei were produced by the following reactions: ^{48}Ti(^{58}Ni, 1p2n)^{103}In at E(^{58}Ni)=210 MeV, ^{54}Fe(^{54}Fe, 3p)^{105}In at E(^{54}Fe)=200 MeV and ^{54}Fe(^{56}Fe, 3p)^{107}In at E(^{56}Fe)=210 MeV. Exit channels were selected by the Si box [1]. The maximum recoil distance allowable improved to 9 mm from 3 mm in the previous measurements [2]. The lifetimes of the $17/2^+$states were determined from the decay curves of the $17/2^+ \rightarrow 13/2^+$ transitions: $T_{1/2} = 0.13(2)$ ns, 0.43(4) ns and 1.3(3) ns for ^{103}In, ^{105}In and ^{107}In, respectively. These $B(E2)$ values are shown in Fig. 1, together with those of the $6^+ \rightarrow 4^+$ transitions in Sn nuclei. Low-lying states in an odd In nucleus can be described within the weak coupling scheme of a hole $(\pi g_{9/2}^{-1})$ to the core Sn nucleus. Then the $17/2^+ \rightarrow 13/2^+$ transition in In is ruled by the $4^+ \rightarrow 2^+$ transition in the core. Although the $B(E2; 4^+ \rightarrow 2^+)$ value is usually larger than the $B(E2; 6^+ \rightarrow 4^+)$ value in Sn nucleus [3], the $B(E2; 17/2^+ \rightarrow 13/2^+)$ value is as low as the $B(E2; 6^+ \rightarrow 4^+)$ value in the core nucleus. It suggests that the $17/2^+$ and $13/2^+$ states in $^{103-107}$In include some admixture of the multiplets with the higher core spin.

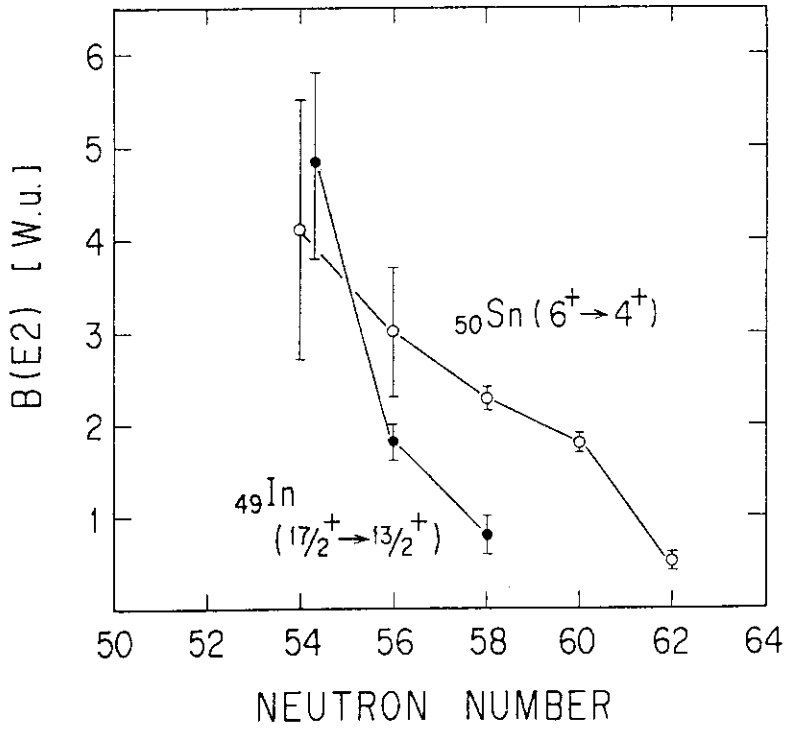

FIG. 1. Comparison of B(E2) between the $17/2^+ \rightarrow 13/2^+$ transition in $^{103-107}$In and the $6^+ \rightarrow 4^+$ transition in $^{104-112}$Sn.

References

[1] M. Ishii et al.: in Nuclei off the line of stability(ed. by R.A. Meyer and D.S. Brenner, A.C.S., Washington D.C., 1986) p.496.
[2] T. Ishii et al.: Z. Phys. A**343**, 261 (1992).
[3] A. van Poelgeest et al.: Nucl Phys. A**346**, 70 (1980).

[1]Department of Liberal Arts and Sciences,National Defense Medical College
[2]Department of Energy Sciences, Tokyo Institute of Technology

2.5 COLLECTIVE STATES IN ^{232}Th AND ^{168}Er

M. OSHIMA, M. KIDERA, T. HAYAKAWA, K. FURUTAKA, Y. HATSUKAWA, M. MATSUDA, H. IIMURA, H. KUSAKARI,[1] Y. IGARI,[1] M. SUGAWARA[2]

Recently new experimental results for two-phonon γ-vibrational states in deformed nuclei are emerging[1-5]. However, there are still some discussion on the assignment of these states as two-phonon γ vibrational state. Rather strong E4 matrix elements between the ground state and the 4^+ state of ^{192}Os may suggest strong mixing with hexadecapole one-phonon state[6]. In order to understand those situation, it is important to determine the electromagnetic properties of these states. Especially, the B(E2) values connected to the one-phonon and zero-phonon states, and the quadrupole moment are important in analyzing the property of this state. Because of this we made a multiple-Coulomb-excitation experiment for ^{168}Er and ^{232}Th, both of which are known to have well established double-γ band with collective B(E2) values; in ^{232}Th a near harmonic vibration has been reported.

The ^{168}Er and ^{232}Th nuclei were multiply Coulomb-excited with beams of 390-MeV and 415-MeV ^{90}Zr, respectively, which were obtained from the new JAERI tandem booster accelerator. The target was a self-supporting metallic foil of 2.4 mg/cm^2. The latter was coated with thin Au layers on both sides. The bombarding energies have been chosen so as to achieve the "safe energy"(4 - 4.5 fm of closest distance). Coulomb scattered particles by target nucleus are detected by two position sensitive detectors which subtended the angle between 75 and 155 degree. γ-rays in coincidence with the scattered particles are detected by four Ge-BGO anti Compton spectrometers. The observed γ-ray spectra were corrected for Doppler shifts kinematically by using the position signals of the scattered particles.

Figure 1 shows a γ-ray spectrum of ^{232}Th obtained in coincidence with back scattered Zr ions. Three transitions deexciting a known level at 1414.8 keV were observed in our experiment. The analysis of particle-γ correlation data would provide E2 matrix elements between the 4^+ state and the one-phonon states and the quadrupole moment of the 4^+ state. Such an analysis for both ^{168}Er and ^{232}Th nuclei is under way.

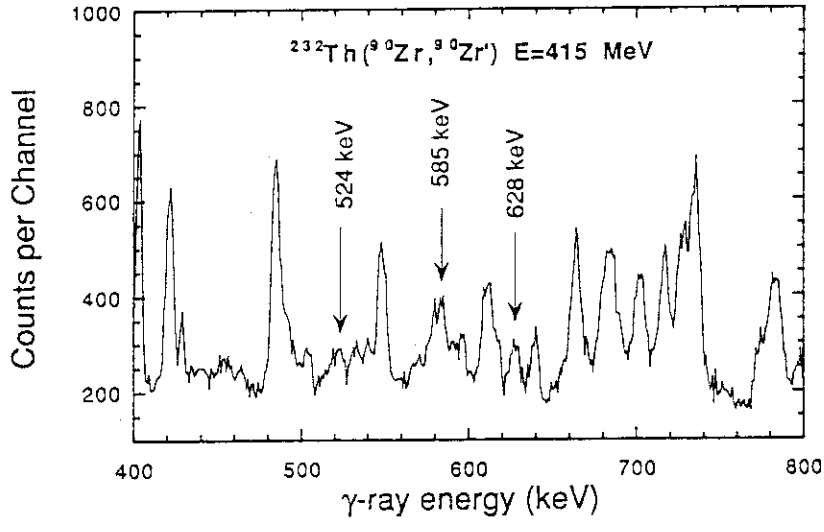

Fig. 1. A partial γ-ray spectrum of ^{232}Th gated by back scattered projectile.

References

1) H.G.Börner *et al.*, *Phys. Rev. Lett.* **66** (1991) 691.
2) M.Oshima *et al.*, *Nucl. Phys.* **A557** (1993) 635c.
3) U. Kneissl *et al.*, *Phys. Rev. Lett.* **71** (1993) 2180.
4) W.Korten *et al.*, *Phys. Lett.* B **317** (1993) 19.
5) M.Oshima *et al.*, *Phys. Rev.* **C52** (1995) 3492.
6) D.G.Burke, *Phys. Rev. Lett.* **73** (1994) 1899.

[1]Faculty of Education, Chiba University
[2]Chiba Institute of Technology

2. 6 HIGH-SPIN STATES IN ^{155,157}Gd

M. KIDERA, M. OSHIMA, T. HAYAKWA, K. FURUTAKA, Y. HATSUKAWA,
M. MATSUDA, H. IIMURA, H. KUSAKARI,[1] Y. IGARI,[1] M. SUGAWARA[2]

We have investigated previously electromagnetic properties of one quasiparticle rotational bands of several rare earth nuclei[1-3], including ^{155,157}Gd[4], based on Coulomb excitation (COULEX). Since the COULEX cross section at high spin is strongly restricted by projectile charge and energy, heavy projectiles available in the new superconducting post accelerator provide a new tool for the COULEX study. It is interesting to see the energy and electromagnetic transition probability at the backbending region, which is expected at the crossing frequency of around 0.3 MeV. For this purpose we made multiple COULEX of ^{155,157}Gd whose ground-state rotational bands are known up to 25/2$^-$.

Self-supporting metallic targets of ^{155}Gd (91.8% enriched) and ^{157}Gd (93.3% enriched) were bombarded with a beam of 390-MeV ^{90}Zr from the tandem and booster accelerators. The bombarding energy was selected so as to achieve the safe energy. The Coulomb-scattered particles were detected with two position-sensitive Si detectors with large sensitive area (45mm x 45mm) covering the angular range of 75° - 155°. γ-rays in coincidence with the projectiles were measured with an array of 10 BGO anti-Compton spectrometers constructed in collaboration with Tsukuba university. The information of γ-γ coincidence has been extracted from this data. Levels up to 2699 keV (31/2$^-$) in ^{155}Gd and to 2115 keV (29/2$^-$) in ^{157}Gd were determined as shown in Figs. 1(a) and 1(b). The data of γ-ray angular distributions will be analyzed to determine *B(E2)/B(M1)* ratios up to high spins.

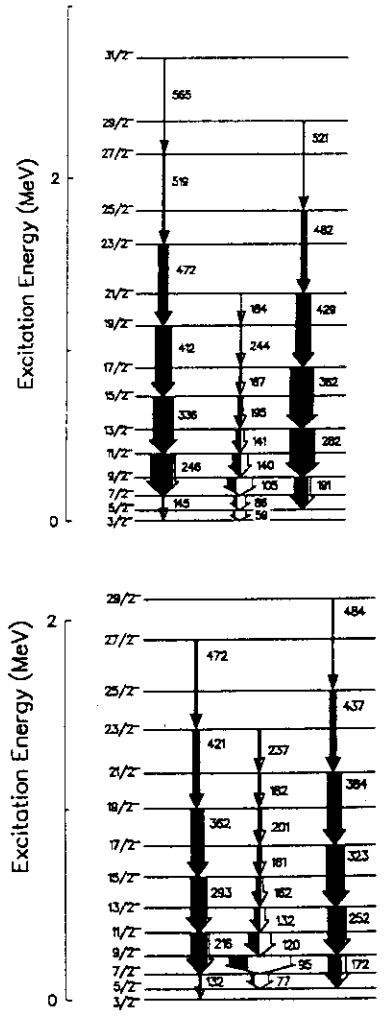

Fig.1. Partial level shemes of (a)^{155}Gd and (b)^{157}Gd.

References

1) M.Oshima *et al., Nucl. Phys.* **A436** (1985) 518.
2) M.Oshima *et al., Phys. Rev.* **C39** (1989) 645.
3) M.Oshima *et al., ibid* **C40** (1989) 2084.
4) H.Kusakari *et al., ibid* **C46** (1992) 1257.

[1]Faculty of Education, Chiba University
[2]Chiba Institute of Technology

2.7 COULOMB EXCITATION OF ^{171}Yb

M. KIDERA, M. OSHIMA, K. FURUTAKA, T. HAYAKAWA, Y. HATSUKAWA,
H. KUSAKARI,[1] M. SUGAWARA,[2] Y. IGARI[1]

The high spins states and their electromagnetic properties of well deformed nuclei, ^{161,163}Dy ^{167}Er ^{155,157}Gd and ^{173}Yb, have been investigated using Coulomb excitation[1]. As the extension of this work, the nucleus ^{171}Yb has been multiply Coulomb excited at the mini-crystalball. The ground-state rotational band of ^{171}Yb is the strongly decoupled one with the decoupling constant, $a \approx 0.85\hbar$ and backbending is expected at $I \geq 27/2$ due to the Coriolis interaction.

A ^{171}Yb target was bombarded by a 390MeV ^{90}Zr beam accelerated by the tandem accelerator and the super-conducting booster at JAERI. The target is a self-supporting foil of thickness of 1.5mg/cm^2. γ-rays were measured in coincidence with the projectile using two position sensitive Si detectors (PSD). The observed γ-ray energy is shifted due to the Doppler effect, so the correction is made by using the information of scattering angle of the projectiles. As shown in Fig. 1, the γ-rays peaks from the levels of ^{171}Yb excited by the ^{90}Zr projectile was observed. Levels up to spin 33/2 have been assigned on the basis of γ-γ coincidences. The analysis of γ-ray angular correlation is under way to extract $B(\mathrm{E2})/B(\mathrm{M1})$ ratios.

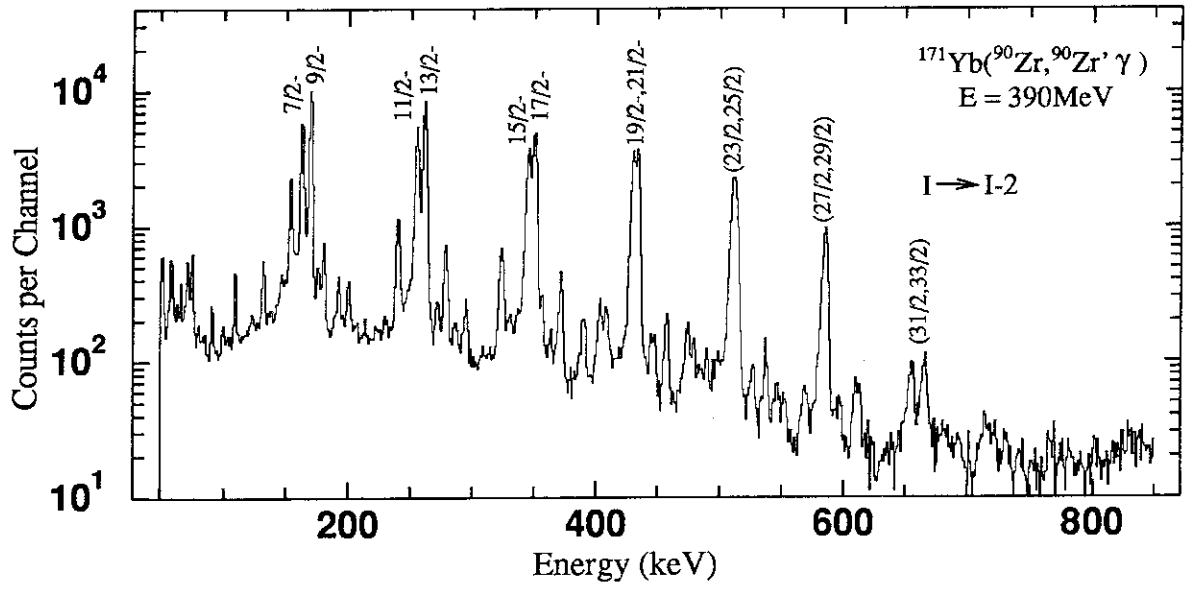

Fig. 1. A γ-ray spectra of ^{171}Yb in coincidence with back scattered projectiles. The numbers on top of peaks are the spin value of their initial states. Spins up to 23/2 is reassigned.

References

1)H. Kusakari *et al.*, Phys. Rev. **C46**(1992)1257; M. Oshima *et al.*, *ibid* **C40**(1989)2084.

[1]Faculty of Education, Chiba University
[2]Chiba Institute of Technology

2.8 HIGH SPIN STATES OF ^{63,64}Zn

T. HAYAKAWA, K. FURUTAKA, M. KIDERA, Y. HATSUKAWA, T. ISHII,
M. OSHIMA, T. SHIZUMA[1], S. MITARAI[1], T. MORIKAWA[1],
Y. GONO[1], H. KUSAKARI[2], M. SUGAWARA[3]

Low spin states of Zn isotopes were reported[1-2]. However, high spin states of Zn populated by fusion-evaporation reaction by heavy ion were unknown. To investigate excited states of nuclei of A~60 mass region, in-beam γ ray spectroscopy has been performed by heavy ion reaction. The nuclei of ^{63}Zn and ^{64}Zn were populated via ^{40}Ca(^{28}Si,4p1n) and ^{40}Ca(^{28}Si,4p) reactions with 120 MeV beam from the tandem accelerator of JAERI. A thick Au-Ca(natural)-Au target was used. A $\gamma-\gamma$ coincidence measurement was made with 10 Compton-suppressed HPGe detectors and a charged particle detector system. A typical Ge detector has 40 % relative efficiency to a 3" ×3" NaI detector and a resolution of 2.1 keV at 1.33 MeV. Each event was recorded when at least two Ge detectors and one charged particle detector fired. Total amount of 5 × 10^8 two fold events was collected. The $\gamma-\gamma$ coincidence data were analysed by using a coincidence matrix gated on three-proton or four-proton channels. The high spin states of ^{63}Zn and ^{64}Zn were observed up to ~ 8 and ~ 10 MeV. Figs. 1 and 2 show excited levels of ^{63}Zn and ^{64}Zn.

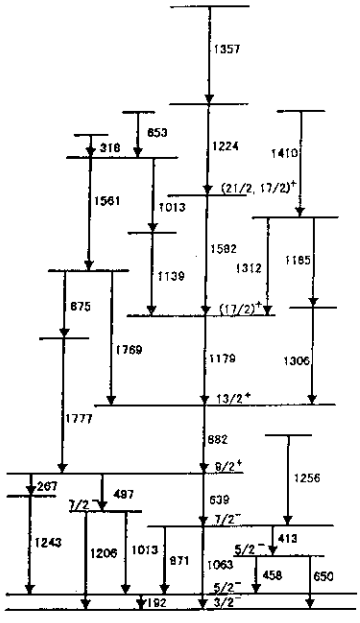

Fig.1 ^{63}Zn

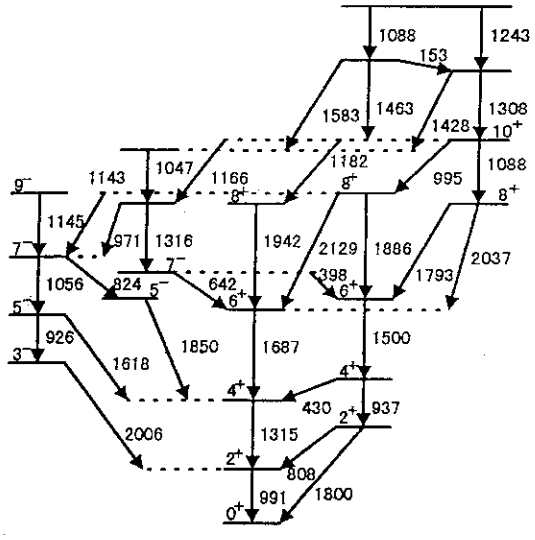

Fig.2 ^{64}Zn

Reference
1)L.Mulligan, R.W.Zurmühle, and D.P.Balamuth, Phys. Rev. C19(1979)1925
2)B.Crowell, P.J.Ennis, C.J.Lister, and W.R.Schief, Jr., Phys. Rev. C50(1994)1321

[1]Department of Physics, Kushu University, Hakozaki, Fukuoka 812, Japan
[2]Faculty of Education, Chiba University, Chiba-shi, Chiba 260, Japan
[3]Faculty of Natural Science, Chiba Institute of Technology, Narashino-shi, Chiba 275, Japan

2.9 DETERMINATION OF THE SIGN OF E2/M1 MIXING RATIO FOR THE TRANSITION FROM $11/2^-$ TO $9/2^-$ STATES IN ^{193}Tl

T. SAITOH[1], N. HASHIMOTO[1], J. LU[1], T. KOMATSUBARA[1], K. FURUNO[1]
M. OSHIMA, Y. HATSUKAWA, T. HAYAKAWA, K. FURUTAKA,
M. MATSUDA, T. ISHII and M. KIDERA[2]

The coexistence of prolate and oblate nuclear shapes is discussed on many nuclei in Pt-Hg region. This phenomenon is investigated in odd Tl isotopes also[1–3]. Reviol *et al.* proposed the coexistence of collective oblate and noncollective prolate shape in ^{193}Tl[1]. A calculation of total routhian surface indicates that the deformation of the lowest band with $\pi[505]9/2$ configuration is oblate[1]. The calculations are performed with the method developed by Satula *et al.*[4] on the basis of the self-consistent Strutinsky-Bogolyubov cranking model using a non-axial Woods-Saxon potential[5].

One of the experimental information about the nuclear shape is the sign of mixing ratios of $\Delta I = 1$ transitions. It can be used to determine the sign of the quadrupole moment from the well-known relation given by sign $\delta = (g_K - g_R)/Q_0$. This is based on the strong coupling model, and of course the sign of $(g_K - g_R)$ must be known. If we assume the $\pi[505]9/2$ configuration for the ground-state band of ^{193}Tl, the value of g_K is calculated to be 0.76. The factor g_R can be estimated to be $g_R \simeq Z/A \simeq 0.4$, so that one obtains $(g_K - g_R) > 0$. With these values of g factors, the sign of mixing ratio corresponds to the sign of quadrupole moment, and then it can be judged whether the deformation is oblate or prolate.

For the transition from the $11/2^-$ to $9/2^-$ state in the lowest band in ^{193}Tl, Newton *et al.* measured the angular distribution of γ rays[6]. On the basis of this measurement, the mixing ratio is derived as $+0.8^{+0.4}_{-0.3}$ in ref. [7]. According to the level scheme reported by Reviol *et al.*[1], however, the $11/2^- \rightarrow 9/2^-$ transition is a doublet with a transition located at a higher excitation energy. Therefore, we have carried out a new experiment aiming at the determination of the sign of E2/M1 mixing ratio for this transition.

The experiment was performed at the tandem accelerator facility in JAERI. Excited states of ^{193}Tl were populated through the ^{181}Ta(^{16}O, $4n$) reaction at a bombarding energy of 84 MeV. The target was a natural tantalum foil of 2.5 mg/cm^2 thickness. Gamma rays were observed with an array of Ge detectors which was constructed in the Tsukuba-JAERI tandem collaboration. It consists of 9 Ge detectors with BGO Compton shields. A magnet system was mounted at 90° with respect to the beam direction in order to measure conversion electrons. The system consists of a quadrupole doublet and a non-dispersive dipole magnet with a bending angle of 270°. The entrance and exit shim angles of the dipole magnet are 45° and 32.5°, respectively, to obtain both horizontal and vertical focusing. The radius of curvature is 65 mm for the central orbit. A cooled Si(Li) detector with a 100 mm^2 active area and 2 mm thick was placed at the focal position of the magnet system. An overall detection efficiency for 624 keV electrons from ^{137}Cs was measured to be 1.3×10^{-3} including the effective solid angle, the transmission through the magnet system and the peak efficiency of the Si(Li) detector. A typical energy resolution was 5 keV for 307 keV electrons emitted

1 Institute of Physics and Tandem Accelerator Center, University of Tsukuba 305 Ibaraki, JAPAN
2 On leave from Kyushu University, Hakozaki, Fukuoka, Japan

from ^{193}Tl. The range of electron momentum having approximately flat efficiency was ± 10 % for a certain value of the magnetic fields .

Ratios of γ-γ directional correlation from oriented nuclei(DCO ratios) were obtained for the direct cascade consisting of the 754.7 and 399.2 keV γ rays. The multipolarity of the 754.7 keV γ ray feeding the $11/2^-$ state is E2, whereas the subsequent 399.2 keV γ ray feeds the $9/2^-$ state with E2/M1 mixed multipoles. The experimental result is displayed in Fig. 1. Two horizontal lines indicate the limits of the experimental DCO ratio. The curves are calculations as a function of arctan δ for assumed spin-alignment parameters, σ/J, in the range from 0.2 to 0.45.

Fig. 2 shows DCO ratios for $e^- - \gamma$ angular correlation. Two horizontal lines are experimental limits and curves are theoretical DCO ratios. In this figure, the yield of electrons is summed up for γ-ray detectors except for one detector which is mounted on the opposite direction to the magnet system for the electron measurement.

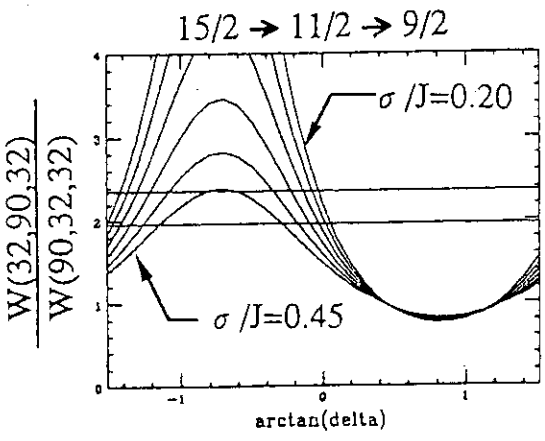

Fig. 1. DCO ratios for $\gamma - \gamma$ correlations

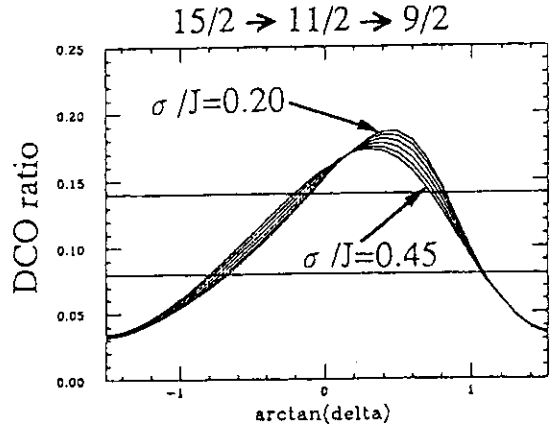

Fig. 2. DCO ratios for $e^- - \gamma$ correlations

From the combination of these two data, we have deduced the mixing ratio of -0.59 ± 0.14. This mixing ratio is comparable to the ratios of heavier odd Tl isotopes. In ^{197}Tl and ^{199}Tl, negative mixing ratios are reported for both $11/2^- \rightarrow 9/2^-$ and $13/2^- \rightarrow 11/2^-$ transitions[8,9]. The present result fits to a systematic trend of mixing ratios together with excitation energies of the $9/2^-$ band which hardly change over a wide range of neutron number from $N = 104$ to 118. The negative sign of the mixing ratio implies that the [505]9/2 band has an oblate shape. Indeed the [505]9/2 Nilsson state lies near the Fermi surface if we assume a slightly oblate deformation.

References

1) W. Reviol *et al*, Nucl. Phys. **A 548**(1992)331.
2) G.J. Lane *et al*, Nucl. Phys. **A 586**(1995)316.
3) A.J. Kreiner *et al*, Phys. Rev. **C 38**(1988)316.
4) W. Satula *et al*, Nucl. Phys. **A 529**(1991)289.
5) W. Nazarewicz *et al*, Nucl. Phys. **A 435**(1985)397.
6) J.O.Newton *et al*, Nucl. Phys. **A 236**(1974)225.
7) V.S. Shirley, Nuclear Data Sheets **61**(1990)519.
8) L.L. Collins *et al*, Abst. Int. **35B**(1979)3834.
9) J.O. Newton *et al*, Nucl. Phys. **A 148**(1970)593.

2.10 IN-BEAM SPECTROSCOPY OF ^{63,65}Ga BY ^{40}Ca + ^{32}S REACTION

S. MITARAI[1], T. MORIKAWA[1], A. ODAHARA[1], H. TSUCHIDA[1], T. SIZUMA[1], T. SHIBATA[1], M. KIDERA[1], H. WATANABE[1], Y. GONO[1], J. MUKAI[2], M. OSHIMA, T. ISHII, Y. HATSUKAWA, K. FURUTAKA, T. HAYAKAWA, M. MATSUDA, T. KOMATSUBARA[3], E. IDEGUCHI[4],

Nuclei far from the valley of beta-stability have proven to be an excellent testing ground for nuclear models involving single-particle and collective degrees of freedom. The nuclei around N=Z in the region of A=60-80 are predicted to show exotic shapes, supper-deformation and hyper-deformaition. But the nuclei with N=Z in the mass=60-70 are difficult to be produced. Accordingly, the identification of in-beam γ transition requires the use of an experimental filter to separate the transitions of interest from the intense back-ground of more prolific fusin-evaporation channels. Most of the experiments in this region were carried out using light heavy ion like as α, Li, C, O and relatively low energy beams. So, only a γ-ray emitted from a stopped residues was mainly measured to get an information of the low-lying levels.

The method employed in the present study has been to utilize coincidences between γ-rays and proton and α particles to identify transitions in specified nucleus. The multiplicity filter for charged particles (Silicon ball)[1] has been installed inside a 100 mm diameter sphere of an array of 11 ACS-Ge detectors at JAERI tandem accelerator. The Silicon ball with 30 detectors works as 21 detctor elements shown in fig. 1. Each of 6 pentagonal detectors with segmentations in backward sphere was interconnected to work as one

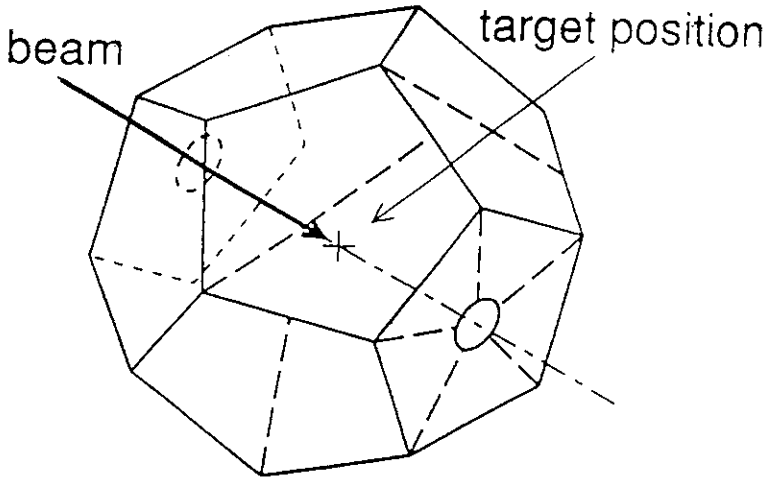

Fig.1 A schematic drawing of Silicon ball consisted of 21 Si detector elements. Silicon ball with high granularity in the forward angles to the beam axis.

1. Department of Physics, Kyushu University
2. Touwa University
3. Institute of Physics, University of Tsukuba
4. Institute of Physical and Chemical Research

detector and the remaining 15 detectors of the array work independently. The thick and thin targets of ^{nat}Ca were bombarded to study the details of low-lying states and high spin states from the measurements of γ-ray emitted from the stopped and in flight residues, respectively. The excited states of $^{63,65}Ga$ were populated by the $^{nat}Ca + ^{32}S$ reaction at a ^{32}S beam energy of 140 MeV.

Figure 2 shows the level schemes of ^{63}Ga and ^{65}Ga which are based on γ-ray energies, relative intensities and coincidence relation. Tentative spin-parity values are based on refs. 2 and 3, systematics in this mass region and branching of γ-rays in the scheme. Data of 90k events of γ-γ coincidence gated by 2α1p can give the relations between 15 γ-rays of ^{63}Ga in the level scheme because of high quality of the data. In previous experiment in ref. [2], only 10 γ-rays of yrast band are assigned to ^{63}Ga with a small cross section. The tentative spin-value of 19/2 for a 4434 keV level of ^{65}Ga is assigned from the γ-ray branching of a 5468 keV level, contradicted to the assignment of the first 21/2 level[3] which indicated a change of band structure. The extension of yrast bands were carried out by clean γ-γ coincidence data in flight, irrespective of large Doppler broadening effect of the γ-ray. Analysis of the data for other exit channels is in progress.

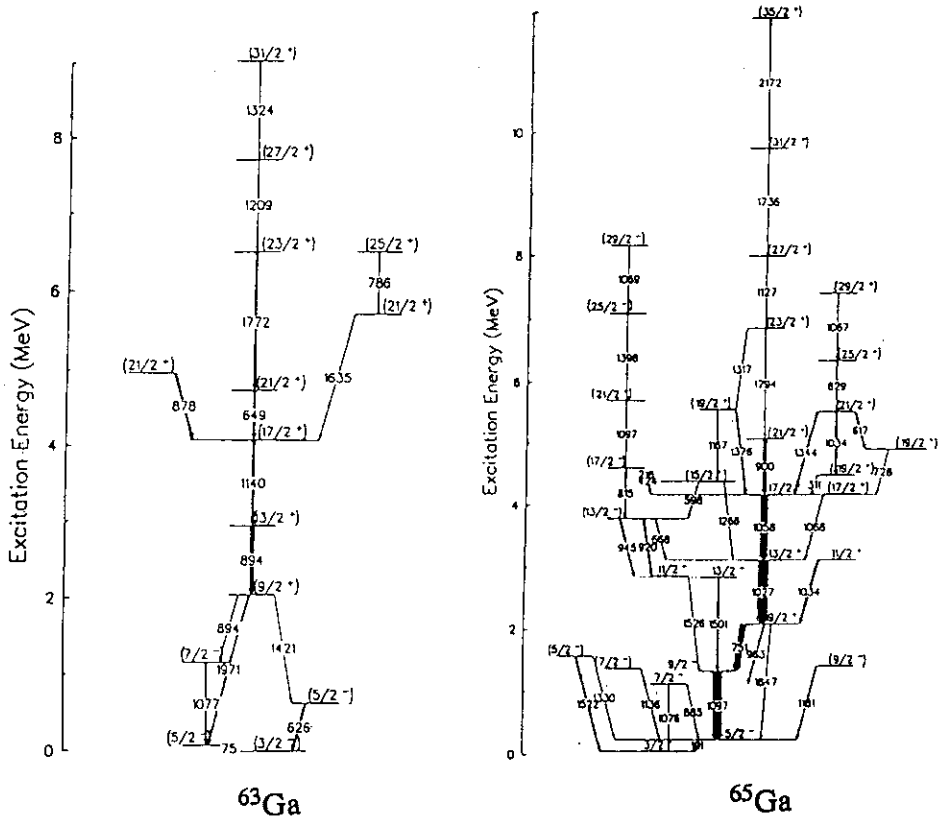

Fig. 2 The level schemes for ^{63}Ga and ^{65}Ga obtained from the present work.

References

1) T. Kuroyanagi et al., Nucl. Instr. and Meth. A 316(1992) 289.
2) D.P. Balamuth etal., Phys. Rev. C. 43(1991) 43.
3) H. Kawakami et al., Phys. Rev. C. 21(1980) 1311.

2.11 IN-BEAM γ SPECTROSCOPY OF ^{62}Zn NUCLEI

K. FURUTAKA, M. KIDERA,[1] M. MATSUDA, T. HAYAKAWA, Y. HATSUKAWA, T. ISHII, M. OSHIMA, S. MITARAI,[2] T. SHIZUMA,[2,3] M. SHIBATA,[2] H. WATANABE,[2] T. MORIKAWA,[2] T. KOMATSUBARA,[4] T. SAITOH,[4] N. HASHIMOTO,[4] H. KUSAKARI,[5] and M. SUGAWARA[6]

Nuclei in $A \sim 60$ region are close to $N = Z$ domain and several interesting phenomena, such as octupole correlation in ground states [1] and superdeformations [2–4], are expected. But experimental data, especially for high spin states, are rather scarce. In order to get more information on high spin states and to search for such exotic phenomena, in-beam γ-spectroscopic study has been performed by using newly constructed mini crystal–ball which consist of 11 Ge γ-ray detectors with BGO anti–Compton suppressor.

Two targets of ^{40}Ca were irradiated by 120 MeV ^{28}Si beam derived from JAERI Tandem Accelerator. Both are sandwiched between Au layers; one is thin(Au(300μg/cm^2) + Ca(300μg/cm^2) + Au(300μg/cm^2)), and the other is thick (Au(500μg/cm^2) + Ca(3 mg/cm^2) + Au(13 mg/cm^2)). γ rays emitted in the reaction were detected with mini-crystal ball in coincidence with light charged particles(LCP) using large solid angle charged particle detector array, Si-ball [5]. The data were sorted by the number and the kind of LCPs (channels) detected in the Si-ball, and γ-γ corelation matrices were constructed and analyzed for each channel. Here we restrict ourselves to the data on ^{62}Zn nucleus ($2p1\alpha$ channel).

A correction for γ-ray energies were made using information on emission angles of γ rays and LCPs, which are required by finiteness of recoiling velocity and its small variation due to LCP emission. By this correction, an extremely good resolution (6.5 keV for 1 MeV γ ray) is obtained for the spectrum of the gamma rays emitted from nuclei in flight.

From the analysis of the γ-γ matrix, new γ rays from ^{62}Zn, including one that seem to be emitted from a level above 14 MeV excitation energy, are observed as shown in fig. 1. Detailed analysis, including angular distribution and DCO ratios, are now under way.

References

1) P. J. Ennis *et al.*, Nucl. Phys. **A535**, (1991) 392
2) T. Bengtsson *et al.*, Phys. Scr., **24**, 200-214 (1981)
3) I. Ragnarsson *et al.*, Phys. Rep., **45**, (1987) 1-87
4) I. Ragnarsson, L.A.N.L. Report **LA-11964**, Oct. 1990
5) T. Kuroyanagi *et al.*, Nucl. Instrum. Method **A316**, (1992) 289

[1]on leave from Kyushu University
[2]Kyushu University
[3]Present address : Tsukuba University
[4]Tsukuba University
[5]Faculty of education, Chiba University
[6]Chiba Institute of Technology

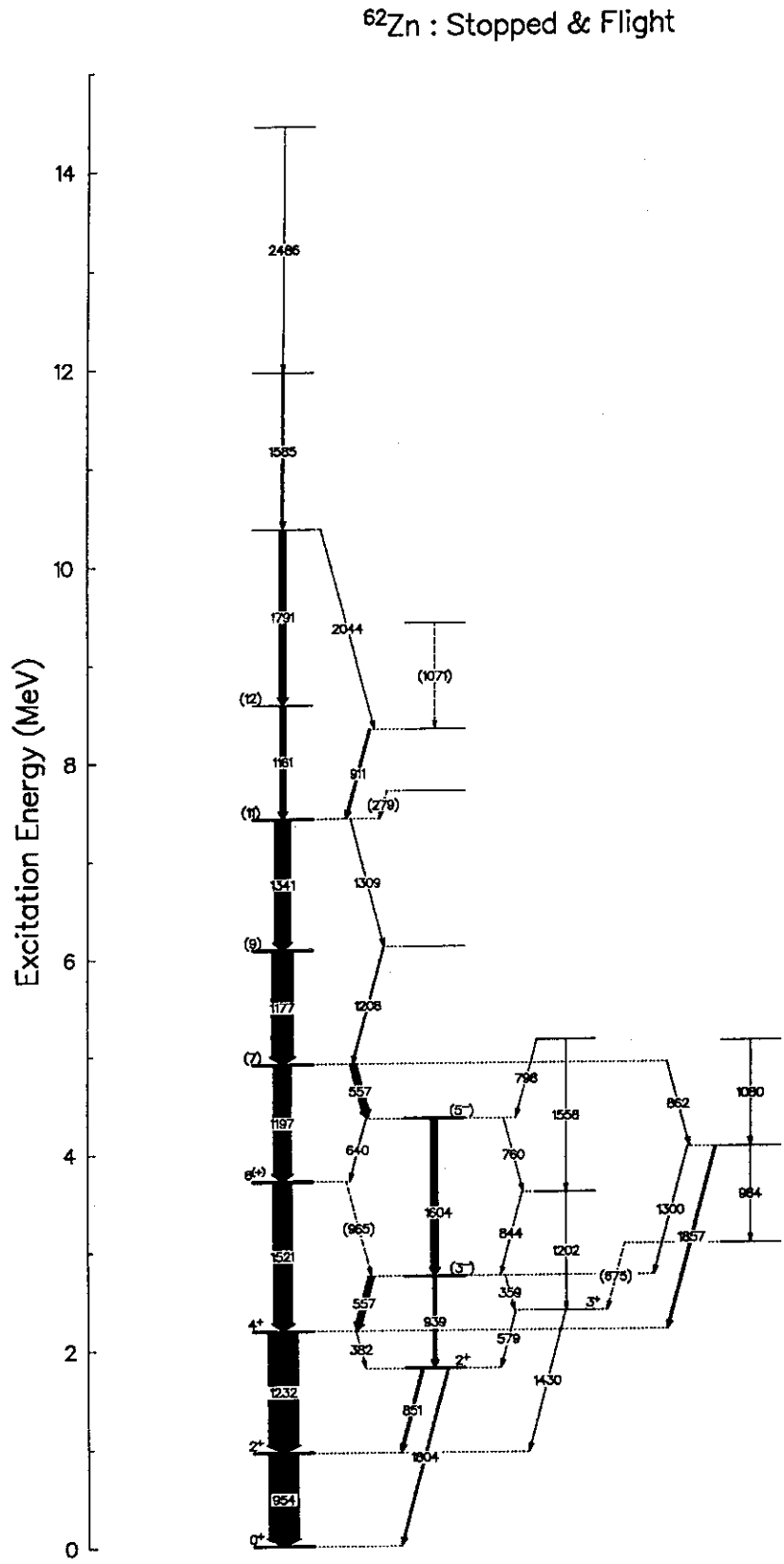

Figure 1: Level scheme of ^{62}Zn obtained in the present study (preliminary).

2.12 AN AUTOMATIC LIQUID NITROGEN FILLING SYSTEM FOR Ge DETECTORS OF MINI-CRYSTALBALL

K. FURUTAKA, M. KIDERA,[1] M. MATSUDA, T. HAYAKAWA, Y. HATSUKAWA, T. ISHII, M. OSHIMA, T. MORIKAWA[2]

Ge detectors must always be coold down to the liquid nitrogen temperature in order to avoid deterioration in energy resolution owing to neutron damage. However, capacity of liquid nitrogen Dewars attached to Ge detectors of the so called crystal ball is so small that it must be refilled about twice a day. To automate this task, an automatic liquid nitrogen filling system for Ge detectors of newly constructed mini-crystalball has been constructed.

The liquid nitrogen filling system consists mainly of three parts (see fig. 1); i) liquid nitrogen distribution components which are made up with reservoir vessel, distribution tubes and valves, ii) programable controller with two timers administrating the whole system, and iii) a monitor computer which fetch and display data concerning filling cycles, which is independent of the controller.

A liquid nitrogen vessel with volume capacity of 250 liters is used as a reservoir. With this vessel, the nitrogen can be supplied for five days without re-filling it, to 11 detectors (5 Dewars (5 littres) which are filled once a day and 6 Dewars (3 littres) twice a day). The nitrogen is taken out of it by applying pressure (1.0 kgw/cm^2) with nitrogen gas. Liquid nitrogen is distributed via Teflon tubes. The system has two manifolds to serve to two type of liquid nitrogen Dewars. Essentially four kind of valves are attached to each distribution tube (see figure 1); a pressure valve V_p, a liq. N_2 take-out valve V_t, an exhaust valve V_m with a thermometer and detector valves V_d. All valves are controlled by programmable controller.

The controller system consists of programmable contoroller and two timers. Each timer initiates filling cycles of the corresponding distributions. As much as 16 cycles a day can be set on each timer. The controller (OMRON SYSMAC C200H) observes timers and thermometers and opnes/closes the valves.

A filling cycle proceeds as the following: When it comes to a preset time, the controller first opens V_p, V_t, and V_e, with V_d closed, to cool down distribution tubes. After the tubes are sufficiently cooled down below a preset temperature, V_e is shut and all V_ds are opened, and actual filling begins. When a Dewar becomes full with liquid nitrogen and a thermometer attached to the outer side of the Dewar senses spilling of nitrogen liquid, the corresponding V_d is shut, and the time during which the valve is open is recorded in the controller. After all Dewars become full, liquid nitrogen supply to the whole system is stopped by closing V_p and V_t, and liquid nitrogen remained in distribution tubes are exhausted by opening V_e. On average it takes 10 minutes to fill a Dewar. One filling cycle is finished in approximately 15 minutes.

A computer system, which is absolutely independent of the controller, monitors the filling cycles, especially the time elapsed to fill each Dewar. The monitor computer periodically

[1]on leave from Kyushu University
[2]Kyushu University

check the controller and, if there are new data (i.e. a supplying cycle has been finished), it fetches and record them. These data are plotted on the monitoring computer and, if there are any detectors which takes longer time than a preset value (now set to 10 minutes) it displays warning. The computer can be remotely controled and monitored via Local Area Network as well as via telephone line using modem.

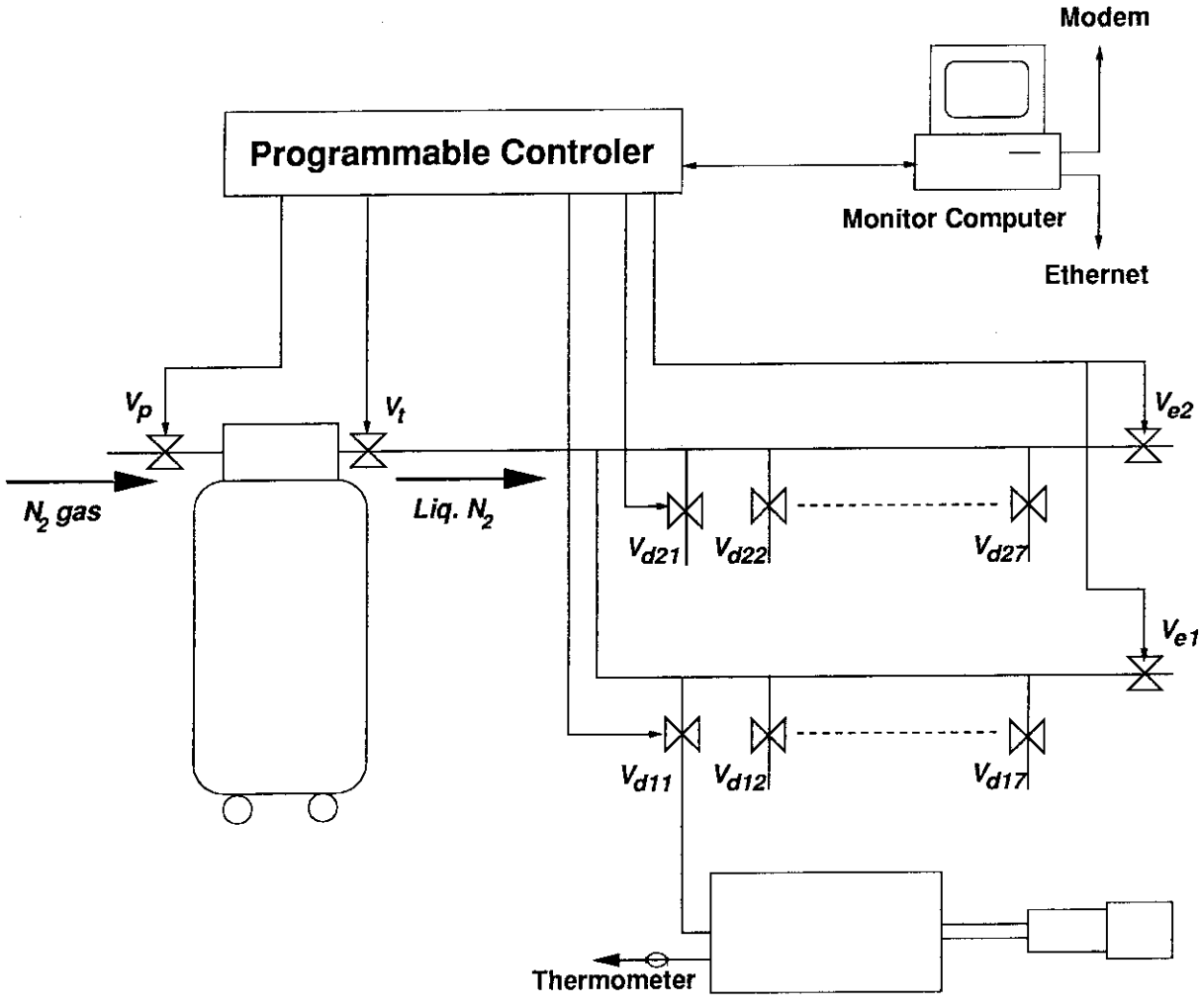

Figure 1: Schematic diagram of the automatic liq. N_2 filling system.

2. 13 DEVELOPMENT OF FREQUENCY-REFERENCE FOR COLLINEAR LASER-ION-BEAM SPECTROSCOPY

Y. ISHIDA[1] , H. IIMURA, S. ICHIKAWA and T. HORIGUCHI[1]

Hyperfine structures (HFS) and isotope shifts (IS) of atomic spectral lines obtaining from laser spectroscopy provide the useful information on nuclear structure, such as nuclear moments and charge radii. A number of elements have been studied by laser spectroscopy in the world. At JAERI-ISOL, we have focused on light lanthanoids, i.e., La, Ce, Pr. By means of collinear laser-ion-beam spectroscopy, we have successfully measured the HFS's of ^{141}Pr stable isotope[1] and ^{143}Pr radioactive isotope[2], and obtained the electro-magnetic moments of those nuclides. However, the IS have not been measured because mass-separated ion-beam from the ISOL does not allow the spectra of two isotopes to be taken simultaneously.

To measure the IS with mass-separated ion-beam, we had to introduce the frequency-reference which can calibrate the absolute frequency of spectral lines. The HFS of $^{127}I_2$ is useful for that purpose because of its dense spectra in the visible region. Polarization spectroscopy is one of the technique to obtain the HFS of $^{127}I_2$, and offers a better signal-to-background ratio with simple optical apparatus.

Figure 1 shows the experimental apparatus for polarization spectroscopy. A single-mode tunable dye laser (Coherent 699-29) with a wavemeter was pumped by an Ar-ion laser (Coherent INNOVA-100-20). A linearly polarized probe beam from the dye laser is sent through an iodine cell. Only a small fraction of this beam reaches a photomultiplier tube (PMT) after passing through a crossed linear polarizer. Any optical anisotropy which changes the probe polarization will alter the light flux through the used polarizer and can be detected with high sensitivity. Such an anisotropy can be induced by sending a circularly polarized laser beam in nearly the opposite direction through the cell. As in conventional saturation spectroscopy, a resonant signal is expected only near the center of a Doppler-broadened absorption line because only the atoms with essentially zero axial velocity can interact with both laser beams. A confocal Fabry-Pérot Interferometer (FPI) with a free spectral range of 150-MHz was used to calibrate the relative frequency of spectral lines.

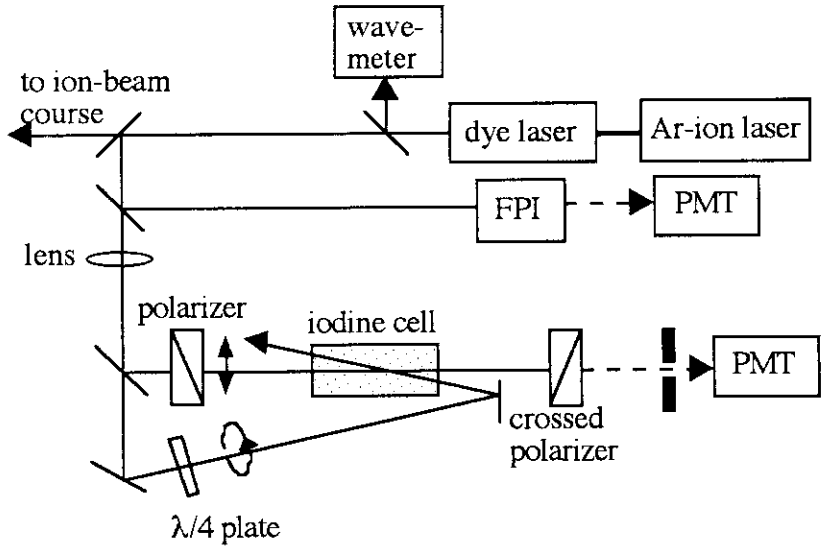

Fig. 1. Experimental apparatus for polarization spectroscopy. FPI; Fabry-Pérot interferometer, PMT; photomultiplier tube.

[1] Department of Physics, Hiroshima University.

Typical HFS spectrum of the $^{127}I_2$ *B-X P*(62) 17-1 transition is shown in Fig. 2. If one uses a perfectly crossed polarizer in polarization spectroscopy, a Lorentzian resonance signal is taken, as in Fig. 2. The relative frequencies between the hyperfine peaks measured by Razet[3] are indicated by vertical lines at the lower part of the spectrum. The relative frequencies obtained in this work are in good agreement with the previous ones. The line width corresponding to one hyperfine transition is about 10 MHz. This ensures that the accuracy of the IS measurement will not be reduced by this frequency-reference system because the line width of collinear laser-ion-beam spectroscopy is typically about 100 MHz.

We are now using this system for the IS measurements of Ce isotopes with collinear laser-ion-beam spectroscopy.

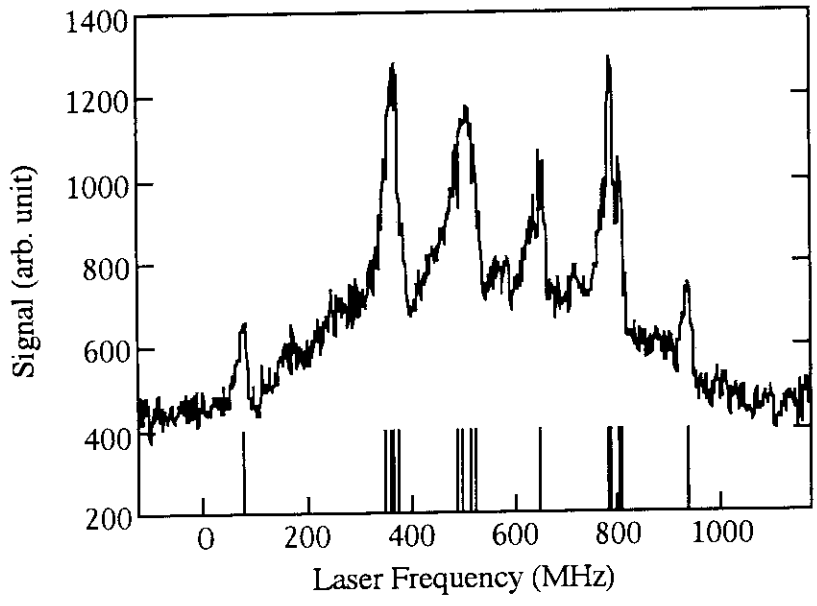

Fig. 2. Polarization spectrum of the $^{127}I_2$ *B-X P*(62) 17-1 transition. The relative frequency scale of the horizontal axis was calibrated by using FPI.

References
1) H. Iimura, Y. Nakahara, S. Ichikawa, K. Kotani, M. Wakasugi, and T. Horiguchi, J. Phys. Soc. Jpn. **59** (1990) 4208.
2) H. Iimura, Y. Nakahara, S. Ichikawa, M. Kubota, and T. Horiguchi, Phys. Rev. C**50** (1994) 661.
3) A. Razet, Metrologia **30** (1993) 193.

2. 14 HOLD-UP TIMES IN A GAS-JET COUPLED THERMAL ION-SOURCE FOR METALLIC AND MONOXIDE IONS OF LANTHANUM AND CERIUM

S.ICHIKAWA, K.TSUKADA, M. ASAI[1], A.OSA, Y.KOJIMA[1], Y.NAGAME, K.KAWADE[2], H.IIMURA, Y.OURA, I. NISHINAKA and Y.HATSUKAWA

A gas-jet coupled thermal ion source was installed in the separator on line at the JAERI tandem accelerator [1]. It was used for decay spectroscopy of short-lived isotopes and search for unknown isotopes in the region of neutron-rich rare earth isotopes. So far a new isotope of ^{166}Tb has been identified [2]. The performance of the thermal ion source with the gas-jet transport system was tested using short-lived isotopes produced via proton-induced fission of ^{238}U. The separation efficiencies of the whole system were measured to be 3.3% for ^{140}Cs($T_{1/2}$ = 63.7s), 2.0% for ^{144}La($T_{1/2}$ = 40.8s), 2.2% for ^{148}Pr($T_{1/2}$ = 2.0 min.), 1.2% for ^{156}Pm($T_{1/2}$ = 26.7s) and 1.0% for ^{160}Eu($T_{1/2}$ = 44s). For very short-lived ^{144}Cs ($T_{1/2}$ = 1.02s) and ^{148}La ($T_{1/2}$ = 1.05s) isotopes, the separation efficiencies were found to be >1% and 0.1%, respectively.

The measured separation efficiency of ^{148}La was 1/20 of that for ^{144}La. The separation efficiency of ^{148}La can be compared with ^{144}Cs whose separation efficiency was 1/3 of that for ^{140}Cs. These relative separation efficiencies give some information about a delay time between the production of isotopes and its extraction from the ion source. If there are no losses coming from decay until it is analyzed with the mass separator, the separation efficiencies for ^{140}Cs and ^{144}Cs, and ^{144}La and ^{148}La are the same within the experimental uncertainty. But, the separation efficiency depends on the half-life $T_{1/2}$ of an isotope and t the delay time and is expressed as being proportional to $\exp[-\ln 2(\frac{t}{T_{1/2}})]$. With their half-lives being taken into account, the above relative efficiencies for ^{144,140}Cs and ^{148,144}La give t =1.7s for ^{144}Cs and t = 4.5 s for ^{148}La, respectively.

To confirm the delay time for La and Cs ions in the gas-jet coupled thermal ion source, we measured the intensity of a mass-separated beam before and after the accelerator beam stopped. It was confirmed that the intensity of a mass-separated beam decrease exponentially after the accelerator beam was switched off and the production of the nuclide of interest stopped [3]. As a result, a delay half-time of the radioactivity after switched off the accelerator beam was obtained; the value $T_{1/2}^{del}/\ln 2$ should be considered as a mean delay time in the whole system.

Fig. 1 shows a release profile of mass-separated beams of $^{140}Cs^+$, $^{144}LaO^+$ and $^{148}CeO^+$ at the ion-source temperature of 2450 K. The delay half-times obtained in the present work are 2 s for $^{140}Cs^+$, 3.4 s for $^{148}CeO^+$ and 5.4 s for $^{144}LaO^+$.

For a gas-jet coupled ion source, the delay time can be analyzed in terms of three components: the sweep-out time of recoil atoms through the target chamber, the transit time through a capillary and the hold-up time in the ion source. A delay time t_d, sum of two components of a sweep-out time and a transit time, was studied experimentally by Moltz *et al.* [4]. With the equation proposed by Moltz, the delay time t_d of our gas-jet system was estimated to be 2.5 s. The hold-up times for many elements were studied by Kirchner [5] with the FEBIAD ion source. His results indicated that the hold-up times are governed by sticking time on the cavity wall, and suggest the possibility that a

1 Department of Nuclear Engineering, Nagoya University
2 Department of Energy and Engineering and Science, Nagoya University

thermal ion source has longer hold-up time for La and Ce ions than for neighboring elements in the periodic table, such as Cs, Ba and Pr. The observed delay time for Cs ion, thus can be regarded as the delay time t_d for gas-jet transport system.

Time difference: $t(^{148}\mathrm{La})$-$t(^{144}\mathrm{Cs})$ = 2.8 s that was indirectly calculated from the relative efficiency for ^{144,140}Cs and ^{148,144}La, is consistent with the time difference of delay half-time: $T_{1/2}^{del}(^{144}LaO) - T_{1/2}^{del}(^{140}Cs) \approx 3.4s$. The time difference of the delay half-time of $T_{1/2}^{del}(^{148}CeO) - T_{1/2}^{del}(^{140}Cs) \approx 1.4s$ can be calculated also. The hold-up time for La^+, LaO^+ and CeO^+ ions in the thermal ion source are ascribable to long sticking time of La and Ce atoms on the Re surface that is construction material of the ion source. The present results are identical with the previous ones [6] that metallic and monoxide ions of La and Ce have a longer sticking time for the Re surface than those of Cs, Ba, Pr and Nd.

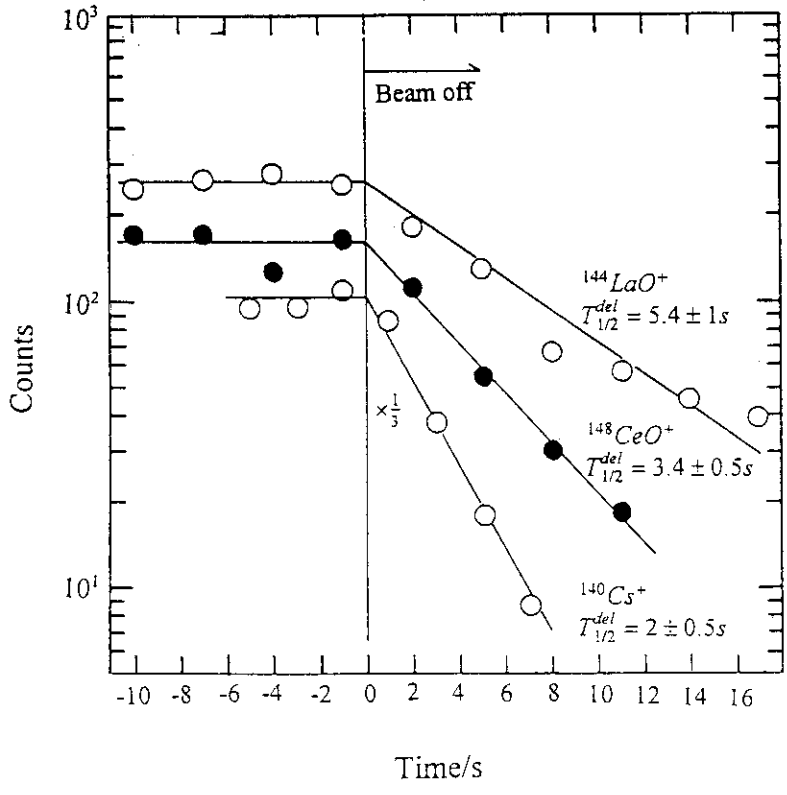

Fig. 1. Release profile of the $^{144}La^{16}O^+$, $^{148}Ce^{16}O^+$ and $^{140}Cs^+$ ions at an ion source temperature of 2450 K. The γ-rays associated with the decay of ^{144}La, ^{148}Ce and ^{140}Cs were detected.

References

[1] S.Ichikawa, M.Asai, K.Tsukada, A.Osa, T. Ikuta, N.Shinohara, H. Iimura, Y.Nagame, Y.Hatsukawa, I.Nishinaka, K.Kawade, H.Yamamoto, M.Shibata and Y.Kojima, Nucl. Instr. Meth. A in press.
[2] M.Asai, K.Tsukada, S.Ichikawa, A.Osa, Y.Kojima, M.Shibata, H.Yamamoto, K.Kawade, N.Shinohara, Y.Nagame, H.Iimura, Y.Hatsukawa and I.Nishinaka, J.Phys. Soci. Japan. in press.
[3] V.A.Karnaukhov, D.D.Bogdanov, A.V.Demyanov, G.I.Koval and L.A.Petrov, Nucl. Instr. Meth 120(1974)69.
[4] D.M.Moltz, J.M.Wouters, J.Aysto, M.D.Cable, R.F.Parry, R.D.Von Dincklage and J.Cerny, Nucl. Instr. Meth. 172(1980)519.
[5] R.Kirchner, GSI 88-1(1988)pp.339, 341.
[6] S.Ichikawa, T.Sekine, H.Iimura and M.Oshima, Nucl. Instr. Ment. B70(1992)156.

3. Nuclear Reactions

3.1 INVESTIGATION OF INTERMEDIATE STRUCTURES IN $^{12}C(^{16}O,^{12}C[2_1^+])^{16}O$ BY THE γ-RAY RECOIL METHOD

H. FUJITA[1], M. HIJIYA[2], T. MUKAE[2], K. NAKAMOTO[2], T. OKAMOTO[2], S. KOJIMA[2], S. TERUYAMA[2], K. MIZUUCHI[2], K. KOGA[2], T. SUGIMITSU[2], N. IKEDA[2], S. MORINOBU[2], Y. SUGIYAMA, Y. TOMITA, H. IKEZOE, K. IDENO, Y. YAMANOUTI, S. HAMADA and T. IKUTA

We have been studying some intermadiate sturctures in $^{12}C+^{16}O$ inelastic scattering leading to the single excitation $^{12}C(2_1^+)$-$^{16}O(0_1^+)$ and mutual excitation $^{12}C(2_1^+)$-$^{16}O(0_2^+,3_1^-)$ channels by mesuaring the magnetic substate populations for the 2^+ state at 4.44 MeV in ^{12}C by the γ-ray recoil method [1]. This method allows us to extract the magnetic substate populations properly from the line shape of excited reaction products which are broadened by γ decay in flight, when a quantization axis is taken along the center of mass scattering angle of the products. Recently we showed that in the above ejectile-axis frame a resonance spin J can be obtained directly from the m-substate angular distributions and a decay L value is sensitive to the relative intensity between each m-substate cross section [2].

Up to now we have measured the angular distributions for the individual m-substates at backward angles around $E_{c.m.} \approx 22$ MeV and 32 MeV. In the energy region around $E_{c.m.} \approx 32$ MeV resonance-like structures have been observed at $E_{c.m.} \approx 30$ and 32 MeV in both the single and mutual excitation channels. As for the single excitation channel the angular distributions for the individual m-substates have been measured at $E_{c.m.} = 29.8$ and 31.8 MeV on-resonance and 33.0 MeV off-resonance. The result of the analysis suggests that the spin value for the structures at $E_{c.m.} = 29.8$ and 31.8 MeV is assigned to be $J^\pi = 16^+$ or 17^- and both structures decay dominatly through the L value of the aligned configuration $L = J - 2$ [2]. In the energy region around $E_{c.m.} \approx 22$ MeV the angular distributions for the individual m-substates have been measured at several energies between 22.0 and 23.1 MeV. A pronounced resonance has been observed previously at $E_{c.m.} \approx 22.5$ MeV in the single excitation channel. The angular distributions for the individual m-substates in this energy region are different from those observed at $E_{c.m.} = 29.8$ and 31.8 MeV and cannot be explained by the calculation under the assumption that the resonance decays dominatly through the L value of the aligned configuration $L = J - 2$ [3].

In the present work we have measured the angular distributions for the individual m-substates in the single excitation channel at the off-resonance energies of $E_{c.m.} = 21.5$ and 28.8 MeV in order to confirm the consistency of the feature obtained by the above analyses. The experiment was performed by bombarding a ^{12}C target with an ^{16}O beam from the JAERI tandem accelerator. Momentum spectra of ^{12}C ejected were measured with a high resolution by the magnetic spectrograph "ENMA". The analysis is in progress.

References
[1] Y. Sugiyama et al., Z. Phys. A - Atoms and Nuclei **322** (1985) 579.
[2] Y. Sugiyama et al., Phys. Rev. C **49** (1994) 3305.
[3] H. Fujita et al., JAERI TANDEM, LINAC & V.D.G. Annual Report 1993, p.36.

[1]Daiichi College of Pharmaceutical Sciences, Fukuoka 815
[2]Department of Physics, Kyushu University, Fukuoka 812

3.2 STUDY OF PROTON RADIOACTIVITIES IN THE VICINITY OF ^{100}Sn

T. IKUTA, H. IKEZOE, S. HAMADA, Y. NAGAME, I. NISHINAKA, K. TSUKADA, Y. OURA, T. OHTSUKI[1] and Y. AOKI[1]

The neutron-deficient trans-tin isotopes have been characterized by their complex decay behavior (β^+/EC decay, β-delayed proton and α emission, ground state α-decay and proton emission) owing to the influence of the magicity of Z=N=50. Especially, the nuclei lying around the proton drip-line exhibit notable features attributed to the onset of deformation and the strong pairing interaction between the odd neutron and proton[1].

Test experiment was performed to study the production of the known proton emitter and the observation of its subsequent decays in the focal plane detector system installed at the JAERI recoil mass separator[2]. A 1.0 pnA beam of 260 MeV ^{58}Ni ion was used to bombard a 600 μg/cm^2 thick isotopically enriched ^{58}Ni target over a period of 56 h in order to produce ^{112}Cs and ^{109}Xe nuclei via the p3n and the α3n evaporation channels, respectively. The recoil mass separator was adjusted for optimum transmission of A=112 in charge state 29$^+$ and A=109 in charge state 28$^+$ in two separate runs. The separated recoils passed through a thin foil (20 μg/cm^2 Au evaporated on a 4.7 μg/cm^2 thick formvar foil) of the large microchannel plate detector (MCP) before being implanted into the double sided position sensitive strip detector (PSSD) surrounded by four other single sided strip detectors[3]. Since energies and positions of the separated recoils could not be recorded with one amplification (up to 6 MeV for protons and alpha particles in this experiment), a 15 μm thick Al foil and a 2 μm thick Al-coated Mylar foil were inserted in front of the MCP in order to degrade recoil energies from some hundred to a few MeV. The present electronic system was ready for the analysis of successive events at least more than 80 μs interval.

The correlated events between the implantation of separated recoil and its subsequent decay obtained within a time window of 30 s are shown in Fig. 1. The α decay of ^{110}I, ^{111}Xe and ^{110}Xe nuclei were tentatively assigned in this experiment, although most of the separated recoils of interest were stopped in the degrader foils. Clearly, additional amplifiers to measure recoil energies are needed to obtain more unambiguous data and is now in progress.

References

1) R. D. Page, P. J. Woods, R. A. Cunningham, T. Davinson, N. J. Davis, A. N. James, K. Livingston, P. J. Sellin and A. C. Shotter, Phys. Rev. **C49** (1994) 3312.
2) H. Ikezoe, Y. Nagame, T. Ikuta, S. Hamada, I. Nishinaka, and T. Ohtsuki, to be published in Nucl. Instr. Meth..
3) H. Ikezoe, T. Ikuta, S. Hamada, Y. Nagame, I. Nishinaka, K. Tsukada, Y. Oura and T. Ohtsuki, submitted to Phys. Rev. C.

[1]Laboratory of Nuclear Science, Tohoku University

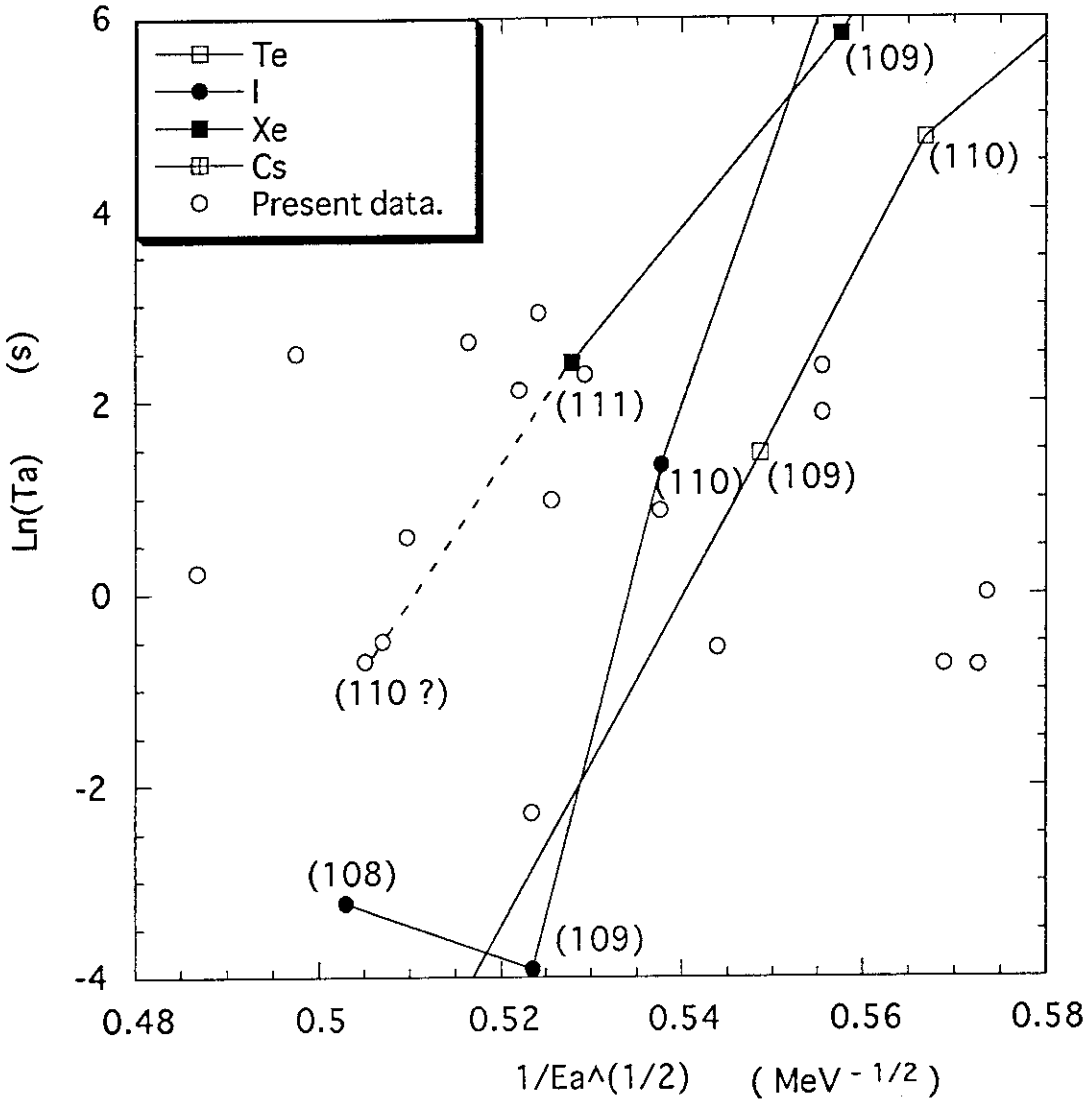

Fig. 1. Systematics of Ln(Ta) vs. 1/Ea^(1/2) for the trans-tin isotopes, where Ta is the partial life time of α decay and Ea is the α decay energy. The Ta value for the present data is taking from the time difference between the preceding implantation of the separated recoil and the energy deposition of the subsequent decay event within a time window of 30 s. No decay chain was observed in this experiment.

3.3 STUDY OF PREEQUILIBRIUM PARTICLE EMISSION IN PROTON-INDUCED REACTIONS

Y. WATANABE[1], S. YOSHIOKA[1], M. HARADA[1], M. HIGASHI[1], K. SATO[1], N. KOORI[2], S. CHIBA, T. FUKAHORI, S. MEIGO, and O. IWAMOTO

Preequilibrium particle emission is one of characteristic reaction mechanisms in nuclear reactions with energies of more than 10 MeV per nucleon. Kyushu university group has so far been intensively studying preequilibrium nucleon emission in nucleon-induced reactions at incident energies of 12 to 26 MeV[1,2,3]. In the collaboration done previously with JAERI group[3], we have measured double-differential proton emission cross sections for proton-induced reactions on ^{98}Mo and ^{106}Pd at energies around 26 MeV and analyzed the data together with (p,n) and (n,n') data in terms of the Feshbach-Kerman-Koonin (FKK) theory[4]. The dependence of the strength of the effective N-N interaction, V_0, on the incident energy and the nature of projectiles and ejectiles was investigated in those analyses. In consequence, we found that the extracted V_0 values are different between (p,p') and (n,n') at the same projectile energies. The similar result has recently been obtained in a consistent FKK analysis of (n,n'), (p,p'), (n,p) and (p,n) by Demetriou et al.[5]. For further consideration about this issue, a set of data for the same nuclei and the same energy is desirable. However, such an ideal set does not exist at present. In this work, therefore, we aim at measuring (p,p') data for the same target nuclei and the same energy as (n,n') data at 25.7 MeV[6] in order to see whether or not the V_0 values derived in a consistent analysis are different between (n,n') and (p,p'). Also, measurements of energy spectra of emitted composite particles (d, t, ^{3}He, and alpha) are planned to investigate the mechanism of preequilibrium cluster emission in detail.

For these measurements, we have developed a new ΔE-E counter telescope with an active collimator made of a thin plastic scintillator. ΔE and E detectors consist of three silicon surface barrier detectors whose thickness are 20, 200, and 5000 μm, respectively. The role of the active collimator is to reduce the tail component of the elastic peak generated by the edge-penetration. Such the background component in the continuum region leads to a serious problem at small angles. Since we used a passive collimator made of stainless steel in the previous measurement[3], we were not able to measure the (p,p') spectra at forward angles less than 40° due to the edge-penetration effect. The usefulness of the active collimator installed in the new counter telescope has been demonstrated in a test measurement of 16 MeV(p,p') for ^{197}Au carried out at Kyushu University Tandem accelerator Laboratory[7,8]. The result is shown in Fig.1. Moreover, Kyushu university group has measured double-differential cross sections of 14.1 MeV (p,p') on ^{56}Fe, ^{60}Ni and ^{93}Nb using the same type of ΔE-E counter telescope with the active collimator[7,8]. Figure 2 shows the measured cross sections for ^{60}Ni as an example.

As for a theoretical progress, the FKK-GNASH code[3,9] based on the FKK model plus the Hauser-Feshbach (HF) model was extended by one of the authors (YW)[10] so that the isospin can be introduced as a conserved quantum number in the multistep compound (MSC) and HF formula. As a result, the calculation with the extended FKK-GNASH code reproduced quite well the experimental (p,p') data at energies below 26 MeV over the whole outgoing energy region. Hence, the remarkable underprediction seen at lower outgoing energies in the previous work [3] was solved and the importance of isospin effect in MSC and compound nucleus (CN) processes in the (p,p') reaction was recognized.

In fiscal year 1996, we will start to measure double-differential emission cross sections of (p,x) reactions on ^{56}Fe, ^{90}Zr and ^{93}Nb at an incident energy of 25.7 MeV using the newly-developed ΔE-E counter telescope with the active collimator at JAERI Tandem accelerator facility. Both

[1] Department of Energy Conversion Engineering, Kyushu University
[2] Faculty of Integrated Arts and Sciences, The University of Tokushima

(p,p') data at 14.1 and 25.7 MeV will be analyzed simultaneously using the extended FKK-GNASH code and compared with the result of (n,n') analysis.

References

[1] Y. Watanabe et al., Phys. Rev. C **36** (1987) 1325.
[2] Y. Watanabe et al., Z. Phys. A **336** (1990) 63.
[3] Y. Watanabe et al., Phys Rev. C **51** (1995) 1891.
[4] H. Feshbach, A. Kerman, and S. Koonin, Ann. Phys. (N.Y.) **125** (1980) 429.
[5] P. Demetriou et al., to be published in J. Phys. G (1996).
[6] A. Marcinkowski et al., Nucl. Sci. Eng. **83** (1983) 13.
[7] M. Hayashi et al., Proc. of the 1994 Symp. on Nuclear Data, Nov. 17-18, 1994, JAERI, Tokai, JAERI-Conf 95-008 (1995), pp. 225.
[8] Y. Nakao et al., Kyushu University Tandem Accelerator Laboratory Report (1993-1994), KUTL report-5 (1995), pp. 115.
[9] M.B. Chadwick and P.G. Young, Phys. Rev. C **47** (1993) 2255.
[10] Y. Watanabe, Proc. of Int. Symp. on Pre-Equilibrium Reactions, Smolenice, October 1995, acta physica slovaca **45** (1995) 749.

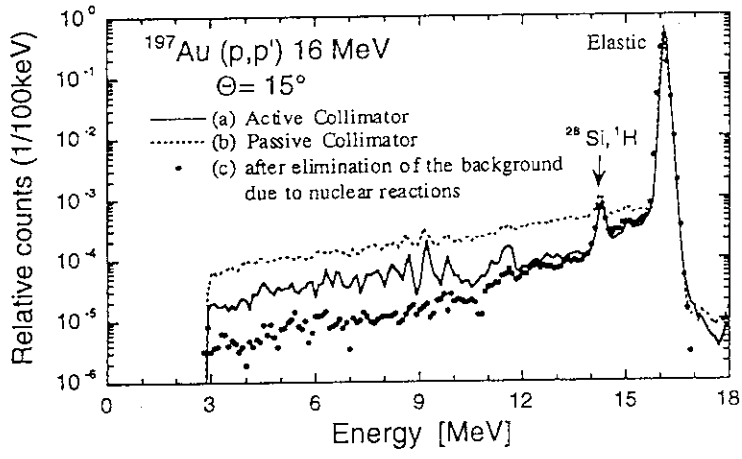

Fig.1 Experimental proton emission spectra of 16 MeV(p,p') for ^{197}Au. (a) with an active collimator (NE102A), (b) with a passive collimator(stainless steel) and (c) after reduction of the background due to nuclear reactions in the E-detector.

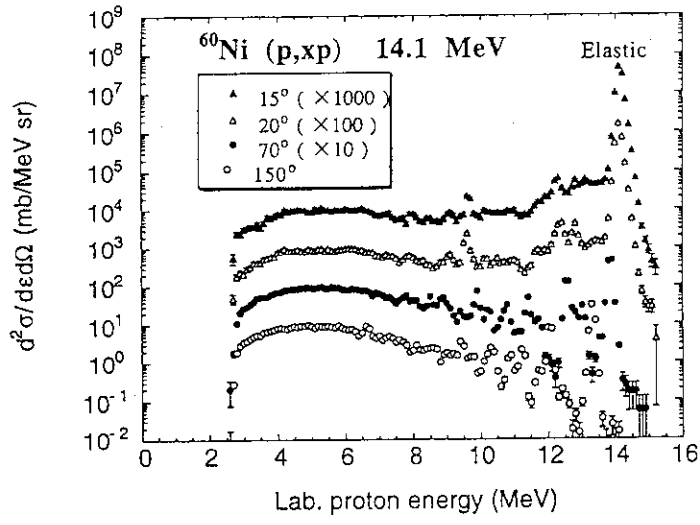

Fig.2 Experimental proton emission spectra of ^{60}Ni(p,p') at 14.1 MeV. The cross sections are given in the lab. system.

3.4 MEASUREMENTS OF ACTIVATION CROSS SECTIONS FOR THE NEUTRON DOSIMETRY AT AN ENERGY RANGE FROM 17.5 TO 30 MEV BY USING ^{7}Li(p,n) QUASI-MONOENERGETIC NEUTRON SOURCE

Y. UNO, S. MEIGO, S. CHIBA, T. FUKAHORI, Y. KASUGAI,
O. IWAMOTO, P. SIEGLER AND Y. IKEDA

Since 1993, an experimental program for systematic measurements of activation cross sections in a neutron energy range from 17.5 to 30 MeV has been underway in order to meet the data requirement from the high energy neutron dosimetry application.

The protons of 20, 22.5, 25, 27.5, 30 and 32 MeV were impinged on the ^{7}Li target and the neutrons were produced by the ^{7}Li(p,n) reaction. The neutron energy spectrum for each proton energy was measured by the time of flight (TOF) technique incorporating an NE213 scintillation counter. Fig. 1 shows the measured neutron spectrum for the incident proton energy of 20, 25 and 32 MeV. One observes a quasi-monoenergetic peak corresponding to the combined reaction of ^{7}Li(p,n)^{7}Be[0.0 MeV] and ^{7}L(p,n)^{7*}Be[0.429 MeV]. The absolute flux of the peak neutrons was determined by a proton recoil telescope (PRT) counter. Also, the angular neutron flux distribution for each irradiation was measured by moving the NE213 around the target.

The samples of Au, Al, Co, Tm, Y, Nb, Cu, ^{58}Ni and ^{48}Ti were irradiated for the cross section measurement. After each irradiation, γ-rays from the irradiated samples were measured with Hp-Ge detectors. From the net counts of full-energy peaks of interest, the reaction rate was derived after necessary corrections. Cross sections were derived by both the neutron flux and reaction rate. In general, there is a considerably large amount of neutrons in the energy region below the peak. Since the obtained reaction rate is given as the integral product of neutron flux spectrum and cross sections over the whole sensitive energy region, the contribution of lower energy neutrons to the total reaction rate should be subtracted. The correction factor F is calculated by using the measured neutron spectrum $\phi(E)$ and estimated cross section $\sigma_{ref}(E)$ as follows:

$$F = \frac{\int_{peak} \phi(E) \cdot \sigma_{ref}(E)\ dE}{\int_{Total} \phi(E) \cdot \sigma_{ref}(E)\ dE},$$

and the cross section σ is calculated by the following equation:

$$\sigma = \frac{R \cdot F}{\phi_{peak}},$$

where R is the obtained reaction rate and ϕ_{peak} is the absolute flux of the peak neutrons. When there is no appropriate evaluated cross section data, the cross sections were calculated with SINCROS-II[1] or ALICE-F[2] code. The main sources of the experimental error were in the γ-ray counting statistics and in the absolute neutron flux determination. The total errors are in a range of 6-7 %.

The experiments of 20, 25, 27.5 and 32 MeV proton energy were made in previous

Table 1. List of measured reactions

Sample	Reaction	Half-life	Q-Value
^{197}Au	^{197}Au(n,2n)^{196m}Au	9.7h	-8.67
	^{197}Au(n,2n)$^{196m+g}$Au	6.183d	-8.07
	^{197}Au(n,3n)^{195}Au	186.09d	-14.72
	^{197}Au(n,4n)^{194}Au	1.646d	-23.10
^{27}Al	^{27}Al(n,α)$^{24m+g}$Na	14.659h	-3.13
^{59}Co	^{59}Co(n,2n)$^{58m+g}$Co	70.916d	-10.45
	^{59}Co(n,3n)^{57}Co	271.77d	-19.03
	^{59}Co(n,p)^{59}Fe	44.496d	-0.78
	^{59}Co(n,α)^{56}Mn	2.5785h	0.33
	^{59}Co(n,2nα)^{54}Mn	312.20d	-17.17
^{169}Tm	^{169}Tm(n,2n)^{168}Tm	93.1d	-8.03
	^{169}Tm(n,3n)^{167}Tm	9.24d	-14.87
^{89}Y	^{89}Y(n,2n)^{88}Y	106.61d	-11.48
	^{89}Y(n,3n)^{87m}Y	12.9h	-21.21
	^{89}Y(n,3n)$^{87m+g}$Y	3.346d	-20.83
^{93}Nb	^{93}Nb(n,2n)^{92m}Nb	10.15d	-8.97
^{58}Ni	^{58}Ni(n,2n)^{57}Ni	1.503d	-12.22
	^{58}Ni(n,p)$^{58m+g}$Co	70.916d	0.40
	^{58}Ni(n,np)^{57}Co	271.77d	-8.17
	^{58}Ni(n,2np)^{56}Co	77.7d	-19.55
^{48}Ti	^{48}Ti(n,p)^{48}Sc	1.821d	-3.21
	^{48}Ti(n,np)^{47}Sc	3.341d	-11.44
	^{48}Ti(n,2np)$^{46m+g}$Sc	83.83d	-22.09
natCu	natCu(n,xn)^{61}Cu	3.408h	-19.74

years. The experiments of the 22.5 and 30 MeV were made in 1995. The first series of measurement, thus, has been completed to give full set of data from 17.5 to 30 MeV. The reactions measured in this study are tabulated in Table 1. In Fig. 2, the measured cross section data of ^{169}Tm(n,2n)^{168}Tm and ^{169}Tm(n,3n)^{168}Tm reactions are shown together with data in literature along with calculated cross section. Our results show the good agreement with the other experimental data below 28 MeV, and we gave the new data at 30 MeV. The calculated cross sections were confirmed by these new experimental data.

References

1)Yamamuro, N. : "A Nuclear Cross Section Calculation System with Simplified Input-Format Version-II (SINCROS-II)," JAERI-M 90-006 (1990).

2)Fukahori, T. : "ALICE-F Calculation of Nuclear Data up to 1 GeV," Proc. Specialists' Meeting on High Energy Nuclear Data, Tokai, Ibaraki, Oct. 3-4, 1991, JAERI-M 92-039, pp114 (1992).

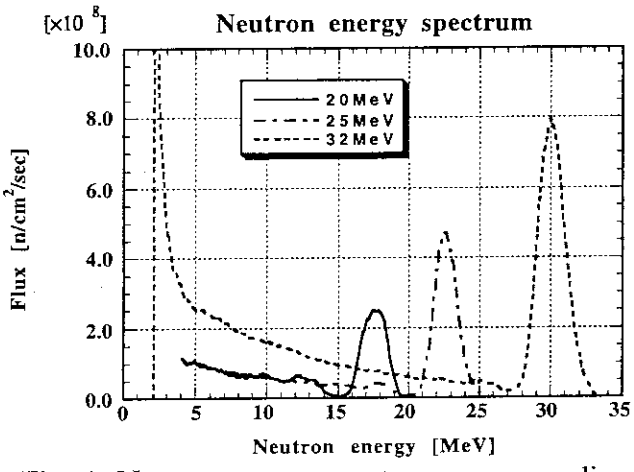

Fig. 1. Neutron energy spectrum corresponding to incident proton energies of 20, 25 and 32 MeV.

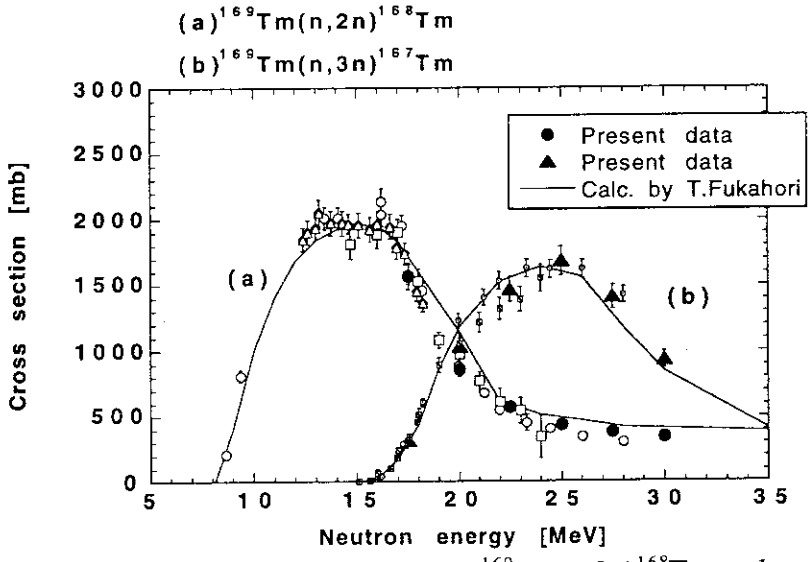

Fig. 2. Measured cross section of ^{169}Tm(n,2n)^{168}Tm and ^{169}Tm(n,3n)^{167}Tm reactions.

3.5 EXCITATION FUNCTIONS OF $^{235,238}U(^{6,7}Li, xn)Am$ REACTIONS

Y. HATSUKAWA, N. SHINOHARA, K. HATA, K. TSUKADA,
Y. OURA, S. ICHIKAWA, I. NISHINAKA, Y. NAGAME and M. OSHIMA.

Bombardments of actinide targets with the lithium beam were expected to find some unknown isotopes of neutron deficient actinide. Only limited study of the excitation functions of the reaction of actinide targets with lithium beam is available. Excitation functions of $^{238}U(^{7}Li, xn)^{245-x}Am$, $^{238}U(^{6}Li, xn)^{244-x}Am$, $^{235}U(^{7}Li, xn)^{242-x}Am$ and $^{235}U(^{6}Li, xn)^{241-x}Am$ reactions were studied. Obtained experimental results were compared with the calculation results of statistical model.

Irradiations, chemical separations, and measurements were described in previous report[1]. The measured excitation functions of $^{238}U(^{7}Li, xn)^{245-x}Am$, $^{238}U(^{6}Li, xn)^{244-x}Am$, $^{235}U(^{7}Li, xn)^{242-x}Am$ and $^{235}U(^{6}Li, xn)^{241-x}Am$ reactions sre shown in Figure. ^{242}Am which obtained by the reaction of $^{238}U(^{7}Li, 3n)^{242}Am$ has two isomer states. Only low spin state (1-), ^{242g}Am, is detectable in this experiment. To obtaine the whole cross sections, $^{242g}Am + ^{242m}Am$, formation cross sections of ^{242m}Am were estimated by the following equations[2].

$$\frac{\sigma_H}{\sigma_L} = \frac{\left(2\langle l_c\rangle + 1\right)^2}{\left(2\langle I_R\rangle + 1\right)^2} - 1,$$

$$\langle l_c\rangle = \frac{1}{\sigma_c}\left[\sum_{l=0}^{l_{max}} (l+1)\sigma_l\right] + \Delta_l - 1,$$

$$\langle I_R\rangle = \frac{I_H + I_L}{2},$$

$\Delta l = 2.5$ for (p,n),

$\Delta l = 2.0$ for (d, xn), and (α, n),

$\Delta l = 1.0$ for others.

Corrected cross sections are also shown in Figure. Experimental results were compared with the statistical model calculation by using ALICE Livermore 91[3]. The calculations with the parameters of number of exciton, TD=2, fission barrier parameter, Cf=1.15, and level density parameter, $a_f/a_n = 1$, obtained good agreement with the experimental data. According to the ALICE calculation by using the parameters which is obtained in this study, the production cross section of unknow nuclide, ^{236}Am, via $^{235}U(^{6}Li, xn)$ reaction is expected to be about 100 μb.

References;

1) Hatsukawa, et al. Jaeri Tandem Annual Rep. 1994(JAERI-Review 95-017), 42 (95)
2)Hata et al. Abstracts of papers, The 34th symposium on radiochemistry 1A05 (1990)
3)M. Blann and H.K. Vonach Phys. Rev. C28 1475 (1883)

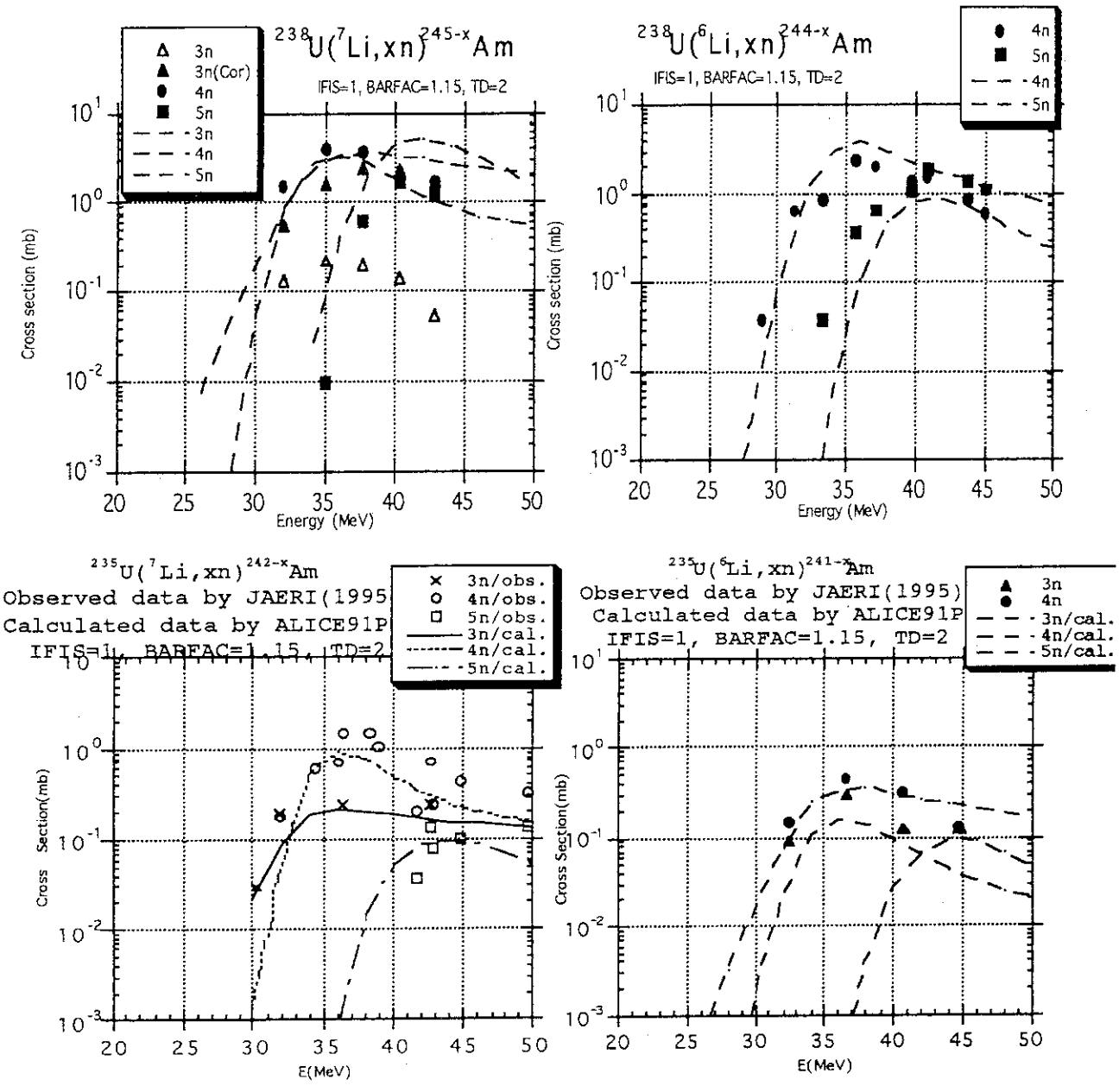

Figure.

Excitation functions for Am isotopes produced in bombardment of ^{238}U with ^{7}Li(upper left), ^{238}U with ^{6}Li(upper right), ^{235}U with ^{7}Li(bottom left), and ^{235}U with ^{6}Li(bottom right). Lines show the calculated results of the ALICE code with the parameters of TD = 2, Cf = 1.15 and $a_f/a_n = 1$.

3.6 SEARCH FOR ^{236}Am

Y.OURA, K.TSUKADA, Y.HATSUKAWA, T.OHYAMA[1], N.SHINOHARA, K.HATA, I.NISHINAKA, Y.NAGAME, and S.ICHIKAWA.

Many neutron deficient actinide nuclides have not been discovered. These undiscovered nuclides will decay mainly by the electron capture, therefore the identification of them, especially their mass number, is difficult. As the first attempt of our continuing study of searching new actinide nuclides, we try to synthesize and identify a new americium isotope, ^{236}Am which is predicted to decay to ^{236}Pu by the electron capture with a half life of 31.2 min[1].

We planned to detect α particles emitted from ^{236}Pu, which was a daughter of ^{236}Am, rather than to measure characteristic X-ray accompanied by the electron capture of ^{236}Am in order to identify the mass number of the new americium isotope clearly. A target of ^{235}U electrodeposited on Al foil was irradiated with 46 MeV of ^{6}Li for 60 min at the JAERI tandem accelerator. After irradiation, Am was separated by the solvent extraction method. The time required for the separation was about 10 min. After 1 week, Pu including daughter of ^{236}Am in the Am fraction was purified by the anion exchange method and electrodeposited on Ta foil to measure α rays with SSD for about 2 weeks. For the purpose of determining a half life of ^{236}Am, eight runs were carried out and the time between the end of irradiation and the chemical separation of Am (hereafter call the separation time) was varied from 15 min to 34 min.

The alpha spectrum of Pu at the run in which the separation time was 15.3 min is shown in Fig.1. It was found that the net counts contributed from ^{236}Pu of the daughter of ^{236}Am were 26 after appropriate corrections. Thus the existence of ^{236}Am was confirmed. And owing to the variation of the activity of ^{236}Pu with the separation time, it was obtained preliminary that the half life of ^{236}Am was 3 to 7 min. This value is about 10 times smaller than the predicted one. The further study will be performed in order to obtain a more accurate value of the half life.

References

1)T.Tachibana, M.Yamada and Y. Yoshida, Prog. Theor. Phys. **84** (1990) 641.

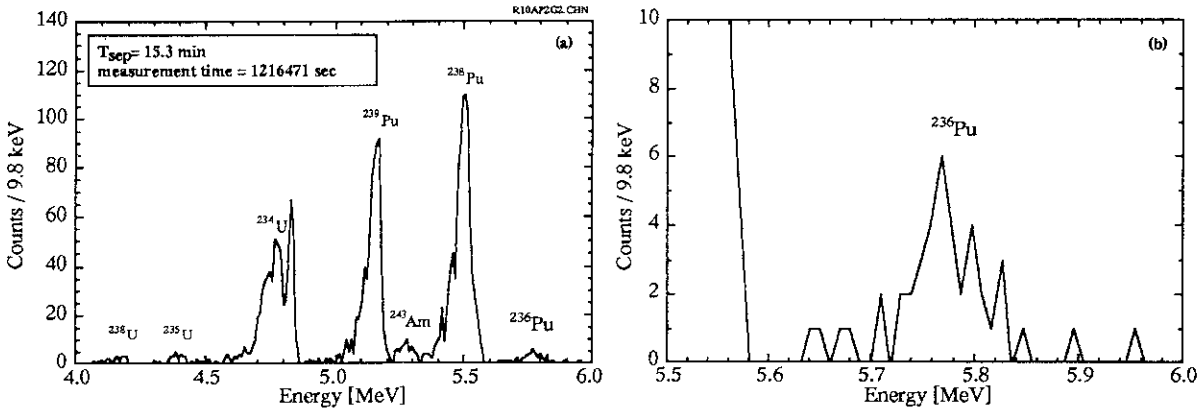

Fig.1. (a) Alpha spectrum of Pu purified from Am fraction of run in which Am was separated at 15.3 min after the end of irradiation. (b) Expanded spectrum of (a).

[1]Faculty of Science, Tokyo Metropolitan University

3.7 SEARCH FOR THE EVIDENCE OF TRANSITION OF THE FISSION MECHANISM IN THE PROTON-INDUCED FISSION OF ^{238}U AROUND E_X = 14 MeV

K.NAKANISHI [1], K.TAKAMIYA[1], T.INOUE[1], A.YOKOYAMA[1], T.SAITO[1], H.BABA[1], I.NISHINAKA, K.TSUKADA, Y.HATSUKAWA, N.SHINOHARA and Y.NAGAME

Spontaneous and thermal-neutron-induced fissions of actinide nuclei reveal different features from those at high excitation energies. In the proton-induced fission of ^{238}U the systematics varies at the region near E_X = 14 MeV[1]. It suggests that the transition of the fission mechanism is expected to occur around this energy. We have investigated that transition by radiochemical method and concluded that there are many evidences of transition of fission mechanism around E_X = 14 MeV[2]. In order to investigate this transition from different point of view we measured ^{238}U(p,f) around E_X = 14 MeV by a double-energy measurement (2E) in the present work.

Proton beams of energies 8.1 and 10.6 MeV (the excitation energies were respectively 13.4 MeV and 15.9 MeV) were used for the bombardment. The present experiment was carried out at R1 course of the JAERI tandem Van de Graaff accelerator. The target of ^{238}U was prepared by evaporation of UF_4 on a 20-μg cm^{-2} carbon foil and the thickness of the target was 110-μg cm^{-2}. To detect the fission fragments two silicon surface-barrier detectors(SSBD) were used. Proton beam currents were generally in the 150 to 350-nA range. About 3.7×10^4 and 1.8×10^5 fission events were analyzed when excitation energies were 13.4 MeV and 15.9 MeV, respectively.

The primary-fragment mass distributions and the fragment kinetic-energy distributions were obtained from the energy-mass correlation data. The number of pre-scission neutron was calculated by using the equation in Ref.[3] and the number of post-scission neutron was taken from available neutrons data [4,5].

The sum of the kinetic energies of complementary fragments gives the total kinetic energy (TKE) for a given mass. The resulting first moments of the fragment kinetic energy (MKE) and TKE distributions are indicated in Fig.1. Remarkable differences are not observed between two cases.

On the other hand, a difference is noticed in the mass distribution between the two cases. The total kinetic energy distribution of a given mass bin was decomposed into two Gaussian components by fixing the width of both components at 25 MeV as an appropriate value. The mass distribution was decomposed into two components, one is symmetric and the other is asymmetric, in proportion to relative intensities of the fitted Gaussians. The asymmetric component of mass distribution could be fitted to a single Gaussian at 15.9 MeV. On the contrary, the resulting asymmetric component could not be fitted to a single Gaussian but two

[1]Faculty of Science, Osaka University.

Gaussians were required to reproduce observed distribution at 13.4 MeV. This consequence is consistent with the results of radiochemical method.

In the present work, the difference was not observed in the energy distribution of the proton-induced fission of ^{238}U between the two cases above and below 14 MeV, though the difference could be found in the mass distribution. In future, refined experiments should be done to confirm whether there is any difference in the energy distribution.

References

[1] H. Baba *et al.*, Nucl. Phys. **A175**(1971) 177.

[2] H. Baba *et al.*, Proc. Specialists' Meet. on Frontier in Nucl. Fission Res. Basic Science and Technology, 1995, Kumatori, pp. 72-88.

[3] H. Umezawa *et al.*, Nucl. Phys. **A160**(1971) 65.

[4] J. Terrell, Phys. Rev. **127**(1932) 880.

[5] M. Strecker *et al.*, Phys. Rev. **C41**(1971) 2172.

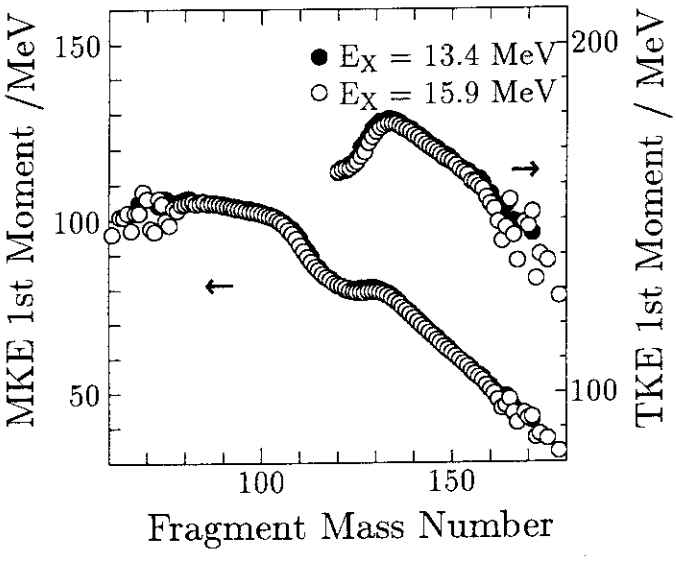

Figure 1: 1st moment of the fragment kinetic and total kinetic energies as functions of the primary fragment mass

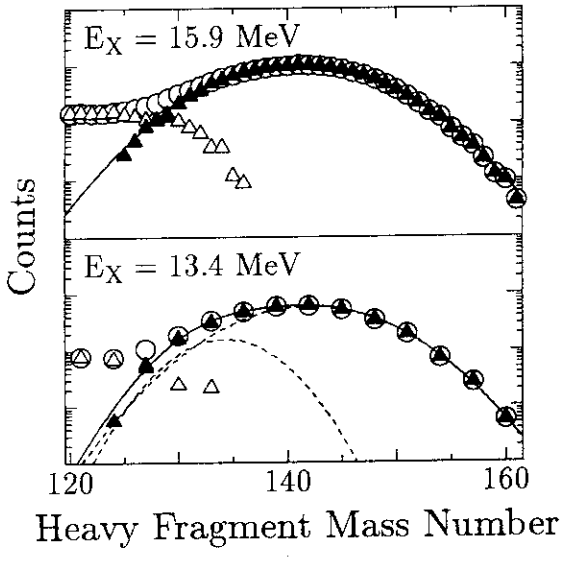

Figure 2: Mass yield curves. Open circles indicate the mass yield, while the closed and open triangles represent decomposed asymmetric and symmetric components, respectively.

3.8 NEUTRON EMISSION IN 13.2 MeV PROTON INDUCED FISSION OF ^{232}Th

I. NISHINAKA, Y. NAGAME, K. TSUKADA, Y. OURA, S. ICHIKAWA, H. IKEZOE, Y.L. ZHAO [1], K. SUEKI [1], H. NAKAHARA [1], T. OHTSUKI [2], M. TANIKAWA [3], Y. HAMAJIMA [4], H. KUDO [5], K. TAKAMIYA [6] and Y.H. CHUNG [7]

In order to investigate the two-mode fission in the region of light actinides, mass distribution, total kinetic energy of fission fragments, and average number of neutrons emitted from fission fragments have been measured for the 13.2 MeV proton-induced fission of ^{232}Th. The experiment was carried out at the JAERI tandem accelerator. Details of the experiment are given in Ref.[1]. The number of neutrons emitted from fission fragments was determined by measuring both fragment velocities and energies for one of the fragments. Primary fragment mass number (m^*) and the one for the secondary fragment (m) are derived from the relationships $m^* = A_f v_{cm2}/(v_{cm1} + v_{cm2})$ and $m = 2E_{cm1}/v_{cm1}^2$, respectively, where E_{cm}, v_{cmi} and A_f denote kinetic energies, velocities of fragments and mass number of the fissioning nucleus, and the subscript $i(= 1$ and $2)$ indicates the complementary fragments. In the present calculation no correction was made for pre-fission neutron evaporation; A_f was set to the mass number of the compound nucleus. The number of emitted neutrons ν is given by $\nu = m^* - m$.

Figure 1 shows (a) the average number of neutrons emitted (open symbols) $\nu(m^*)$, (b) the average total kinetic energies of fission fragments TKE(m^*), and (c) primary mass yield Y(m^*) as a function of primary fragment mass number. Also in Fig. 1(a) the total number of neutrons ($\nu_T(m^*)$) emitted from both fragments is plotted as closed symbols. The trend of $\nu(m^*)$ is similar to that obtained from proton induced fission of ^{226}Ra [2, 3] and ^{233,238}U [4]. $\nu(m^*)$ does not drop at or near symmetry, which corresponds to the existence of the symmetric mode. The pronounced dips of $\nu(m^*)$ are observed at the mass numbers ~106 and ~132. The dips of ($\nu_T(m^*)$) at the mass numbers ~90 and ~132 corresponding to nuclei with $Z \simeq 50$ and $N \simeq 82$ are located in the mass region where the average total kinetic energies of fragments show the maxima.

We are going to analyze the correlations among the distributions, Y(m^*), TKE(m^*) and $\nu(m^*)$.

References

1) Y. Nagame et al., to be submitted.
2) E. Konecny and H.W. Schmitt, Phys. Rev. **172**(1968)1213.
3) A. Gayetr and Z. Fraenkel, Phys. Rev. C**16**(1977)1066.
4) S.C. Burnett et al., Phys. Rev. C**3**(1971)2034.

[1]Faculty of Science, Tokyo Metropolitan University
[2]Laboratory of Nuclear Science, Tohoku University
[3]School of Science, The University of Tokyo
[4]Faculty of Science, Kanazawa University
[5]Faculty of Science, Niigata University
[6]Faculty of Science, Osaka University
[7]Faculty of Science, Hallym University

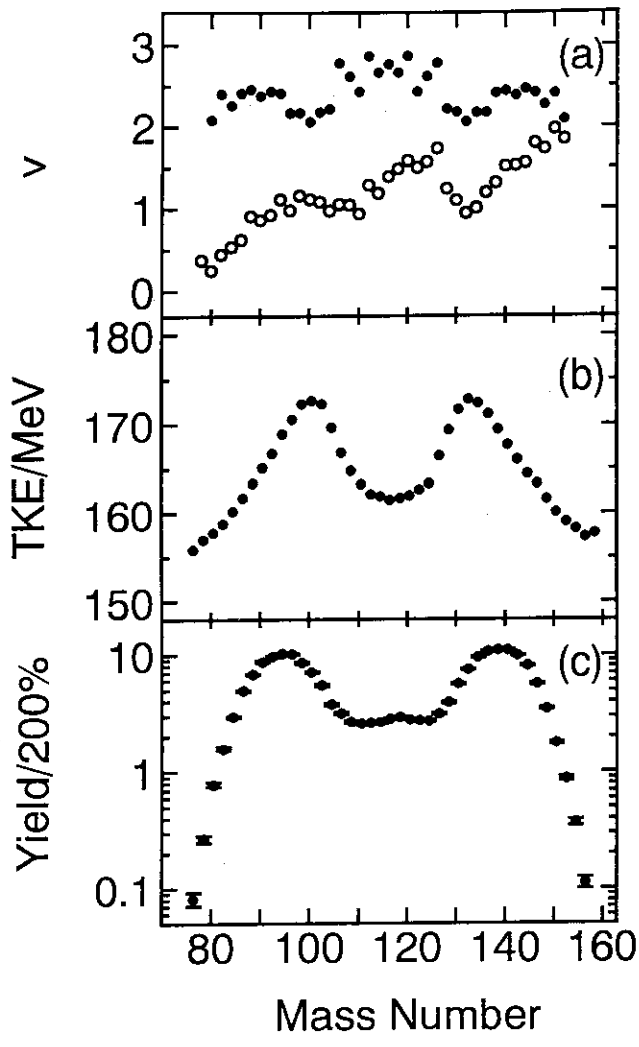

Figure 1: (a) Average number of neutrons emitted per fragments (open symbols) and average total number of neutrons emitted from both fragments (closed symbols), (b) average total kinetic energies, and (c) mass distribution of primary fragments as functions of primary fragment mass.

3.9 TWO DEFORMATION PATHS IN PROTON-INDUCED FISSION OF ^{232}Th

Y. NAGAME, I. NISHINAKA, K. TSUKADA, Y. OURA, S. ICHIKAWA, H. IKEZOE, Y.L. ZHAO[1], K. SUEKI[1], H. NAKAHARA[1], T. OHTSUKI[2], M. TANIKAWA[3], H. KUDO[4], Y. HAMAJIMA[5] K. TAKAMIYA[6] and Y.H. CHUNG[7]

Systematic studies on mass division phenomena, excitation functions, angular distributions and total kinetic energy distributions of fragments, in low energy proton-induced fission of light actinides have been performed by using the JAERI tandem accelerator. The following statements have been experimentally derived; (i) there are two kinds of fission threshold energies, i.e., symmetric and asymmetric mass divisions require different threshold energies and the energy being about a few MeV higher for symmetric mass division than that for asymmetric one [1], and (ii) at least two kinds of scission configurations for certain mass division are verified: compact and elongated scission configurations [2]. In our recent experiments, a correlation between the two fission threshold energies and the two scission configurations has been revealed.

Velocities of complementary fission fragments have been accurately measured by a double velocity time-of-flight method in the proton-induced fission of ^{232}Th with incident energies from 12.0 to 14.7 MeV. A binary structure was observed in total kinetic energy (TKE) distributions in the fragment mass region of A=125-135 with the difference of the lower TKE and the higher TKE being about 15 MeV.

The intensity ratio of each TKE component obtained by two-Gaussian analyses are used to decompose the mass yield distributions, and the results are shown in Fig. 1 as a function of the heavy fragment mass number for the reactions of 14.7 and 12.0 MeV p + ^{232}Th. The yields at the peak top (A$\sim$140) of the mass distributions are normalized to unity and the triangles show the mass yields corresponding to the low-TKE component while the squares are those for the high-TKE. The overall mass yield curves are smoothly decomposed into two in the mass region A$\sim$130 where the asymmetric peak merges into the symmetric region. The square symbols constitute the cliff of the lower mass side of the asymmetric mass yield peak and the triangles are located at the extended region of a broad peak centered around A=A_f/2. A clear difference in the symmetric yields are observed between the two different incident energies, and the same amount of difference is also observed for the decomposed yields of the low-TKE components (the difference between open and closed triangles). On the other hand, no difference is observed in the relative yields of asymmetric mass division products and also for the open and closed squares in the mass region of A$\sim$130 for the two inicident energy systems. The result clearly indicates that the excitation energy dependence of the yields for the low- and high-TKE components is quite different, and the former is similar to that of the symmetric fission products while the latter to that of the asymmetric fission products.

This excitation energy dependence leads us to conclude that the elongated scission configuration with low-TKE is related to the fission process that requires a higher threshold energy and results in the symmetric mass division mode while the compact scission configuration with high-TKE is related with the process that experiences a lower threshold and ends up with the asymmetric mass division mode.

[1]Department of Chemistry, Tokyo Metropolitan University
[2]Laboratory of Nuclear Science, Tohoku University
[3]Department of Chemistry, University of Tokyou
[4]Department of Chemistry, Niigata University
[5]Department of Chemistry, Kanazawa University
[6]Department of Chemistry, Osaka University
[7]Department of Chemistry, Hallym University

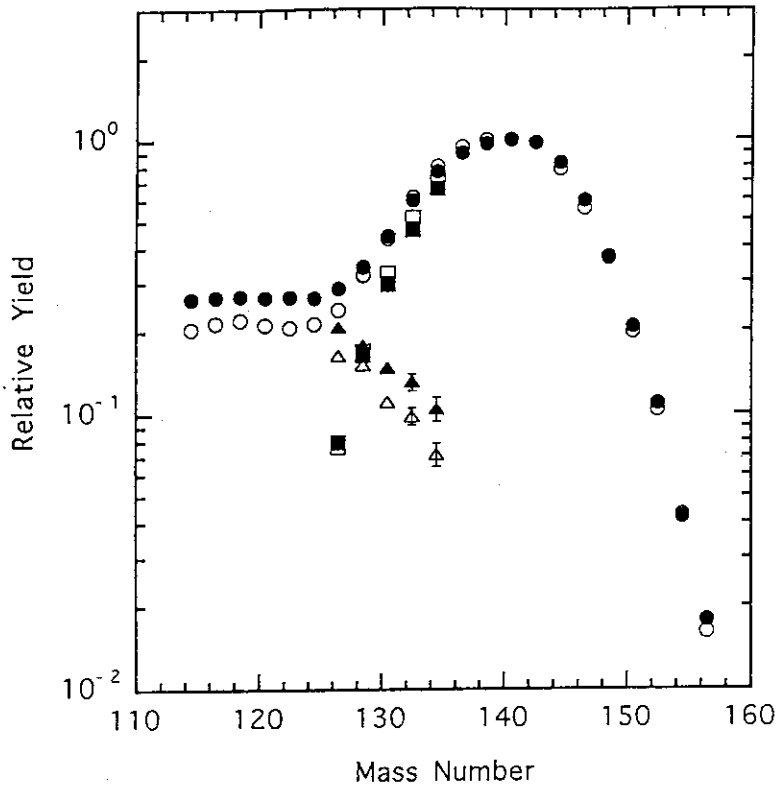

Fig. 1. Comparison of the decomposed mass yields at the 14.7 (closed symbols) and 12.0 MeV (open symbols) incident proton energies. The yields at the peak top (A~140) are normalized to unity. The triangle symbols show the mass yields corresponding to the low-TKE components and the squares are those to high-TKE components.

References

1) T. Ohtsuki, H. Nakahara and Y. Nagame, Phys. Rev. C **48**, 1667 (1993).
2) T. Ohtsuki, Y. Nagame, H. Ikezoe, K. Tsukada, K. Sueki and H. Nakahara, Phys. Rev. Lett **66**, 17 (1991).

3.10 ^{50}Ti (^{12}C, ^{12}C') ^{50}Ti* REACTION AT E=115MeV

Y. YAMANOUTI, Y. SUGIYAMA, Y. TOMITA and K. IDENO

Scattering of light heavy ions has played a major role in obtaining information on the applicability of microscopic double folding model potentials. In order to study the reaction mechanism of heavy ion scattering from intermediate nuclei differential cross sections for elastic and inelastic scattering of 115MeV ^{12}C ions from ^{50}Ti were measured. The experimental data were analyzed using the coupled-channel (CC) formalism with the microscopic optical potentials calculated by the double folding model. The CC calculations with the phenomenological optical potentials of the Woods-Saxon form were also performed to make a comparison with the result of the microscopic optical potentials. Information on the isospin character of nuclear transitions, of which quantitative description is ordinarily represented as M_n/M_p, the ratio of neutron and proton transition matrix elements, can be obtained from comparison of inelastic scattering data by projectiles as an isoscalar probe with electromagnetic transition rates.

Measurements of scattering cross sections were made using a 115MeV ^{12}C beam from the JAERI tandem accelerator. The target was a self supporting foil of 83.2% enriched ^{50}Ti with thickness of 235 μ g/cm^2. Scattered particles were detected using a magnetic spectrograph with a 40cm long hybrid focal plane detector. Angular distributions of differential cross sections were obtained for elastic and inelastic scattering over the angular range from 5° to 40° in lab system.

The double folding potentials were generated by the folding of an effective nucleon-nucleon interaction with the projectile and target density distributions using the computer code DFPOT[1]. Two different effective interactions, the M3Y form of Bertsch et al and the 100MeV Franey-Love form[2] were used in the folding model calculations. In the M3Y calculations it was assumed that the real and imaginary parts of the effective interaction have the same shape. While in the 100MeV Franey-Love calculations the complex effective interaction strengths were employed. The transition density for inelastic scattering was calculated in the Tassie model. The experimental cross sections were well reproduced with the double folding potentials as well as the phenomenological optical potential. These CC calculations were done with the computer code FRESCO[3]. The CC analysis of the (^{12}C,^{12}C') reaction yielded the M_n/M_p value consistent with those derived from other types of reactions such as proton and alpha particle scattering.

References

1) J. Cook, Comp. Phys. Commun. 25 (1982) 125
2) M. A. Franey and W. G. Love, Phys. Rev. 31 (1985) 488
3) I. J. Thompson, Comput. Phys. Rev. C13 (1976) 1502

3.11 ELASTIC TWO-NEUTRON TRANSFER REACTIONS IN $^{58}Ni+^{60}Ni$ AND $^{62}Ni+^{64}Ni$ AROUND THE COULOMB BARRIER

Y.SUGIYAMA,Y.TOMITA, Y.YAMANOUTI, S.HAMADA, T.IKUTA,K.IDENO and H.FUJITA[1]

It is known that angular distributions of elastic scattering show oscillatory patterns in collisions of almost identical nuclei. These characteristic patterns have been attributed to an interference between the truly elastic process and the one involving the transfer of particles. In fact, the choice of almost identical projectile and target make it possible, through the exchange of nucleons, to reach a final mass partition which again coincides with that of the entrance channel configuration.

Detailed analyses of elastic transfer reactions have been performed and reviewed by von Oertzen and Bohlen[1]. They have pointed out that, in the vicinity of the Coulomb barrier, elastic two-nucleon transfer reactions in superfluid nuclei of medium- and heavy-weights seem to be the best way to measure pair exchange as a test of a possible existence of the nuclear Josephson effect. However there have been no experimental data of elastic two-neucleon transfer reactions for superfluid systems, since such measurements are very difficult mainly due to the limited energy resolution. The heaviest system so far measured was $^{32}S+^{34}S$ [2].

We measured elastic two-neutron transfer reactions for the $^{58}Ni+^{60}Ni$ and $^{62}Ni+^{64}Ni$ systems by using the JAERI tandem accelerator and the heavy-ion magnetic spectrograph "ENMA"[3]. The spectrograph has a characteristic feature that the kinematic momentum shift k is well compensated, so that a high energy resolution is achieved over a wide range of k. Angular distributions for $^{58}Ni+^{60}N$ at E_{cm}=127MeV and for $^{62}Ni+^{64}Ni$ at E_{cm}=123 MeV are shown in Fig.1.Bell shaped structures are observed at the backward angles for both systems which are due to the two-neutron transfer process. The data were analyzed with the computer code Ptolemy. The cross section σ for the elastic two-neutron transfer reaction is expressed by using the amplitude of f_{el} for elastic scattering and of f_{tr} for two-neutrontransfer as

$$\sigma(\theta)=|f_{el}(\theta)+f_{tr}(\pi-\theta)|^2 . \qquad (1)$$

The elastic scattering amplitude was obtained by the coupled-channels calculation including the first 2^+ and 3^- states of target and projectile nuclei. The nuclear ion-ion potential we use was based on the semi-empirical expression given by Broglia and Winther[4] . We used the same geometry for the imaginary part and adjusted the strength W. The two-neutron transfer amplitude was calculated by using the macroscopic pair-transfer form factor F(r) which was given by

$$F(r)=(\beta_p R/3A)(\delta U/\delta r) \qquad (2)$$

where β_p was the pair-deformation parameter which measured the collective strength of the pair modes[5]. R,A and U are the nuclear radius, mass number and the optical potential, respectively. For the case of superfluid systems, a large pair-transfer cross section is predicted by the BCS approximation in which the pair-deformation

[1]Daiichi College of Pharmaceutical Sciences

parameter β_p is expressed as $\beta_p=2\Delta / G$, where Δ and G are the gap parameter and the pairing strength[6].

The calculated results are shown by solid lines in Fig.1. The data of the $^{58}Ni+^{60}Ni$ system are reproduced well with a pair-deformation parameter of $\beta_p=7$, while for the $^{62}Ni+^{64}Ni$ system the parameter increases to $\beta_p=9$. The result indicates the pair-transfer cross section increases as the number of valence neutrons. In the BCS approximation mentioned above,the pair-deformation parameter for the Ni+Ni system is estimated as $\beta_p\sim10$ with the approximated values of $\Delta=12/A^{1/2}$ (MeV) and G=19/A (MeV). Therefore the $^{62}Ni+^{64}Ni$ system is seen to have the large pair-transfer cross section comparable to the one predicted for the the g.s. BCS wave function nuclei. More precise theoretical calculations are under way in order to check a possible existence of the nuclear Josephson effect.

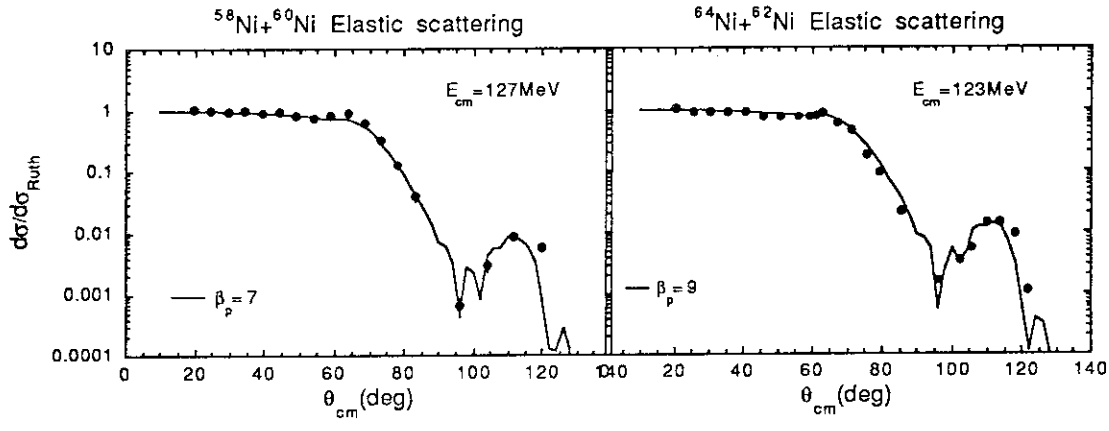

Fig.1 Elastic scattering angular distributions for the $^{58}Ni+^{60}Ni$ (left) and $^{64}Ni+^{62}Ni$ (right) systems. The dolid lines are the results of theoretical calculations.

References
1)W. von Oertzen and H.G.Bohlen, Phys. Rep. 19C (1975).
2)M.C.Mermaz, B.Bilwes, R.Belwis and J.L.Ferrero, Phy. Rev. C27(1983)2408.
3)Y.Sugiyama et al, Nucl. Instr. and Meth. A281(1989)512.
4)R.A.Broglia abd A.Winther, Heavy Ion Reaction, Lecture Notes(Benjamin, New York 1981) Vol 1.
5)C.H.Dasso and G.Pollarolo, Phys. Lett.155B(1985)223.
6)D.R.Bes, P.Lotti, E.Maglione and A.Vitturi, Phys. Lett. 169B(1986)5.

3.12 STUDY OF ^{60}Zn IN THE rp-PROCESS

S. KUBONO[1], P. STRASSER[1], M. H. TANAKA[1], H. FUCHI[1], T. MIYACHI[1], T. NOMURA[1], S. KATO[2], K. SUGIYAMA, H. IKEZOE, H. TOMITA, K. IDENO, S. HAMADA, and Y. YAMANOUCHI

Proton deficient unstable nuclei play a crucial role in the explosive hydrogen burning process (rp-process[1]) in stellar sites. Among them, ^{60}Zn is involved in a possible bottle neck reaction of ^{59}Cu(p,γ)^{60}Zn that determines the passway of the rp-process at high temperature. However, the structure of ^{60}Zn is not known well. Nuclear structures of the proton deficient nuclei can be studied using multi-proton stripping reactions with heavy ion beams. In the last years, we have tested the (^{12}C,^{10}Be) reaction, and found it to be a useful spectroscopic tool for these nuclei.

The measurement of the (^{12}C,^{10}Be) reaction was first tested at the JAERI-Tandem accelerator using the heavy-ion spectrograph ENMA. As reported in the last annual report, the time-of-flight measurement is very powerful for particle identification in a condition of relatively high background. The test experiment was performed for the ^{26}Mg(^{12}C,^{10}Be)^{28}Si reaction at 115 MeV. The levels of ^{28}Si were observed with negligibly small background.

The experimental investigation was made on the nuclear structure of ^{60}Zn at the cyclotron facility of the Institute for Nuclear Study, University of Tokyo. The ^{58}Ni(^{12}C,^{10}Be)^{60}Zn reaction was used to determine the excitation energies and the spin-parity of the residual states. The angular distributions usually have the characteristic feature that the forward angle shapes have a clear transferred angular momentum (L) dependence at this energy region, which enables us to assign spin-parity for the states observed.

The experiment was performed using a ^{12}C beam of 78 MeV from the sector focusing cyclotron, which was directed onto a-thin ^{58}Ni target foil of about 400 μg/cm^2. The momentum spectra of the ^{10}Be^{4+} particles were measured with a high resolution QDD-type magnetic spectrograph and a hybrid-type gas proportional counter placed on the focal plane. The detector which has a hybrid structure of a drift-space with a large vertical acceptance is composed of two position counters and two ΔE counters for particle identification. In addition a plastic scintillator placed just behind the proportional counter is used for energy and time-of-flight measurements. Several levels were observed above the proton threshold ^{59}Cu+p (5.121 MeV) including the states observed previously[2,3] in ^{60}Zn. The angular distributions were also measured at forward angles, and the energy calibration was made. The data are presently being analyzed using DWBA calculations in order to determine the most probable L for each level. Further measurements at other angles are needed, and also a run with a thin target of ^{58}Ni to check possible doublets.

References

1) R. K. Wallace and S. E. Woosley, Astrophys. J. Suppl. **45** (1981) 389.
2) A. Boucenna *et al.*, Phys. Rev. C **42** (1990) 1297.
3) D. J. Weber *et al.*, Nucl. Phys. **A313** (1979) 385.

[1] Institute for Nuclear Study, University of Tokyo, 3-2-1 Midori-cho, Tanashi, Tokyo, 188 Japan.
[2] Physics Department, Yamagata University, Yamagata, 990 Japan.

3. 13 HEAVY ION INDUCED D-D FUSION IN DEUTERIDE SOLID

M.TESHIGAWARA[1], K. KONASHI[1], T. YAMAMOTO[1], H. KAYANO[1]
Y. ARATONO, K. FURUKAWA and E. TACHIKAWA

Experimental data of D-D fusion at low energy are necessary for understanding of cold fusion phenomena, nuclear reactions of astrophysical interest, and so on. Nuclear cross sections at low energies may be different from the cross sections which are extrapolated by cross sections at high energies. An electron screening effect may be responsible for increase of cross section at low energies. In the last few years, there have been significant improvements in extending measurements towards low energies. For example, D-D reactions have been studied down to a (center-of-mass) energy E of about 1.6 keV. In particular we are interested in D-D fusion in solid, and the cross sections of D-D fusion in TiD_x using heavy ion beam have been measured . It is well known that an energetic heavy ion particle generates collision cascade in solid, which especially includes a large number of low energy deuterons in deep region. The experimental data were compared with the theoretical predictions. The total fusion probability and the depth profile of fusion probability in solid were calculated by computer code. We have attempted to evaluate the enhancement effect through the comparison of the experimental data with the calculation results. The titanium deuteride, TiD_x, was bombarded by Iodine(I^{7+}), which was accelerated by JAERI Tandem accelerator with the beam energy of 90 MeV. Target samples TiD_x(x =0.14,0.82,1.61,and so on) were prepared by deuterium absorption method. The D-D fusion in solid was measured by detecting neutrons and protons. The BC-501 liquid scintillation counter (14.1 cm in diameter and 13.7 cm thickness) and ^{6}Li glass scintillator counter were used for neutron detection. The neutron detector was placed at 35 cm from target and angle of 90^0 was selected to the beam axis. The detector was shielded by Lead block of 5 cm thickness to reduce γ-ray background. Protons were detected by SSD detector with sensitive depth of 500 μm, active area of 200 mm^2 and 19 m sr of solid angle. Aluminum foil (thickness of 6 μm) was placed in front of SSD detector to prevent the detector from incidenting of scattered particles. The neutron detectors and the SSD detector were calibrated by ^{252} Cf neutron source and ^{241} Am α source respectively. The total fusion yields have been measured for target samples of TiDx.

The profile of the fusion probability along the depth in the target was measured for specially designed target sample ($TiD_{1.6}$). The pure Ti foils with thickness of 0 ~8 μ m were placed on the

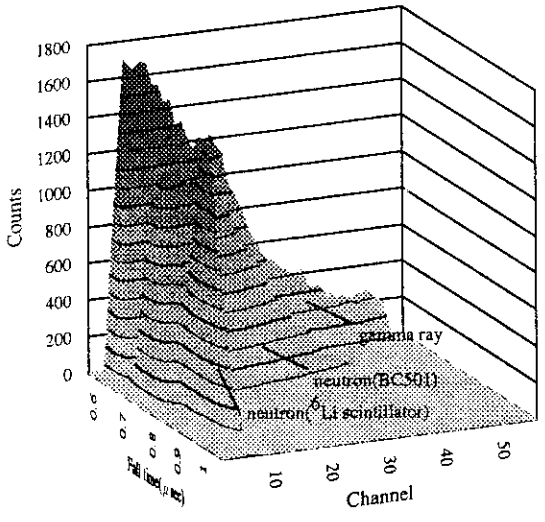

Fig.1 3-demensional curve of D(d,n)^{3}He in $TiD_{1.6}$ irradiated by I(90MeV)

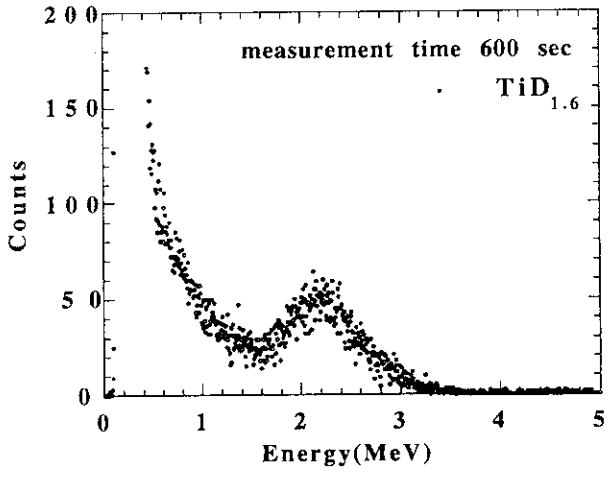

Fig.2 Energy spectrum of emission particle from $TiD_{1.6}$ irradiated I(90 MeV)

1 Oarai Branch,Institute For Materials Research,Tohoku University

target sample during irradiation. The heavy ion passes through the Ti foil without fusion, loses the energy and enters into TiD target. In this type of target, the fusions occur in the region of the target with the depth from the foil thickness to the ion range. The experiments conducted with various thickness foils provide the information of the depth profile of the fusion probability.
The neutron and proton yield were keeping constant obtained during irradiation time of 1 h. Figure 1 shows an example of 3-dimensional spectrum taken by the scintillation counters. The signal for γ ray is presented by ridge peak at about 0.66 μs fall time. The neutron appears as a ridge peak at 0.74 μs fall time and sharp peak at 0.8~0.96 μs fall time. The ridge peak at 0.74 μs fall time is made from signal by the BC501 liquid scintillator, and the sharp peak is from signal by ^{6}Li glass scintillator. The neutron of D(d,n)^{3}He reaction between lattice D atom and recoiled D atom was detected under the irradiation of heavy ion with very low background.

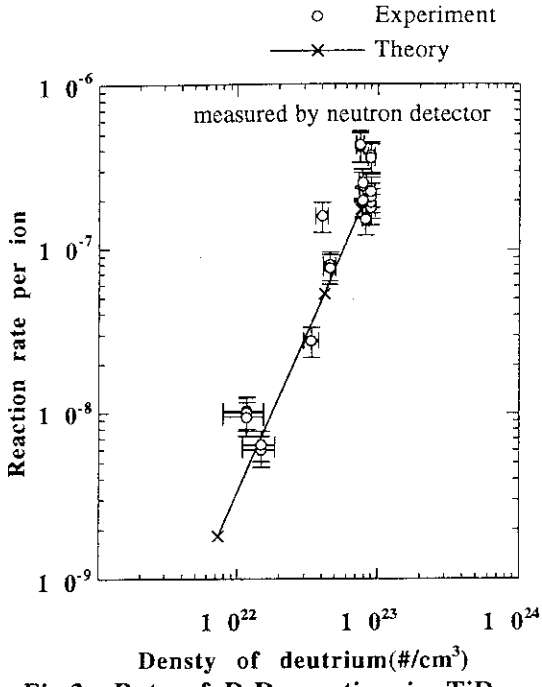

Fig.3 Rate of D-D reaction in TiDx irradiated by I with energy of 90 MeV

Figure 2 shows an example of energy spectrum of proton from D(d,p)T reaction. Since incident heavy ion penetrates into TiD_x target with depth of about 9 μ m, energy spectrum of proton has a wide hem peak. After the irradiation, the TiD_x samples were analyzed by X ray diffraction method. Only single phase was found in sample of $TiD_{1.6-1.9}$. Two phases were found in the sample with low concentrations of deuterium(TiD_x $x<1.6$); Ti phase and $TiD_{1.97}$ phase.

The simulation of the D-D fusion process was also performed by Monte Carlo code. The calculation was based on atomic collision theory without any enhancement effect such as electron screening effect. The D-D fusion rate has been calculated for the following process;
(1) TiD_x are irradiated by Heavy ions.
(2) Lattice D atoms are recoiled by heavy ion irradiation.
(3) D-D fusion occurs between lattice D atom and recoiled D atom.

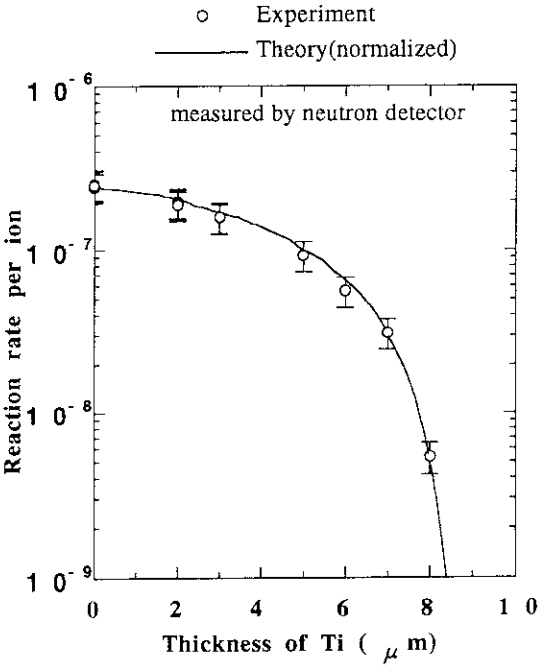

Fig.4 Depth profile of experimental results compared with those of the theoretical predictions

Figure 3 shows the comparison of experimental results on the rate of the D-D fusion with those of the theoretical predictions. Experimental values of D-D fusion values were almost equal to those of the theoretical predictions calculated by Monte Carlo code. Figure 4 shows the comparison of experimental results of depth profile of fusion probability in the target with those of the theoretical predictions. The depth profile of experimental results is very close to that of calculation results.

Consequently, experimental results are in agreement with fusion probabilities calculated by computer code. This means that no enhancement has been found in the experimental data of total probability.

3.14 JAERI RECOIL MASS SEPARATOR

H. IKEZOE, T. IKUTA, Y. NAGAME, S. HAMADA, I. NISHINAKA, T. OHTSUKI, K. TSUKADA, and Y. OURA

A recoil mass separator has been constructed at the JAERI tandem-booster facility [1]. It has a symmetric configuration of Q_1Q_2-ED_1-MD-$ED_2Q_3Q_4$-O, where two electric dipoles ED_1 and ED_2, and the magnetic dipole MD are used to disperse reaction products by their mass/charge ratio(m/q) and focus their energies. Two quadrupole doublet (Q_1Q_2 and Q_3Q_4) are used for focusing reaction products spread spatially. The octupole magnet O is used to correct a non-linearity of the m/q dispersion. The m/q and energy acceptances are designed to be ±4% and ±12%, respectively. In order to reduce a background originating from beams scattered from the ED_1 anode, the anode is split into two parts, so that the primary beam can pass through without hitting the anode. The performance of the recoil mass separator has been tested by using the ^{28}Si and ^{127}I beams from the JAERI tandem accelerator. The capability of the background suppression at the beam direction is excellent as shown in Fig.1 and the obtained mass resolution is $A/\Delta A \cong 300$. By using the JAERI-RMS, the new neutron deficient isotope ^{209}Th has been produced in the reaction of ^{32}S on ^{182}W at beam energy of 171 MeV [2]. An α-decay energy and a half-life of ^{209}Th have been determined to be 8.080(50) MeV and $3.8^{+6.9}_{-1.5}$ ms, respectively.

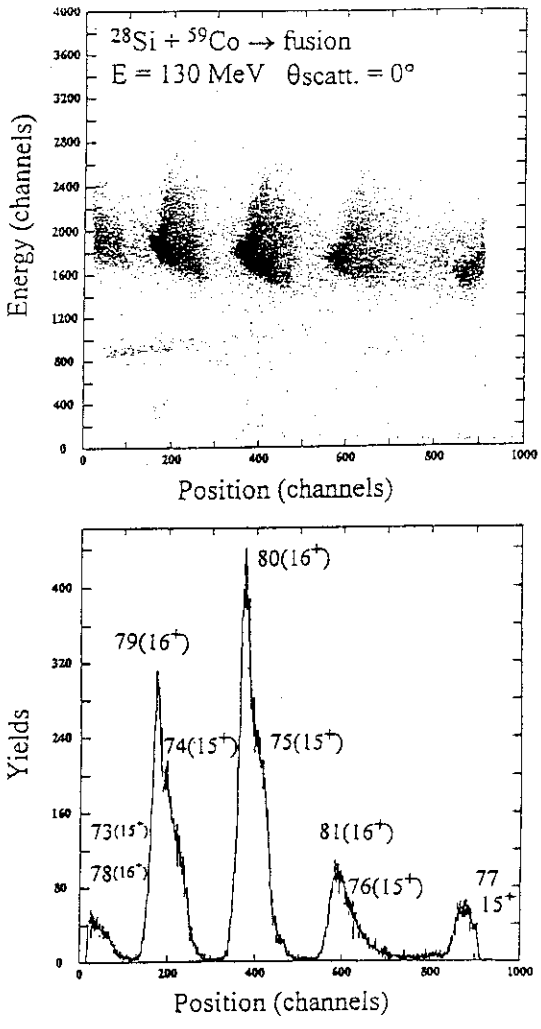

Fig.1 Measured two dimensional position versus energy spectrum (upper part) and position spectrum (lower part) obtained by projecting the two dimensional spectrum on to the position axis without setting any gate.

References

[1] H. Ikezoe, Y. Nagame, T. Ikuta, S. Hamada, I. Nishinaka, T. Ohtsuki, to be published in Nucl. Instr. & Meth.

[2] H. Ikezoe, T. Ikuta, S. Hamada, Y. Nagame, I. Nishinaka, K. Tsukada, Y. Oura, to be submitted in Phys. Rev. C

3. 15 MEASUREMENT OF RADIO-ACTIVE NUCLEI BY RECOIL MASS SEPARATOR

S.HAMADA, T.IKUTA, H.IKEZOE, S.MITUOKA, Y.NAGAME, K.TUKADA, I.NISHINAKA, K.SUGIYAMA, Y.TOMITA, T.OHTUKI*

Measurement of radio-active heavy particles from the fusion reaction and the application to the production of heavy nucleus near the proton drip line are great concern. For the isotope production projects, which are conducted under the JAERI superconducting linear accelerator and the Recoil Mass Separator(RMS) at heavy-ion nuclear physics facility, heavy-ion fusion products of atomic mass region $100 \leq A \leq 260$ are the recent objects. Since the construction of RMS, several experiments were done to investigate the optimal condition of RMS beam optics in the first order, production rates of nuclei around A=200, transmission coefficents, and the signal test of the double sided strip detecter(DSSD), in order to know the total perfomance of the RMS system[1,2].

We performed the test of measurements of recoil nucleus ^{197}Au from the elastic scattering of ^{32}S of incident energy $E_{lab.}$=100 and 80 MeV, at detection angle $\theta_{lab.}$=0° in the beam direction, bombarded on a thin gold foil, for which the energy elastic recoiled particle was degraded by various thin aluminium foil into 37.7, 31.9, 22.4 and 18.1 MeV, respectively.

The entrance aperture of RMS in the first magnet stage was set variable by a vertical/horizontal slit, of which the solid angle is estimated to be varied geometrically from sevreal str. to about 10 str. in wide-open aperture. The RMS consists of electromagnetic field, the micro channel plate(MCP) placed behind the exit of octupole magnet in order to get the signal of transported particles, and the DSSD which are segmented into fifteen strips at the front side and into 128 at the back side, by which the third quarter of all the escape solid angle are surrounded in the front side as well as other four strip detectors set in the upper, left, down and right directions. Distance between the MCP and the DSSD front surface was about 10 cm and the particle focal point was estimated to be several centimeter behind the MCP.

Position signals multiplied by enrgy for each strip detectors were flowed into each fast amplifiers, for which the posion signals were labeled by the 12 bit input register, and then distinguisded by software labeling of position and energy information in online/offline analysis. A SSD monitor was placed in the scattering chamber at laboratory angle θ=150° for counting the backward elastic scattering of ^{32}S particles, which corresponds to the Rutherford scattering cross section[5] 533 mb with solid angle 35 mstr. The elastic counts were used for normalizing the detected counts of elastic recoil ^{197}Au particles, which are to 464 mb in the same elastic calculation[5] mentioned above. Energy calibration were done using alpha source, which are of kinematic energy below the recolied particle energy done in the precedent measurements.

The measured total solid angle of RMS system is defined by the ratio of the event counts of time-of-flight(TAC) of the MCP and DSSD, to the monitor counts of backward elastic scattering, multiplied by solid angle of monitor counter and also by the ratio of both calculated cross sections. We obtained the measured solid angle of 19.2 mstr for recoil energy 18.1 MeV which is typically suitable energy for detecting the fusion synthesized nucleus. For higher energy larger than several ten MeV, it is suspected that the measured solid angle could be overestimated because of the contamination of nearest neighbouring

* Laboratory of Nuclear Science, Faculty of Science, Tohoku University

charge, because the definite energy acceptance defined by the ratio of energy and mass E/q, δ(E/q) $\cong$3 percent, have large enough acceptance to permit the contaminaiton of relatively larger q value.

Because of the problem of the resolution for position/energy and the low counts statistics, it is severe to eliminate the charge contamination in the position spectrum without the time of flight discrimination in about 10 channel, which corresponds to the time difference of about several nano second. The figure below is one typical profile for recoil particle beams in the horizontal positions, which are distinguished by several different charge q values. The verification of total counts are done by reducing the possible contamination of different q values, with checking several gating methodes for time-energy spectra.

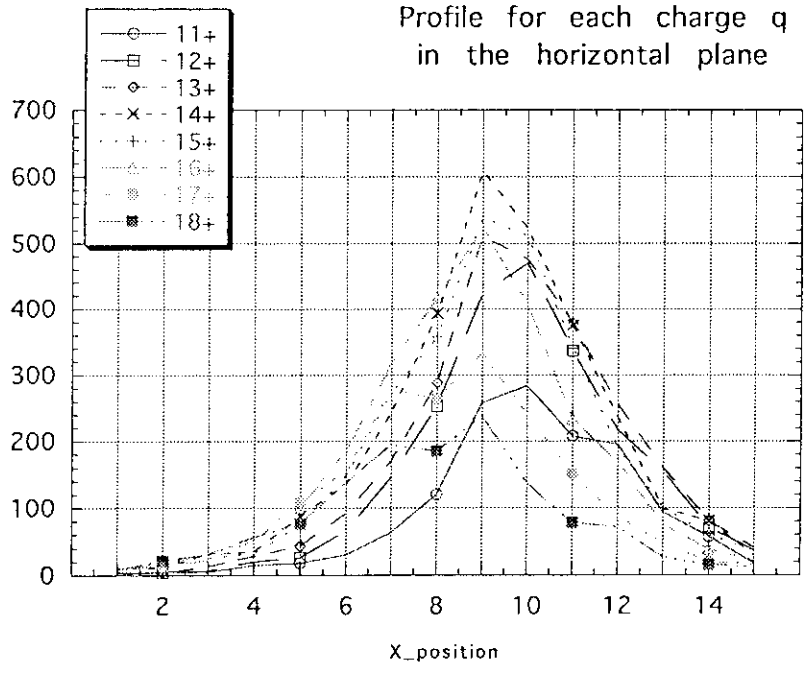

Fifure caption
Vertical- and horizontal- axis stand for the detected counts and position label of front strip dectors, respectively. The remarked numbers are the charge of recoil particle for each different field set.

Refereces
1) H. Ikezoe, Y. Nagame, T. Ikuta, S. Hamada, I. Nishinaka and T. Ohtsuki, JAERI RECOIL MASS SEPARATOR, IN2P3-RIKEN symposium, 1995
2) H. Ikezoe, Y. Nagame, T. Ikuta, S. Hamada, I. Nishinaka and T. Ohtsuki, JAERI RECOIL MASS SEPARATOR, Nucl. Inst. Meth. to be published.
3) C.N. Davids, B.B. Back, K. Bindra, D.J. Henderson, W. Kutschere, T. Lauritsen, Y. Nagame, P. Sutathan, A.V. Ramayana and W.B. Walters, Nucl. Inst. Meth. B70 (1992) 358-365
4) C.N. Davids, B.B. Back, K. Bindra, D.J. Blumenthal, D.J. Henderson, and H.T. Penttilä, Annual report of Argonne National Laboratory, 1995
5) Ptolemy computer code

4. Nuclear Theory

4.1 SPONTANEOUS FISSION VIEWED AS MANY-BODY TUNNELING PROCESS

A. IWAMOTO

To attack the spontaneous fission dynamics from a many-body point of view, we proposed a model[1] based on the Vlasov dynamics. We will briefly review this model and present some results of numerical calculations.

The basic model is the Vlasov equation. It is the classical analog of the TDHF equations and is obtained after the Wigner transform of TDHF equation in the limit of small $\hbar$. The classical nature of our model comes from this fact. One possible and promising way to incorporate the "shell" effect in the model is to include the higher order terms in the expansion of $\hbar$ in Wigner transformation of TDHF [2] which is under consideration for our future work. The Vlasov equation is solved by means of the test particle method. [3]. For the mean field, we used a simple Skyrme force with 225MeV compressibility and the symmetry energy term.

For the description of the dynamics below the barrier, we used the method which was originally developed for the description of subbarrier fusion reactions [4]. The idea is to choose a set of variables which describe the fissioning motion. For simplicity, we choose the distance R between the centers of two fragments and its conjugate momentum P. In order to calculate the tunneling process, we change the force acting on each test particle at the time when P becomes zero. The equation of motion for a test particle now changes to

$$\partial \vec{p}_i / \partial t = -(\vec{\nabla} U(\vec{r}_i) - 2 \cdot \vec{\xi}_{A(B)}) , \qquad (1)$$

where the first term of the r.h.s. is the standard force coming from the gradient of the mean potential U and the second term is the special force defined as

$$\vec{\xi}_{A(B)} = \frac{1}{A(B)} \int_{A(B)} d\vec{r} d\vec{p} \nabla U(\rho) f(\vec{r}, \vec{p}, t) , \qquad (2)$$

where A and B denote the regions to the right and to the left of the dividing plane which separates the right and left fragments. The mean field U and one-body distribution function f are calculated from the Vlasov equation. It is well known that the imaginary-time treatment of the tunneling process for one dimensional problem is equivalent to simply change the signature of the potential term. When we apply eq.(1) not to the test particle but to the collective variable R itself, it just realizes this situation. The subtraction of twice the force acting on the center of one fragment is equivalent to replace grad$U$ by -grad$U$ in this case.

We calculated the final kinetic energy of the fragments and the results are shown in Fig. 1 for the fission of several actinide nuclei. Here the symbol with error bar represents the calculated results and two lines represent the experimental systematics. As is seen in this figure, the agreement between the data and the calculation is not bad. To check the ability of our model to describe the mass asymmetric fission, we calculated the fragment kinetic energies for the fission of ^{252}Cf for various mass splitting. In Fig.2, we show this results together with the data. This nucleus undergoes a typical asymmetric fission, which is caused by the shell effect. A bump structure with a peak near mass=132 is related to this shell effect. In this mass division, the binding energy of the sum of two fragments becomes large, which favors the high relative kinetic energy. Our

model calculation doesn't take this effect into account and thus shows no bump structure. Apart from this structure, however, our model explains the gross structure of the kinetic energy distribution for each mass asymmetry. The absolute values are rather well reproduced although we have no fitting parameter. From this figure, we find that our model gives a reasonable description of the asymmetric mass division.

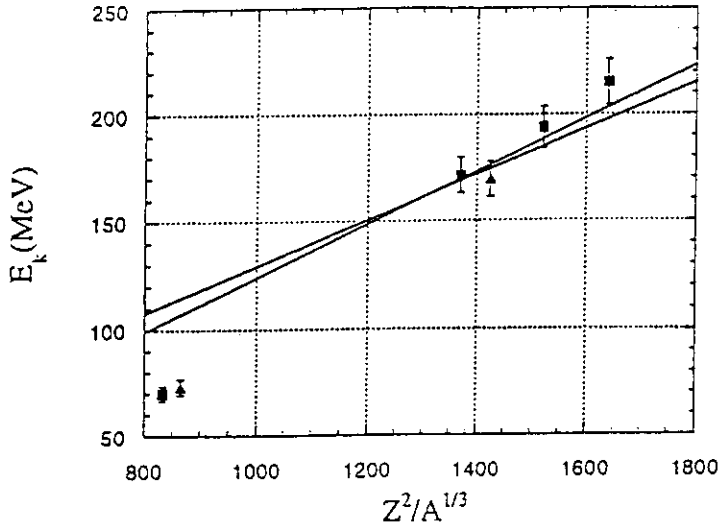

Fig.1. Final kinetic energy between two fragments for the symmetric fission as a function of the $Z^2/A^{1/3}$ of the compound nuclei. The full lines give the Viola fits to the data and solid squares are our calculations. The triangles refer to the calculated spontaneous fission of exotic ^{210}U and ^{147}Ho.

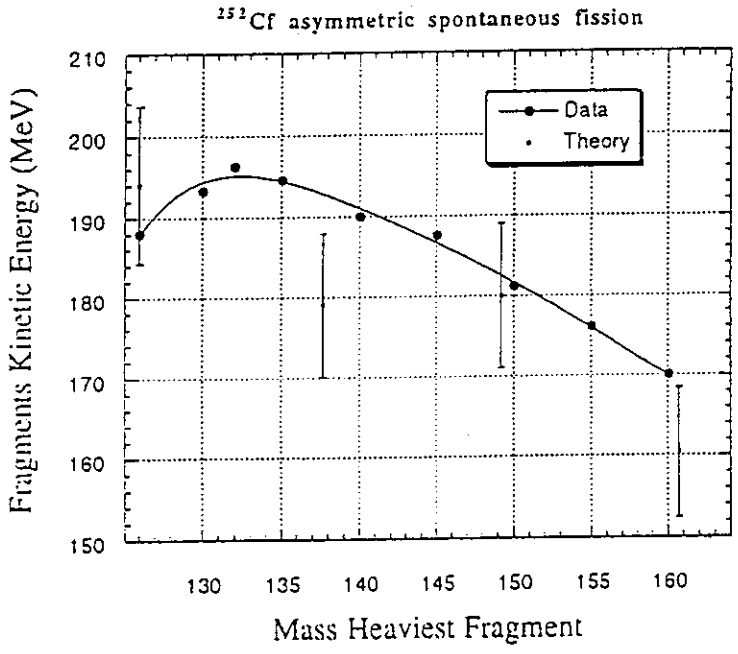

Fig.2. Final kinetic energy between two fragments for asymmetric fission of ^{252}Cf. Solid circles are data and the calculations are shown as small open squares with error bars.

References

1) A. Bonasera and A. Iwamoto, submitted to Phys.Lett.B.
2) S. John and E.A. Remler, Ann. of Phys. **180** (1987) 152; A. Bonasera, V.N. Kondratiev, A. Smerzi and E.A. Remler, Phys.Rev.Lett. **71** (1993) 505.
3) C. Wong, Phys.Rev. C**17** (1978) 1832.
4) A. Bonasera and V.N. Kondratiev, Phys.Lett. **B339** (1994) 207.

4.2 MULTIFRAGMENTATION THROUGH EXOTIC SHAPE NUCLEI IN α(5GeV/u) + Au REACTIONS

TOMOYUKI MARUYAMA

Multifragmentation attracts attention as one of the most important aspects of light- and heavy- ion reactions in the high energy region. It is speculated that the decay of a highly excited nuclear system carries the information about the nuclear EOS and the liquid-gas phase transition of low density nuclear matter. Recently, the KEK experimental group has reported very interesting results for the distribution of the intermediate mass fragments (IMF) in proton (12 GeV) and alpha (5 GeV/u) induced reactions [1]. The experimental data for the angular-distributions of IMF have clear peaks at $\theta_{\rm lab} = 70°$.

Then we investigate the origin of the experimental results for the IMF angular-distribution by simulating the dynamical stage of α(5 GeV/u) + Au collisions with RQMD/S [2]. We show the baryon and pion distributions in the coordinate space at several time steps, projecting on the xz- plane, restricted with positions $|y| < 1$fm (upper columns), and the xy- plane, restricted with positions $|z| < 1$fm (lower column). The figures include the

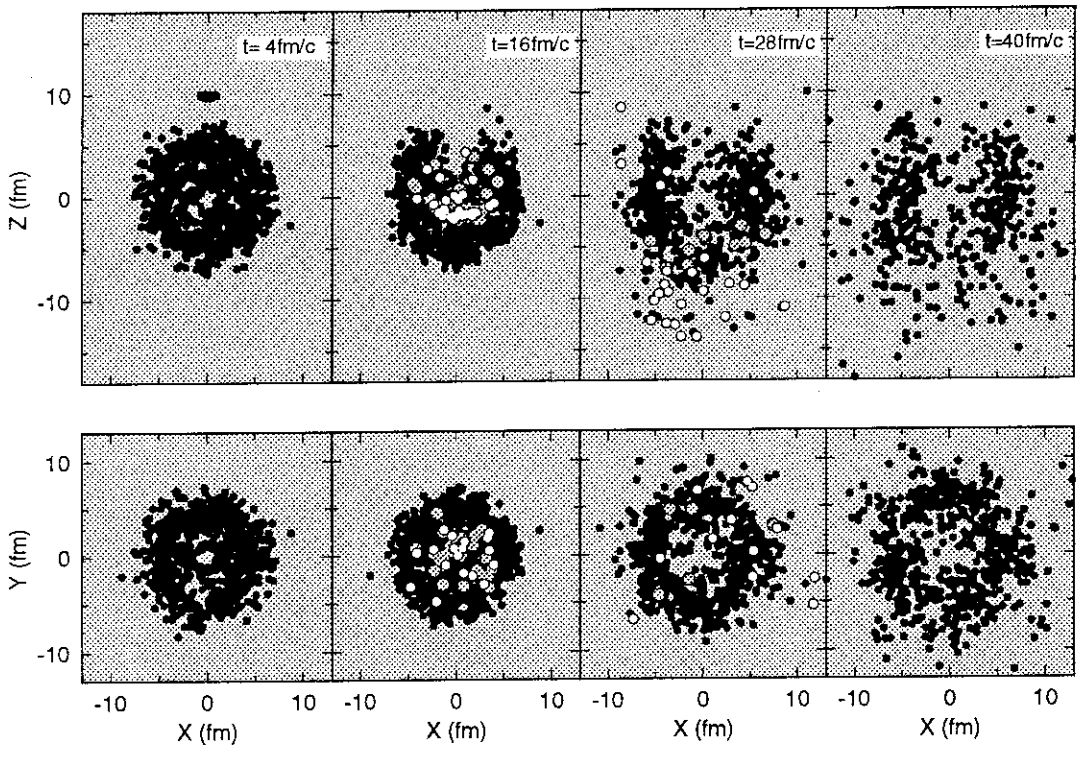

Fig. 1: The time evolution of the baryon and meson distributions in the coordinate space at time steps 4, 16, 28 and 40 fm/c in α(5 GeV/u) + Au collisions for the impact-parameter $b = 0$ fm. The upper columns show the distributions on xz- plane, restricted as $|y| < 1$ fm, while the lower columns on xy- plane, restricted as $|z| < 1$ fm. The black, grey, and white circles denote the nucleons, resonances and mesons, respectively.

results of twenty simulations for the impact-parameter $b = 0$ fm, and the black, gray, and white circles denote the nucleons, resonances and mesons, respectively.

Around the time step $t = 16$ fm/c a lot of resonances and pions are produced and propagate forwards. After $t = 28$ fm/c, these high energy pions and nucleons are emitted forwards. At this moment, the big empty region appears in the center; namely the intermediate residual nucleus with the annular eclipse shape is constructed through the reaction. After that this exotic residual nucleus slowly expands sidewards, and finally nucleons gather, connect and form many fragments. Apparently this fragmentation process is the multifragmentation.

In Fig. 2, we show the angular-distribution of two kinds of fragments with the charge $Z = 1$ (open circles), $3 \leq Z \leq 20$ (IMF) (full squares), for this simulation, where events are restricted with the impact-parameter $b \leq 3$ fm. The IMF angular-distribution has a sideward peak and this result agrees with the experimental one qualitativerly. We have found in the simulations that this sideward peak of the IMF angular distribution is very much correlated with the shape of the intermediate residual nucleus, i.e. the **annular eclipse** shape.

From these results we can conclude that the α + Au reaction at 5 GeV/u constructs a hot nuclear system with the annular eclipse shape in the central collision. This exotic residual nucleus expands sidewards and causes a multifragmentation. As a result of this process the IMF angular-distribution has a side-directed peak. Thus this expermental result must be a clear evidence of the multifragmentation.

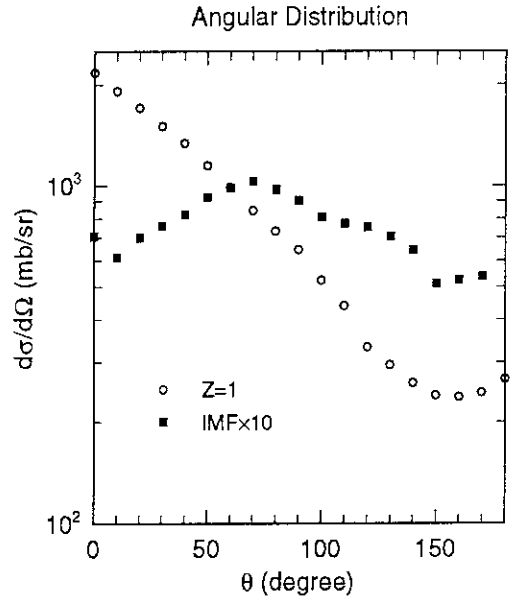

Fig. 2: The angular-distributions of fragments: $Z = 1$ (open circles) and $3 \leq Z \leq 20$ (full squares). The cross-section for the second fragment is multiplied by 10. Events are restricted with the impact-parameter $b \leq 3$ fm.

References

1) K.H. Tanaka et al., Nucl. Phys. **A583**, 581 (1995).

2) T. Maruyama et al., Prog. Theo. Phys. Vol.96 (1996) in press.

4.3 EXTENSION OF QUANTUM MOLECULAR DYNAMICS AND ITS APPLICATION TO HEAVY-ION COLLISIONS

TOSHIKI MARUYAMA, KOJI NIITA[1] AND AKIRA IWAMOTO

Microscopic many-body treatments of the heavy-ion reaction, i.e., molecular dynamics methods such as quantum molecular dynamics (QMD)[1], antisymmetrized MD (AMD)[3] and Fermionic MD (FMD)[2], have been successfully applied to medium and high energy phenomena. However in the very low energy region, such as the near-barrier energy, fully many-body treatment has not yet been tried, especially for heavy systems. In using molecular dynamics for low energy phenomena, sufficiently stable ground state nuclei with good density profiles and binding energies are indispensable.

For this aim, we have extended the QMD method in two respects[4]. One is to include the so called Pauli potential[5] to simulate the Fermion many body system. The other is to treat the width of each Gaussian wave-packet of nucleon as a dynamical variable. We solve the $8A$-dimensional classical Hamilton equation of motion[6] instead of $6A$ (position and momentum coordinates of all wave-packet centers) ones. The additional $2A$ dimensions originate from the complex parameters of wave packet width. We call here this extended version of QMD as EQMD.

We determine the ground state of nucleus as the energy-minimum state which is obtained by solving a damped EOM with the friction term. We can reproduce properties of nuclei, such as binding energy, density distribution and so on, from light to heaviest systems by a unique interaction parameter set. Furthermore, alpha-clustering structures appear in the light nuclei, while this kind of feature is lacking in the standard QMD framework.

Two effects due to the dynamical treatment of wave-packet width are observed in nucleus-nucleus collisions. One is the enhancement of nucleon emissions from the excited nuclei. In Fig. 1 we compare the full EQMD calculation with that of fixed-width constraint for fragment production cross sections in the $^{12}C+^{12}C$ (29 MeV/nucleon) reaction. The fixed-width calculation is to solve the equation of motion only for the centers of nucleon wave-packets keeping the widths as constants ($6A$-dimensional calculation) using exactly the same interactions and the initial conditions as in the full EQMD. The cross sections of nucleons and light fragments in the full EQMD calculation are larger than that in the fixed-width calculation. This cross section is that after the statistical decay process. If we compare the same quantity before the statistical decay, the difference between full and fixed-width calculations is more conspicuous. This enhancement, we consider, is due to the increase of the path of emission process by the dynamical change of the width.

The other effect is the enhancement of the fusion reaction. Fig. 2 shows the fusion cross section of $^{16}O+^{16}O$ system with the incident energy dependence. Note that there have been few works which treat fusion reactions with molecular dynamics due to the insufficient stability of initial nuclei. Two kinds of calculations, namely, full EQMD and fixed-width calculation and experimental data are compared. The full EQMD calculation with dynamical width can reproduce the energy dependence of the fusion cross section, though the absolute value is not perfect. On the other hand, the fixed-width calculation much underestimates the fusion cross section especially in the higher energy region. At

⋆ 1 Research Organization for Information Science and Technology

very low energies, two nuclei can fuse if they overcome the barrier. At higher energies, however, the dissipation of the incident energy into the internal excitation is necessary. The dynamical change of wave-packet widths offers more degrees of freedom for the dissipation than the case of fixed width. Thus the dynamical treatment of wave-packet width plays much important roles rather at higher energies where dissipation of the incident energy is important for the fusion process.

References

1) J. Aichelin and H. Stöcker, Phys. Lett. B **176** (1986) 14; J. Aichelin, Phys. Rep. **202** (1991) 233.
2) H. Feldmeier, Nucl. Phys. **A515** (1990) 147; H. Feldmeier, K. Bieler and J. Schnack, Nucl. Phys. **A586** (1995) 493.
3) A. Ono, H. Horiuchi, T. Maruyama and A. Ohnishi, Prog. Theor. Phys. **87** (1992) 1185.
4) T. Maruyama, K. Niita and A. Iwamoto, Phys. Rev. C **53** (1996) 297.
5) Similar way to A. Ohnishi, T. Maruyama and H. Horiuchi, Prog. Theor. Phys. **87** (1992), 417.
6) P. Valta, J. Konopka, A. Bohnet, J. Jaenicke, S. Huber, C. Hartnack, G. Peilert, L. W. Neise, J. Aichelin, H. Stöcker and W. Greiner, Nucl. Phys. **A538** (1992) 417c.
7) J.Czudek, et al.,Phys. Rev. **C43** (1991) 1248.
8) B. Fernandez, C. Gaarde, J. S. Larsen, S. Pontoppidan and F. Videbaek, Nucl. Phys. **A306** (1978) 259.
9) F. Saint-Laurent, M. Conjeaud, S. Harar, J. M. Loiseaux, J. Menet and J. B. Viano, Nucl. Phys. **A327** (1979) 517.

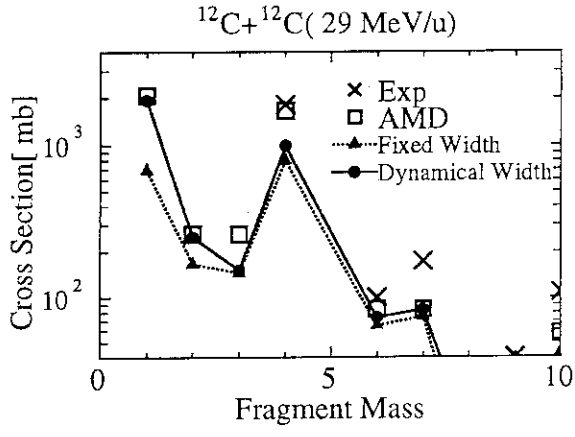

FIG. 1. Fragment mass distribution in the ^{12}C(29 MeV/u)+^{12}C reactions. Compared are experimental data[7], EQMD calculation (dynamical width), fixed-width calculation and the AMD calculation[3] which reproduces the data of $A_f \geq 4$ fragments.

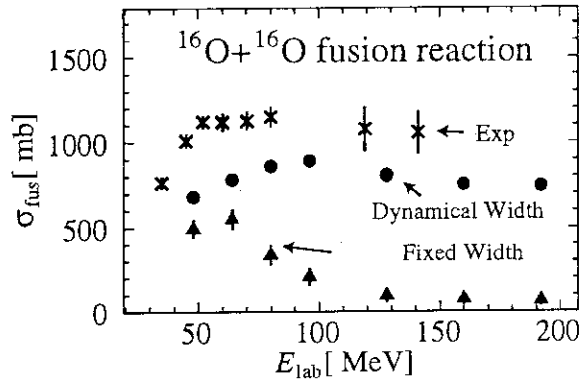

FIG. 2. Fusion cross section of ^{16}O+^{16}O system. Experimental data are from [8,9].

5. Atomic Physics, Solid State Physics and Radiation Effects of Materials

5.1 ELECTRON CAPTURE DIFFERENTIAL CROSS SECTIONS FOR PROTON-RARE GAS COLLISIONS

M. Sataka, S. Kitazawa, K. Komaki[1], Y. Yamazaki[1], T. Azuma[1], H. Shibata[2]
K.Kawatsura[3], K. Kanai[4] and H. Tawara[5]

We have been studying the electron emission processes in the collision of multi-charged ion and atoms and solids and ionic structure of the multi-charged ions, by means of 0 degree electron spectroscopy[1-2]. We started the measurement of the scattering angle in charge changing collision between fast ions and atoms. We are also planning to study the correlation of electron production processes and charge changing processes.

The electron capture differential cross sections, differential in scattering angle of projectile ions, were measured 5 MeV H^+ ion impact on rare gases. H_3^+ ion (15MeV) was accelerated by the JAERI tandem accelerator and H^+ ion of 5 MeV was obtained from dissociated H_3^+ by transmitting a carbon-foil. The ion beam was introduced to collision cell and outgoing ions were separated using electro-static deflector and detected by Faraday cup. Neutral H atoms were detected by 2-dimensional position sensitive detector.

In Fig. 1, we show the experimental result of angular distribution of neutral H atoms after collisions of He, Ne and Ar targets. The full width at half maximum was 0.22, 0.29 and 0.27 mrad for He, Ne and Ar target, respectively. The ratio of total electron capture cross section (integrated cross sections of the differential cross sections) for He, Ne and Ar target is 1: 260: 840. The ratio is consistent with the results of the total capture measurements. It is easily seen from the figure that the angular distribution of Ne target is almost same as that of Ar target. The width of the angler distribution is not likely to depend on the nuclear charge. In this energy region, H ions should capture the K-shell electrons for

[1]Colledge of Arts and Sciences, University of Tokyo,
[2]RCNST, University of Tokyo,
[3]Faculty of Engineering, Kyoto Institute of Technology,
[4]National Institute for Fusion Sciences,
[5]The Institute of Physical and Chemical Research (RIKEN)

the Ne target. The other hand, H ions capture L-shell electrons for Ar target. We suppose the angler scattering process accompanied with electron capture may depend on the target shell of the active electron for the capture process.

References

1) Sataka, M., Imai, M., Yamazaki, Y., Komaki, K., Kawatsura, K., Kanai, Y., Tawara, H., Schultz, D.R. and Reinhold, C.O., J. Phys. B27 (1994) L171.

2) I.Yu.Tolstikhina, H.Tawara, U.I.Safronova, M.Imai, M.Sataka, K.kawatura, K.Komaki, Y. Yamazaki and Y. Kanai, Phys. Scripta. in press.

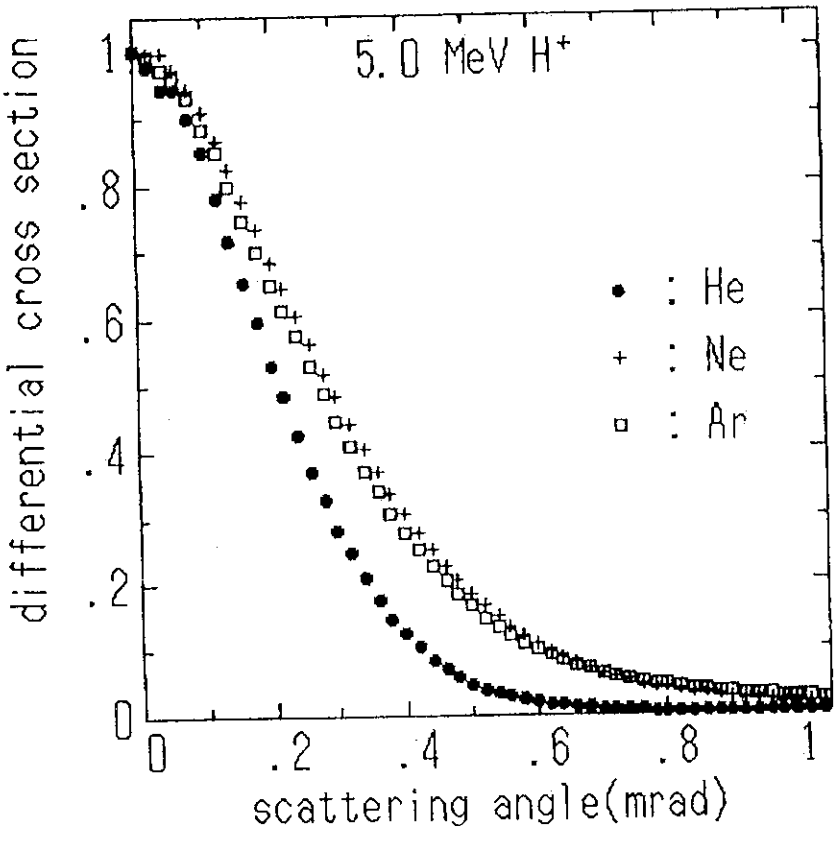

Fig.1 Neutral H beam profile after collision of He target.

5. 2 RADIAL DOSE DISTRIBUTION AROUND AN ENERGETIC HEAVY ION AND AN ION TRACK STRUCTURE MODEL

K. FURUKAWA, S. OHNO[1)] . H. NAMBA, M. TAGUCHI and R. WATANABE

Chemical effects caused by a rapidly moving ion in matter are mainly due to secondary electrons generated along the ion's path. Radiolysis yields for energetic electrons are fairly well known at least for some cases(e.g., Fricke solutions) as a function of radiation dose. Therefore, we can estimate the radiolysis yields for heavy ion irradiations if we know the spatial dose distribution around the heavy ion's path and integrate the probability of reaction due to electrons all over the space. The method has been developed by Katz and collaborators using a simplified track structure model[1,2]. In the present paper, the radial dose distribution is obtained from the measured radial distribution of local ionization currents produced in a gas-filled chamber traversed by a beam of 3.5MeV/u particles[3]. We make use of these measurements together with the LET-values to construct our own track structure model and we have tried to calculate the yield of oxidation of ferrous ions in the Fricke dosimeter irradiated by 200 MeV Ni $^{12+}$ ions.

The expeimental setup used and procedure have been reported earlier[3]. To get information on the spatial distribution of the deposited energy around ion's path, we measured radial distribution of inization currents produced in a small wall-less inization probe. The measured ionization currents at varying distance from the ion beam and at varying gas pressure have been normalized as follows:(1)Simulated radial distance R:

$$R = R_{gas}(d_{gas}/d_{water}) \quad (1)$$

where R_{gas} is the observed distnace (between the small chamber and the ion beam) and d_{gas} and d_{water} are the densities of Ar gas and the liquid water, respectively.
(2)Dose in eV/g at the distance R is:

$$\text{Dose} = (I_p/I_i)(ZW_e/(vd_{gas}))(d_{water}/d_{gas})^2, \quad (2)$$

where I_p and I_i are the ionization current in the small wall-less chamber and incident ion beam current, Z is

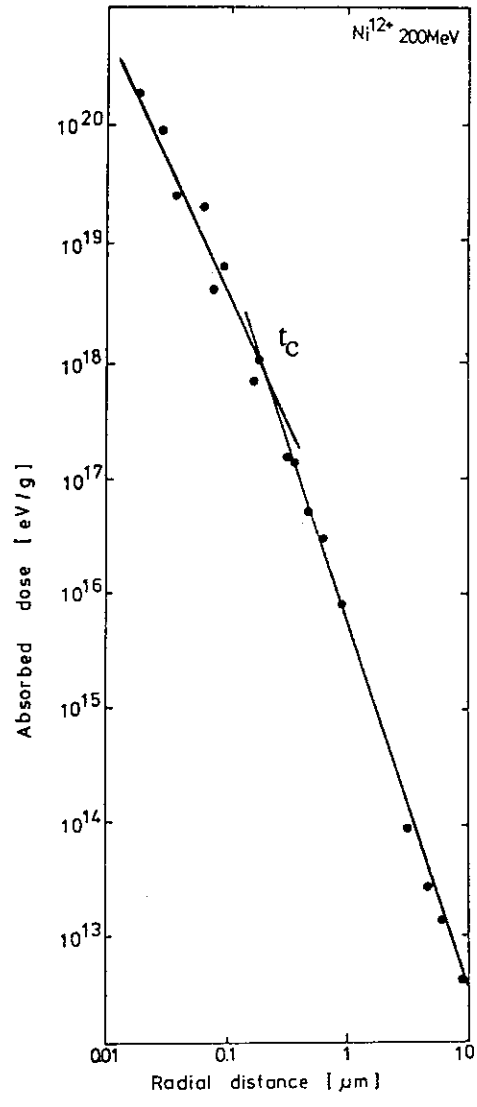

Fig.1. Absorbed dose as a function of radial distance for 200MeV Ni^{12+} ions.

1)Institute of R&D, Tokai University

the charge of the incident ion, W_e is the W-value of the gas for the fast electron(26.2 eV for A r) and v is the volume of the small wall-less ionization chamber.
Fig.1 shows the radial dose distribution obtained in Ar gas around the path of a 200 MeV Ni^{12+}ion. The results indicate that the radial dose distribution decreases as 1/2 power law in the inner region and as 1/3 power law in the outer region of the ion track.

According to the target theory developed in the field of radiation biology and later extended by katz et al [1,2]to the field of radiation chemistry, the probability of reaction for any "target" (a ferrous ion surrounded by water molecules) irradiated "homogeneously" at the dose D by fast electrons is expressed as $[1-\exp(-D/D_0)]$, where D_0 is the average dose which gives 1-reaction per target. For the case of 1mM ferrous sulfate solution where the yield saturation occurs and $G(Fe^{3+})$ is known to be 15.4, we have

$$N_0[1-\exp(-100eV/D_0]=N_0 100/D_0=15.4. \quad (3)$$

If $N_0=6\times10^{17}$ cm^{-3}, one may obtained $D_0=4\times10^{18}eVcm^{-3}$.
As the probability of oxidation of Fe^{2+} located at the distance t from the ion path is $\{1-\exp[-D(t)/D_0]\}$ for heavy ion irradiation, the probability of reaction induced by a single ion is given by

$$\sigma=\int 2\pi t dt(1-\exp[-D(t)/D_0]). \quad (4)$$

For an ion beam of flux F and of the linear energy transfer LET, the probability of reaction is $[1-\exp(-\sigma F)]$ and the dose transferred from the ion beam to a medium of unit thickness is $D=F\cdot LET$. Hence,

$$G_{ion}= N_0[1-\exp(-\sigma\, 100/LET)]. \quad (5)$$

Since the results shown in Fig.1 can be expressed as:

$$D(t)= 5\times10^8/t^2 \text{ eV/g for } 0<t<t_c \quad (6)$$

$$D(t)= 3.4\times10^3/t^3 \text{ eV/g for } t>t_c \quad (7)$$

where $t_c=2\times10^{-5}$ cm, we get

$$\sigma = \int 2\pi t dt(1-\exp[-5\times10^8/t^2D_0])+\int 2\pi t dt(3.4\times10^3/t^3D_0)=4.0\times10^{-10}cm^2 \quad (8)$$

and $$LET=\int 2\pi t D(t)dt=4.8\times10^9 eV/cm \quad (9)$$

from numerical calculation.
From Eq.5 with these values, the $G(Fe^{3+})$ for 200MeV Ni^{12+} ion is given by

$$G_{ion}=N_0\sigma\, 100/LET=5.0\,. \quad (10)$$

We can extend the present calculation to other bombarding ions if the radial dose distribution D(t) of the ions is known. A study of this line is now in progress.

References

1) J. J. Butt and R. Katz, Radiat. Res. 30, (1967) 855
2) M. P. R. Waligorski et al, Nucl. Tracks Radiat. Meas. 11, (1986) 309
3) K. Furukawa et al, JAERI-M91-170, (1991) 61

5.3 DEFECT PRODUCTION DUE TO ELECTRONIC EXCITATION IN $EuBa_2Cu_3O_y$ IRRADIATED WITH HEAVY IONS

N.ISHIKAWA, A.IWASE, Y.CHIMI, H.MAETA, K.TSURU[1], and O.MICHIKAMI[2]

Irradiation with energetic ions in solid materials results in production of defects mainly due to interactions between incident ions and target atoms, commonly termed as nuclear stopping power (S_n) and electronic stopping power (S_e).

Increase of c-axis lattice parameter (c) in $YBa_2Cu_3O_y$ when irradiated with Xe ion has been reported[1] and electronic excitation was suggested as a possible origin for defect production. However systematic study of irradiation effect on c-axis lattice parameter by changing Se has not been performed so far. We have investigated irradiation effect on c-axis lattice parameter of $EuBa_2Cu_3O_y$ (EBCO) using various ions with wide energy range and discussed in terms of Sn[2] and Se.

We prepared c-axis oriented $EuBa_2Cu_3O_y$ thin films which have T_c values of about 83K. Magnetron sputtering method was used for the preparation of as-sputtered films. The value of c-axis lattice parameter before irradiation , c_0, was around 11.735Å. We performed irradiations with high-energy ions, such as Ni(200MeV), I(80MeV), and I(200MeV), using Tandem Accelerator at Tokai Establishment. The samples were irradiated along the direction of c-axis at room temperature. The values of c-axis lattice parameter were estimated before and after the irradiations by measuring X-ray diffraction pattern.

Fig.1 and 2 show $\Delta c/c_0$ as a function of fluence, Φ, for Ni-irradiation and I-irradiation, respectively. Δc is the change of c value caused by ion irradiation; $\Delta c = c - c_0$. In Fig.1 and 2 we note that $\Delta c/c_0$ increased linearly as Φ increased, suggesting that defect density increased linearly as Φ increased. This behavior can be seen for all the irradiations we have performed. The slope of $\Delta c/c_0$ against Φ, $(\Delta c/c_0)/\Phi$, for each irradiation differed one another, indicating each irradiation has a different defect production rate. The values of $(\Delta c/c_0)/\Phi$ in EBCO irradiated with relatively low energy ions (Se <4MeV/(mg/cm^2)) can be regarded as a linear function of nuclear stopping power,S_n[2], meaning that elastic displacement is a dominant defect production process in the low energy ion irradiation.

On the other hand, for Ni-,and I-irradiation, defect production due to elastic displacement could not account for the $(\Delta c/c_0)/\Phi$ values which are far higher than expected from

[1]Electron Devices Laboratory, NTT Interdisciplinary Research Laboratories.

[2]Faculty of Engineering, Iwate University.

elastic displacement. As the most probable defect production other than elastic displacement is defect production due to electronic excitation, for Ni- and I-irradiation we plotted $(\Delta c/c_0)/\Phi$ values against Se in Fig.3. From the figure we can conclude there is an obvious correlation between $(\Delta c/c_0)/\Phi$ values and Se, indicating that defect production are dominated by electronic excitation in the region $Se > 20MeV/(mg/cm^2)$. For Ni-irradiation it is conceivable that defect production due to Se is comparable to defect production due to Sn[2].

Reference

1)B.Roas, B.Hensel, S.Henke, S.Klaumunzer, B.Kabius, W.Watanabe, G.Saemann-Ischenko, L.Schultz and K.Urban, Europhys. Lett. 11 (1990) 669.

2)N.Ishikawa, A.Iwase, Y.Chimi, H.Maeta, K.Tsuru, O.Michikami, Physica C 259(1996) 54.

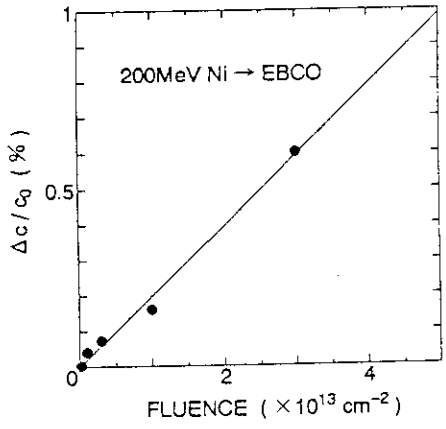

Fig.1 $\Delta c/c_0$ as a function of Φ for EBCO irradiated with 200MeV Ni.

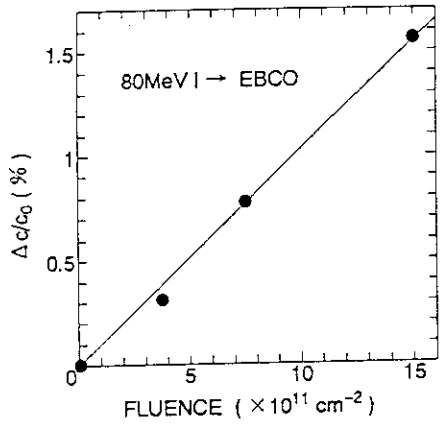

Fig.2 $\Delta c/c_0$ as a function of Φ for EBCO irradiated with 80MeV I.

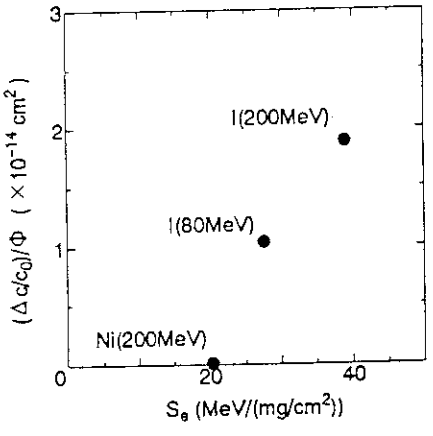

Fig.3 $(\Delta c/c_0)/\Phi$ as a function of electronic stopping power, S_e, for various irradiations.

5.4 EFFECTIVE ACTIVATION ENERGY OF 16MeV PROTON IRRADIATED QMG-YBCO

S.Okayasu and Y. Kazumata

It is well known that the critical current density Jc flowing within high-Tc superconductors exhibits a large long time decay. This phenomenon is resulted from shorter coherence length of the materials and larger thermal fluctuation due to higher working temperatures. Effective activation energy of vortices is one of the keywords to understand the mixed state of high-Tc materials. Melt growth YBCO (QMG-materials) can flow large critical current densities, but the origin of such a strong pinning is still uncertain. To investigate this problem, we focus on the relation between ion irradiation and change of the effective activation energies.

The QMG-materials of YBCO were prepared and synthesized with 30 molar of Y211 inclusions [1]. The inclusions are about 1 μm diameter and are finely dispersed in the matrix of 123. All samples were made in Nippon Steel Corp. Samples were cut into small pieces (1x1x0.3 mm^3) for experiments. Ion irradiation with 16MeV proton was performed at liquid nitrogen temperature using the 20MV tandem accelerator at JAERI. A series of measurements for time decaying magnetization were performed with a commercial magnetometer (PPMS, Quantum Design). These measurements were performed with the following procedures: A sample was settled at desired temperatures. After applying a cyclic field from 9 to -9 Tesla, the sample was then applied to some desired field. This process ensures the entire sample to be in the critical state. Then time decaying magnetization measurements were started. Using the Bean's model and Maley's formula [2], the measured data are converted to the relation between the effective activation energies and the critical currents.

Fig.1 shows the effective activation energies of proton-irradiated QMG-YBCO ($5x10^{15}$ p/cm^2) in different fields. To remove the temperature dependence of J, the U_{eff} values were divided by an empirical function $g(T)=[1-(T/Tx)^2]^{2/3}$ where Tx is the irreversibility temperature. Thus, Fig.1 represents J- and H-dependence of U_{eff}. Concerning the field dependence of U_{eff} these data can be scaled with the factor as $\propto H^{-1/3}$ (see Fig.2). At lower irradiation dose below $5x10^{15}$ p/cm^2, the J-dependent function of U_{eff}, f(J) is expressed as a power-law of J. From a log-log plot of U_{eff} vs J, two different power-law regimes are observed. The power is about -1.5 in higher J regimes and about -0.5 in lower J. This suggests different flux bundle sizes in the two regimes according to the theory of collective flux creep [3]. A similar result is obtained by Kung et. al. with some melt-growth YBCO materials [4]. Increase of the irradiation dose up to $1x10^{16}$ p/cm^2, the f(J) changes qualitatively from the power-law to quasi-exponential one. On the other hand, the effects of the irradiation on T-dependent function g(T) are the minor change of the irreversibility temperatures. The irradiation effects are mainly reflected on the f(J) functions of U_{eff}. The f(J) of U_{eff} is more sensitive to the bombardment because the critical current densities are strongly related to the pinning. In contrast to this, g(T) is affected with an electron irradiation case on LSCO single crystal [5]. In that situation, oxygen atoms are collided preferentially. Oxygen defects are affected with g(T). Conversely, the proton irradiation does not affect g(t), defects are introduced in the sample homogeneously.

The power-law of f(J) is generally observed with melt-growthed YBCO. This property should be explained with being due to the pinning centers preexisting in the material (Y211-inclusions? not clear!). After the irradiation up to $1x10^{16}$ p/cm^2, the pinning properties are qualitatively changed by the defects introduced with the irradiation. This should be reflected in the change of the effective pinning potentials. What type of defects are introduced by the irradiation? In our case, the primary knock-on atoms collided by the bombarded ions can make defects of their average size about 10Å, the order of unit cell. The density of the defects with the dose of $1x10^{16}$ p/cm^2 is estimated about 20 ppm. In spite of the small amount of defects introduced with the irradiation, the effective activation energies are affected. One possible reason is as follows; the defects' sizes are comparable to the coherence length of this material and these small defects act as effective pinning centers. Phenomenological studies are in progress, however, the pinning mechanism of is still unclear.

In summary, effective activation energies of 16MeV proton irradiated QMG-YBCO change their formulas in J-dependence functions from power-law (below $5x10^{15}$ p/cm^2) to exponential (over $1x10^{16}$) with the irradiation doses. T- and H-dependence functions of U_{eff} are not sensitive to the irradiation.

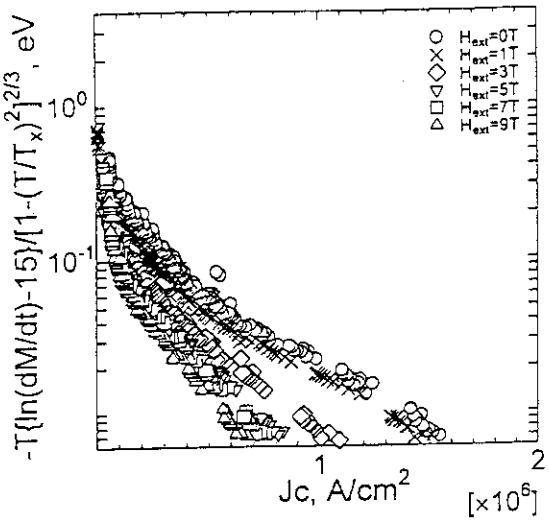

Fig.1 The effective activation energies of 16MeV proton irradiated QMG-YBCO ($5x10^{15}$ p/cm^2) in different field. The irreversibility temperatures are 91K(Hext=0T), 89K(1T), 79K(3T) and 72K(5T), respectively.

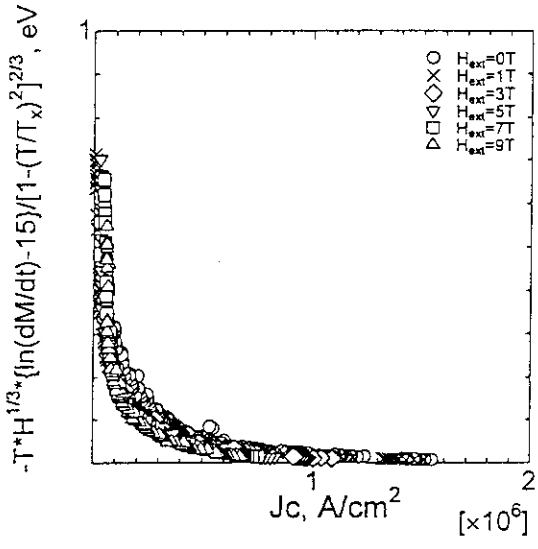

Fig.2 The activation energies in different field can almost be scaled with the factor

References

1)M.Morita, et.al.,Jpn.J.App.Phy.30(1991)813.

2)M.P.Maley, et.al., Phys.Rev.B42(1990)239

3)M.V.Feigel'man, et.al.,Phys.Rev.Lett63(1989)2303

4)P.J.Kung, et.al., Phys.Rev.B46(1992)6427

5)S.Okayasu, et.al.,Trans.Mat.Res.Soc.Jpn.V19A(1994)421

5.5 LINE NATURE OF VORTEX IN Bi-2212 TAPES IRRADIATED WITH 230 MeV Au^{14+} IONS

Y. Kazumata, H. Kumakura[1] and K. Togano[1]

Recent attention for vortex in high T_c superconductors has been forcused on line vortices pinned by columnar defects produced by high energy heavy ions. These line vortices are considered to be most promising for the enhancement of critical current density. However, some experiments showed that the line vortices are divided into the stacks of pancake vortices in the substance with the strong 2D character such as Bi and Tl high T_c superconductors[1,2]. On the contrary to these experimental results, Klein et al[3]. indicated the line nature of vortices (3D) above 50 K from the angular dependence of the applied field relative to columnar defects in a Bi-2212 single crystal. Zech et al[4]. confirmed anisotropic pinning due to columnar defects from the detailed study of the orientation variation of irreversibility line (IL) between the applied field and columnar defects.

In this paper, vortex pinning was compared between columnar and point defects in Bi-2212 tapes irradiated with 230 MeV Au^{14+} ions and 120 MeV O^{7+} ions. The IL observed by O^{7+} irradiation was followed to the scaling rule, but that regarding to columnar defects showed strong uniaxial pinning. Angular dependence of critical current density (J_c) depended on the strength of applied field distant from the irreversibility field (H_{irr}), and a dip in J_c was observed at H//ab-plane. The dip was interpreted as the similar manner to the twin boundary pinning in a YBCO single crystal.

Specimens used in this experiment were grain-oriented Bi-2212 tapes prepared using a doctor blade method. The size of the specimens is 3x4x0.015 mm^3.Irradiations were carried out with 230 MeV Au^{14+} ions and 120 MeV O^{7+} ions by the tandem van de Graaaf accelerator at Japan Atomic Energy Research Institute. The electronic energy loss due to Au^{14+} ions was estimated to be 30 keV/nm[5], of which value was enough to create columnar defects, while point defects were produced by O^{7+} ion irradiation because of the smallness of the electronic stopping power of the ions. All the measurement were performed using the Quantum Design model MPMS superconducting Quantum Interference Device (SQUID).

Angular dependence of H_{irr} at 55K is shown in Fig.1 before and after irradiation, where H_{irr} was obtained from the measurements of hysteresis loops and was defined as the fields at $J_c=1x10^2$ A/cm^2 which was about 0.1% of maximum J_c. The solid lines in this figure were calculated by the eq.

$$H_{irr}=H_{90}/\varepsilon(\theta) \quad (1)$$

$$\varepsilon(\theta)=(\gamma^2\cos^2(\theta)+\sin^2(\theta))^{1/2} \quad (2)$$

where θ is the angle between the applied magnetic field and the ab-plane, and H_{90} is H_{irr} at 90 (H//c-axis). Although γ is the ratio of effective mass m_c/m_{ab}, it was used as a fitted parameter for the experimental values in this case. Double peaks are observed in Au-irradiation. The one at 0 is caused by the intrinsic pinning and the other, a smaller peak, at 90 is due to columnar defects. The double peaks indicates uniaxial vortices(3D). For O-irradiation only a single peak corresponding to the intrinsic pinning is observed because of isotropic nature of point defects. Figure 2 represents J_c at 20 K in 0.5 T and also at 55 K in 0.1 T, respecively. For comparison, J_c at 55 K in 0.6 T is shown for Au-irradiation. Before irradiation, H_{irr} as shown in Fig.1 is lower

than 0.1 T for the angles above 35°. In this case the angular dependence of J_c reflects that of H_{irr}. For O-irradiation, minimum H_{irr} at 90° locates at 0.22 T, of which the value is slightly higher than 0.1 T. J_c shows only a slight field oriantation dependence, although a small maximum due to intrinsic pinning is observed at 0°. For Au-irradiation, H_{irr} is much larger than 0.1 T. A dip on the J_c curve is obseved at 0° and J_c increases slightly with an increase of angles away from the ab-plane. The detailed study of the orientation dependence of the applied field revealed that these characteristic features described just above entirely depended on the strength of the applied field relative to H_{irr}. When J_c in the applied field near H_{irr} was measured, a peak would be observed at 0°, while in the field far lower than H_{irr}, J_c would show a dip at 0°. A similar dip was also observed in a twin boundary in a YBCO single crystal at low temperatures. The twin planes were less effective pinning at low temperatures while the enhancement of J_c due to twin planes was observed at high temperatures. Similar consideration will be applied to the intrinsic pinning between the ab-planes in Bi-2212. Vortices will move along the ab-planes in large J_c region, but can be pinned between the planes in the high applied field near H_{irr}. This interpretation will lead the dip or peak at 0 in the angluar dependence of J_c, depending on the applied field.

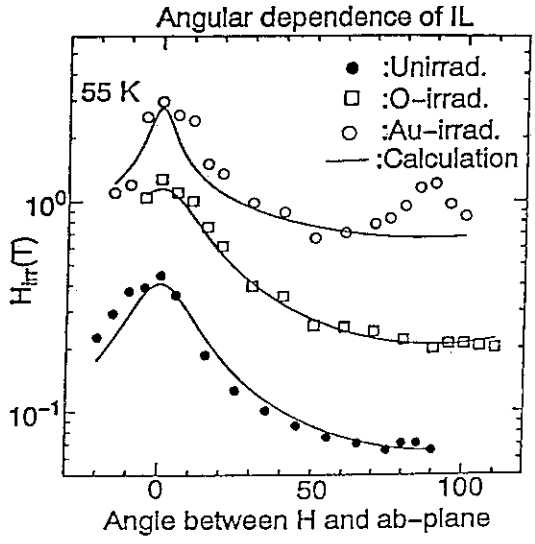

Fig.1 Angular dependence of H_{irr} in the direction of the applied field relative to the ab-plane at 55 K.
○ :Au-irradiation
□ :O-irradiation
● :Before irradiation
—— :Calculation

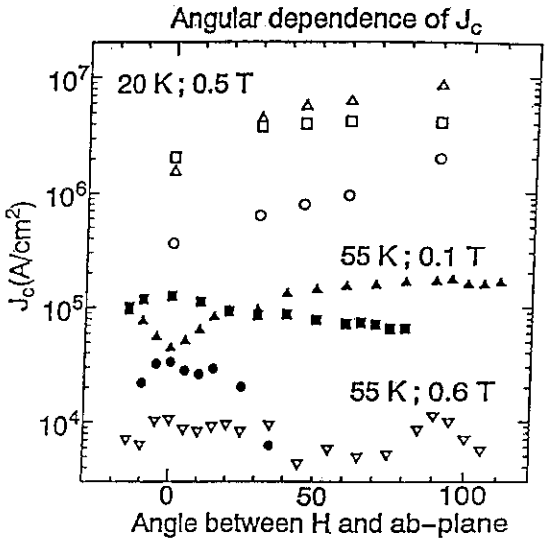

Fig.2 Angular dependence of J_c at 20 and 55 K in 0.5 and 0.1 T field, respectively.
Solid symbols at 55 K.
▲ :Au-irradiation,
■ :O-irradiation,
● :Before irradiation.
For comparison J_c at 55 K in 0.6 T is also shown, ▽.

References
1) W. Gerhauser et al. Phys. Rev. Lett. 68(1992)879
2) J.R. Thompson et al. Appl. Phys. Lett. 60(1992)2306
3) L. Klein et al. Phys. Rev. B48(1993)3523
4) D. Zech et al. Phys. Rev. B52(1995)6913
5) T. Aruga et al. Nucl. Instrum. Method B33(1988)748

1 National Research Institute for Metals

5.6 OBSERVATION OF FLUX-LINE RELAXATION IN ION IRRADIATED $Bi_2Sr_{1.8}CaCu_2O_x$ BY LORENTZ MICROSCOPY

K. HARADA[1], H. KASAI[1], O. KAMIMURA[1], T. MATSUDA[1], A. TONOMURA[1], S. OKAYASU and Y. KAZUMATA

Irradiation with heavy ions of energy of hundreds of MeV creates columnar defects along their linear tracks in the crystal of high-T_C superconductors. These defects act as strong pinning centers for flux lines, thus they enhance the critical current density J_C[1]. The dynamical interaction of flux lines with the defects is a main topic not only of applications but also of the fundamentals of superconductivity. Such dynamics, however, had not been able to be observed until the establishment of the coherent electron beam technique[2]. The columnar defects on $Bi_2Sr_{1.8}CaCu_2O_x$ (BSCCO) were investigated here by observing the dynamic behavior of flux lines by Lorentz microscopy[3].

The experimental setup is illustrated in Fig. 1. A BSCCO film, about 200-nm thick, was cleaved from a single crystal and set on a cold stage with tilting to both the magnetic field and the electron beam. A flux line is seen as a spot consisting of bright and dark regions. The polarity of the flux line is determined from the side on which the dark region is found. Columnar defects were produced by 240-MeV Au^{14+} irradiation by a Tandem accelerator after cleaving. Both irradiated and non-irradiated regions were prepared in one specimen using a mask with 25 X 25 μm^2 windows for the ion irradiation. The dynamical behavior of the flux lines in both regions was simultaneously observed.

Figure 2 (a) shows a Lorentz micrograph of the film cooled to 4.5 K within the field of 15 G, of the area containing both irradiated and non-irradiated regions, whose boundary is indicated by lines. Although flux-line density was initially uniform in (a), the density in both regions changed depending on the magnetic field applied, that is flux-line relaxation. Figure 2(b) is recorded 26 min after switching off the magnetic field. The density decayed in both regions and the difference in density between the two regions increased.

Furthermore, a novel relaxation process was found after the initial flux-line density decreased to less than 0.2 flux lines/mm^2. The reversely polarized flux lines indicated by an arrowhead in (b) began to appear and increased in number with time. This phenomenon has never been observed on non-irradiated or whole-area-irradiated specimens. It is, therefore, considered that a remanent magnetic field held by pinned flux lines produces the opposite magnetic field just out side of the film and generates the reversely polarized flux lines. Newly induced flux lines are gradually attracted to the initial flux lines, and they are

[1] Advanced Research Laboratory, Hitachi, Ltd., Hatoyama, Saitama 350-03, Japan

annihilated to each other. This generation of the flux lines and the occurrence of pair annihilation cannot be observed by macroscopic techniques. Lorentz microscopy revealed the details of the relaxation process by showing the individual flux lines with their polarities.

Figure 3 shows changes in the flux-line density in both regions within 20 min after switching off the magnetic field. The density D(t) in both regions decays logarithmically with time, which is similar to magnetization relaxation. The normalized relaxation rate $S=-1/D_0*(dD/d(\ln t))$ is 0.13 for the non-irradiated region, and 0.11 for the irradiated region with about 20 % difference between them. This difference in the relaxation rates shows the pinning effect of the columnar defects. The logarithmic decay suggests that the flux-line dynamics can be described by the flux creep model. However, the generation and pair-annihilation can not be explained directly from this model.

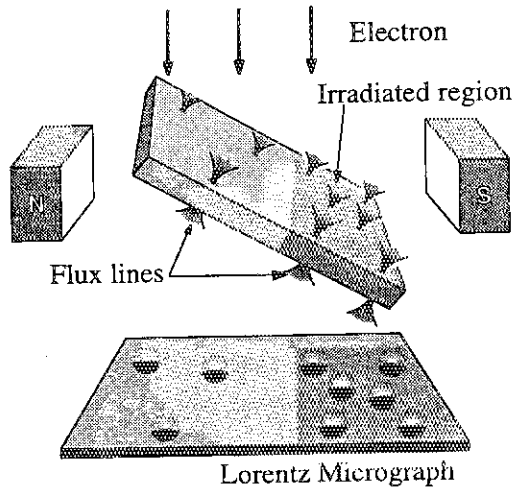

Fig. 1 Experimental arrangement.

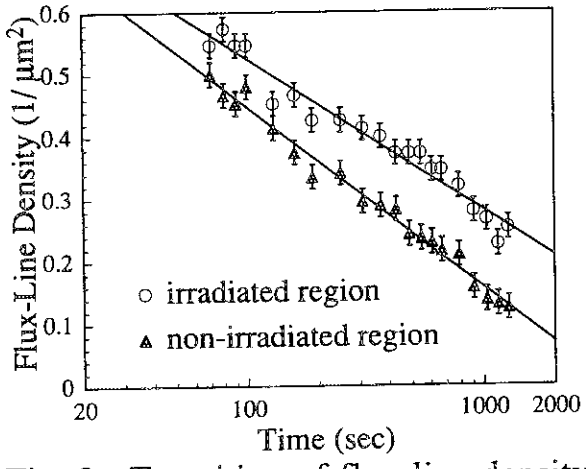

Fig. 3 Transition of flux-line density.

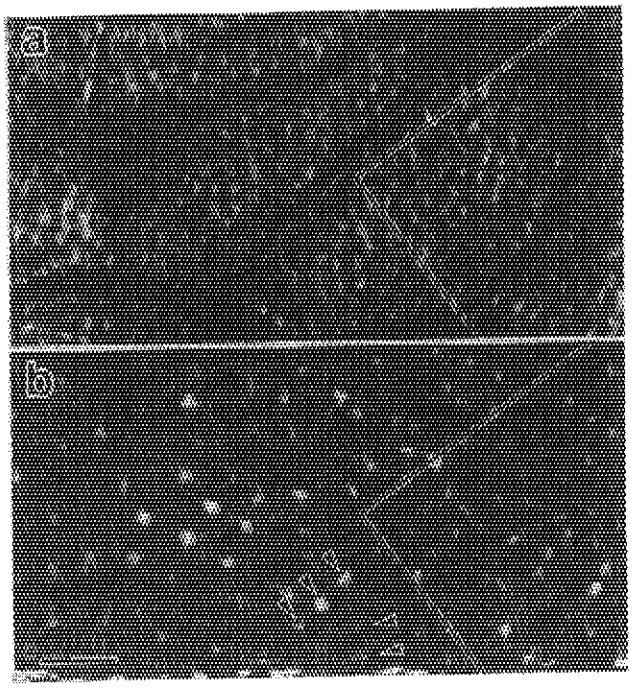

Fig. 2 Lorentz micrographs at 4.5 K: (a) within the magnetic field of 15 G, (b) 26 min after switching off the field.

References

[1] H. Kumakura et al., J. Appl. Phys. **74**, (1993) 451.
[2] K. Harada et al., Nature **360**, (1992) 51.
[3] K. Harada et al., Phys. Rev. **B 53**, (1996) 9400.

5. 7 Effect of Cu^{11+} irradiation on the flux-pinning of $YBa_2Cu_3O_x$ and $Bi_2Sr_2CaCu_2O_y$

H. KUMAKURA[1], H. KITAGUCHI[1], K. TOGANO[1], S. OKAYASU and Y. KAZUMATA

In general, there are large differences in the critical current density J_c and flux-pinning characteristics between $YBa_2Cu_3O_x$(Y-123) and $Bi_2Sr_2CaCu_2O_y$(Bi-2212), especially at high temperatures. From the stand point of conventional flux-pinning theory, this difference should be attributed to the difference of pinning centers and/or their densities. In fact, J_c of high-T_c oxide superconductors strongly depends on the defect structure as in the case of metallic type-II superconductors. A columnar defect introduced by high-energy heavy-ion irradiation is one of the most effective pinning centers[1,2]. However, the effect of the irradiation on the J_c is much different between Y-123 and Bi-2212 as mentioned in our previous report on Cu^{11+} irradiation[3] . In this report, we have done more detailed experiments on the effect of Cu^{11+} irradiation on the flux pinning in Y-123 and Bi-2212.

Samples were textured Y-123 and Bi-2212 thick films. 180MeV Cu^{11+} irradiation was performed at 100K with fluence of 10^{11}-$3x10^{13}$. Pinning characteristics were evaluated from the hysteresis in D.C. magnetization curves. Figure 1 shows the fluence dependence of magnetic hysteresis ΔM at 1T and 24K for Cu^{11+} irradiated Y-123 and Bi-2212. A similar behavior was also observed at different magnetic fields and temperatures. ΔM significantly increased with increasing fluence for both oxide systems, and then, ΔM rapidly decreased for higher fluences. The fluence which gives a maximum ΔM of Y-123 is an order of magnitude larger than that of Bi-2212. This is consistent with the difference in the fluence versus T_c curve between Y-123 and Bi-2212, indicating that the decrease in ΔM at larger fluence is primarily due to the decrease of T_c. The maximum of the enhancement factor, ΔM(irrad.)/ΔM(no irrad.) of Bi-2212 is larger than that of Y-123. However, this is not due to the large ΔM(irrad.) of Bi-2212 but due to the large ΔM(no irrad.) of Y-123. The increase in the absolute J_c values by the irradiation $\Delta J_c=(J_{c,\ \text{after irrad.}}-J_{c,\ \text{no irrad.}})$ for Y-123 is much larger than that for Bi-2212 when compared at optimized fluences. This indicates that the defects introduced by the irradiation act as much more effective pinning centers in Y-123 than in Bi-2212. This difference of pinning behavior between Y-123 and Bi-2212 is due to the difference of two-dimensionality as will be discussed later.

The flux-pinning force density $F_p(J_c \times B)$ versus magnetic field curve of Y-123 is much different from that of Bi-2212. After the Cu^{11+} irradiation, a large difference of the F_p-B curves between Y-123 and Bi-2212 is still observed. Figure 2 shows the normalized pinning-force density $F_p/F_{p,\ max}$ at normalized temperature $T/T_c=0.9$ for Y-123 and Bi-2212 before and after the irradiation as a function of magnetic field. In this figure, the magnetic field is also normalized with irreversibility field B_{irr}. After the irradiation, the normalized field where the F_p becomes maximum shifted to lower field for both Y-123 and Bi-2212. However, this field of Y-123 is still much higher than that of Bi-2212, indicating that the pinning characteristics are much different between the two oxides even after the irradiation.

The decay of magnetization was measured as a function of time. Figure 3 shows examples of Cu^{11+} irradiation effects on the time dependence of the magnetization. The decay of magnetization increases with increasing temperature and magnetic field for both non-irradiated and irradiated oxides. The decay of magnetization of Y-123 is much smaller than that of Bi-2212 not only for non-irradiated samples but also for irradiated samples, suggesting that the decay of magnetization depends more sensitively on the material rather than on the kinds of pinning centers. This difference of the decay of magnetization between Y-123 and Bi-2212

[1]1st Research Group, National Research Institute for Metals

becomes larger with increasing temperature and magnetic field.

The results mentioned above indicate that the defects in Y-123 are more effective as pinning centers than those in Bi-2212. This difference can be understood in terms of the difference in two-dimensionality of the oxides. For flux lines in superconductors such as Bi-2212 having a weakly coupled layer structure, the so-called two-dimensional pancake model is applicable when magnetic fields are parallel to the *c*-axis. In this model, the stacks of pancakes are easily sheared along the *a* or *b* direction, and hence flux lines are not rigid but very flexible. Hence, depinning of one or a few pancakes from the columnar defects occurs with the aid of thermal activation, and a small J_c and small pinning energy is obtained. For Y-123, having a stronger coupling of the superconducting Cu-O layers, flux lines are more rigid and simultaneous depinning of a larger number of pancakes are associated with depinning of a flux line resulting in a larger pinning force and higher J_c values.

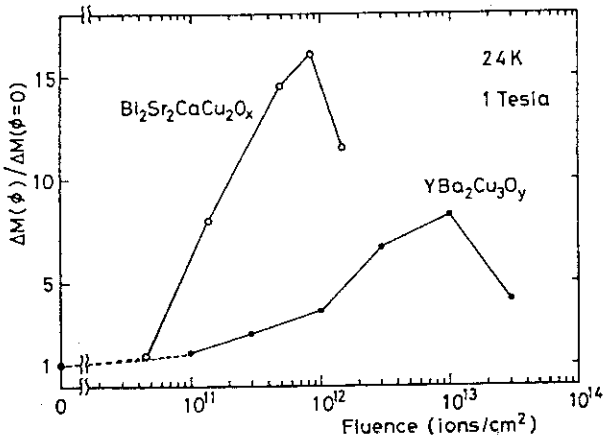

Fig. 1. Fluence dependence of ΔM at 24K.

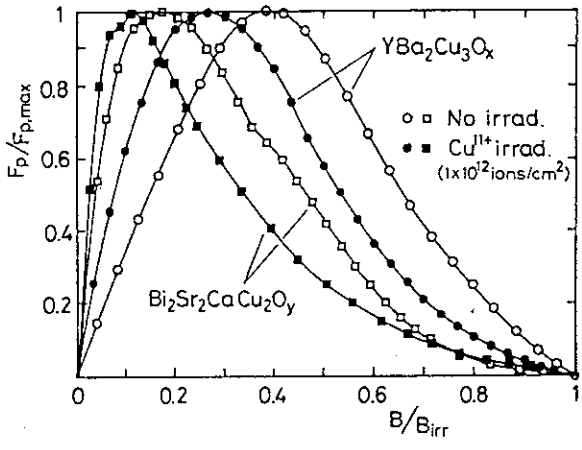

Fig. 2. Pinning force density vs. field curves.

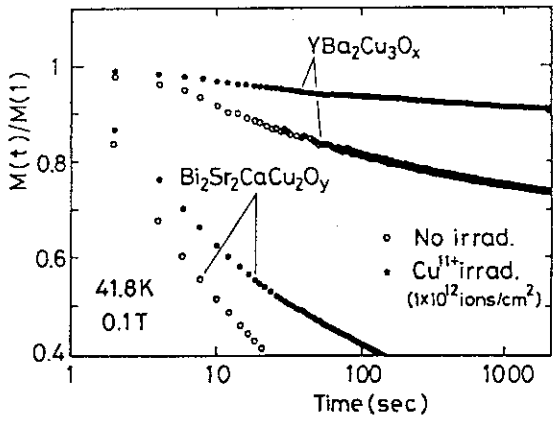

Fig. 3. Decay of magnetization at 41.8K

References

1)L.Civale, A.D. Marwick, T.K. Worthington, M.A. Kirk, J.R. Thompson, L. Krusin-Elbaum, Y.R. Sun, J.R. Clem and F. Holtzber, Phys. Rev. Lett. 67(1991)648.
2)H. Kumakura, H. Kitaguchi, K. Togano, H. Maeda, J. Shimoyama, S. Okayasu and Y. Kazumata, J. Appl. Phys. 74(1993)451.
3) H. Kumakura, H. Kitaguchi, K. Togano, S. Okayasu and Y. Kazumata, JAERI-Review 95-017(1995)p.65.

5.8 IRRADIATION DEFECTS WITH Fe IONS AS FLUX PINNING CENTERS IN $Bi_2Sr_2CaCu_2O_x$ SINGLE CRYSTAL

Y. SASAKI, W.L. Zhou and Y. IKUHARA[1]

$Bi_2Sr_2CaCu_2O_x$ single crystals irradiated with 18 MeV Fe^{8+} ions were investigated by TEM [1],[2]." Optimum fluence for the enhancement of critical current density was found to be strongly dependent with size and distribution of the cascade defects. Moreover, the irradiations with 180 MeV Fe ions were tried for inducing defects with another shape. The critical current density was enhanced in the several samples of them, comparing with that of 18 MeV Fe^{8+} ion irradiation samples in lower fluence.

Thin pieces of $Bi_2Sr_2CaCu_2O_x$ single crystal employed for irradiation experiment were cut out from a sample rod (FZ sample) prepared by floating zone melting method [3]. The experiments of ion irradiation were performed with tandem-type ion injection systems at Japan Atomic Energy Research Institute and Ion Engineering Center Corporation. The orientation of ion irradiation was set parallel to the c-axis. The modification effect of superconductivity by ion irradiation was evaluated by changes in magnetic moment ΔM at 50K before and after irradiation using SQUID.
Irradiation damages were observed both parallel and perpendicular to the axis of ion irradiation using a high-resolution TEM. The defect density and average defect diameter were determined from these observation results using an image processing system.

Fig.1 presents the magnetization property of samples after the irradiation of Fe^{8+} ions in the fluence range of $1x10^{11}$~10^{13} ions/cm^2 at 18MeV. ΔM and the saturation field increase monotonously under the fluence of $1x10^{12}$ ions/cm^2, and it decreases at $1x10^{13}$ ions/cm^2. This indicates that defect formed by irradiation act as magnetic flux pinning centers until their density reaches a certain value, over which they do not function.
Fig.2 shows the image of high-resolution electron microscope of a sample after Fe^{8+} ion irradiation ($1x10^{12}$ ions/cm^2). The damage caused by irradiation is observed as a white, oval

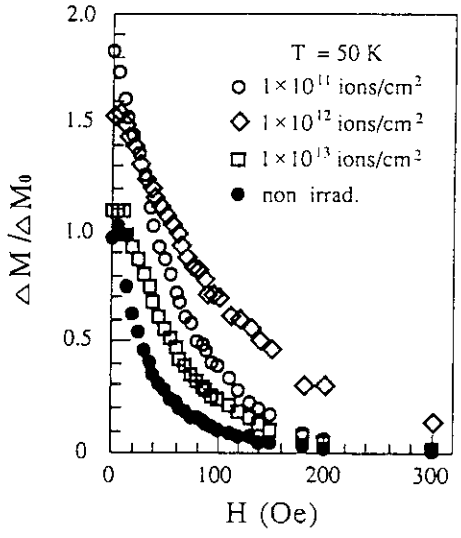

Fig 1. Effect of 18 MeV Fe irradiation on ΔM/ΔMo vs. magnetic field at 50k for Bi2Sr2CaCu2Ox single crystals.

[1] Japan Fine Ceramics Center

contrast. The irradiation defects were distributed in the range approximately 0.5um wide at approximately 4.5um form the surface, and no defect was observed in the region from the surface. Considering the thickness of observation samples and defect distribution width, it is estimated that defects $7\pm 1x10^{12}$ ions/cm^2 in number were formed. Furthermore, the average size of a single defect was approximately 10nm.
However, the cascade defects introduced by low energy irradiation are not effective as flux pinning center to be distributed over only a part of domain. For introduction of more effective flux pinning center, we have tried to introduce columnar defects by the ion irradiation at high energy (180MeV). As the result, we confirmed improvement of Jc largely as shown in Fig.3.
In future, we will observe the irradiation defects in these samples by TEM, and consider the relations between the defect structure and flux pinning. Furthermore, we will investigate the influence of stacking fault and point defects in superconductor on the creation of irradiation defects.

Fig 2. High magnified cross-sectional micrograph of 18 MeV Fe ion irradiation sample.

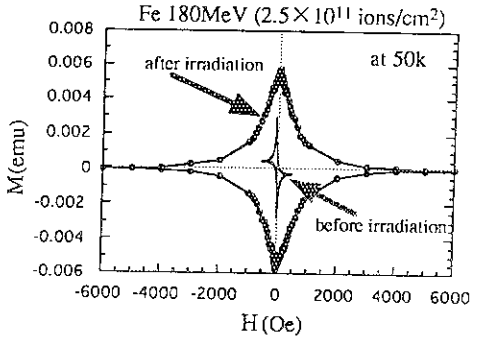

Fig 3. Effect of 180 MeV Fe irradiation on magnetization vs. magnetic field at 50k for Bi2Sr2CaCu2Ox single crystals.

Reference

1) Y. Sasaki, W.L. Zhou, Y. Ishiguro and Y. Ikuhara, J. Ceram. Soc. Jpn., 103 (1995) 195-198
2) W.L. Zhou, Y. Sasaki and Y. Ikuhara, Physica C, 234 (1994) 323-332
3) Y. Kubo, K. Michisita, Y. Higashida, M. Mizuno, H. Yokoyama, N. Shimizu, E. Inukai, N. Kuroda and H. Yoshida, J. Appl. Phys., 28 (1989) L606

5.9 EFFECTS OF 240MeV Au^{14+} ION IRRADIATION ON THE CRITICAL CURRENT DENSITY OF Bi-2212 SINGLE CRYSTALS

T.TERAI[1], Y. ITO[1], S. OKAYASU and Y. KAZUMATA

Particle-beam irradiation is one of the most promising methods to introduce strong pinning centers into High-Tc superconductors. It has been reported that the critical current density (Jc) is enhanced by the irradiation of high-energy particles such as ions, neutrons and electrons[1-3]. In particular, high energy heavy ions are expected to produce columnar defects of a diameter close to the coherence length, which give a very large pinning force for vortices. In order to realize a particle-beam irradiation technique as a method for Jc enhancement, many different conditions such as the kind, the energy and the fluence of particles should be examined. We have been studying magnetic property change due to irradiation with several kinds of particles such as ions, neutrons and electrons on $Bi_2Sr_2CaCu_2O_{8+y}$ (Bi-2212) single crystal. In this paper, we show some experimental results on the critical current density (Jc) of Bi-2212 single crystal irradiated with 240MeV Au^{14+} ions.

The Bi-2212 single crystal specimens used were prepared by the floating-zone method (FZ). Their size was 2mm x 2mm x 50-80μm. The specimens were irradiated with 240MeV Au^{14+} ion beam parallel to the c-axis with a Tandem accelerator at JAERI. The fluences were $5x10^{10}$, $5x10^{11}$ and $1x10^{12}$ cm^{-2} corresponding to the matching field of 1T, 10T and 20T respectively. Magnetization curves of the specimens before and after irradiation were measured with a vibrating sample magnetometer at 4.3K, 20K, 40K and 60K as a function of applied magnetic field. The magnetic field was applied up to 7.5T parallel to the c-axis with the sweep rate of $1mT\cdot s^{-1}$ to $20mT\cdot s^{-1}$. The critical current density was calculated from the magnetization hysteresis using the modified Bean's model expressed in the following equation[4]:

$$\Delta M = \frac{J_c^{ab} t}{2}\left(1-\frac{t}{3l}\right) \quad \text{for} \quad l > t ,$$

where ΔM is magnetization hysteresis in Am^{-1}, J_c critical current density in Am^{-2}, and l, and t, the width and the length of specimen in m, respectively.

Figure 1 shows the magnetization curves at 4.3, 20, 40 and 60K before and after irradiation with different fluences. The magnetic field dependence of critical current density (Jc) calculated from the magnetic hysteresis at 40 K is shown in Fig. 2. Figure 3 shows the fluence dependence of Jc in typical conditions of temperature and magnetic field. The critical current density increased due to the irradiation all over the range of temperature and magnetic field investigated except 4.3K. At 4.3K, Jc slightly decreased with fluence. This little change in the low temperature of 4.3K means that the defects existing in the specimen before irradiation can act as effective pinning centers even after irradiation at such a low temperature. Above 40K, on the other hand, Jc took a maximum value at the fluence of $5.0x10^{10}$ cm^{-2}. The enhancement ratio of Jc mainly depended on temperature and it was larger at the relatively high temperatures of 40 and 60K. The enhancement ratio was the largest (~3000) at 60 K in Fig. 3. This very large increase in the relatively high temperatures of 40 and 60K indicates that contribution of radiation-induced defects is dominant after irradiation. Figure 4 shows the irreversibility field, where Jc disappears, also increased due to Au ion irradiation at 40K and 60K.

References

1) K. Kusagaya, T. Terai, T. Kobayashi, N. Chikumoto, K. Kishio and K. Park, Advances in Superconductivity VI (Springer-Verlag, Tokyo, 1994) pp. 555-558.

[1]Department of Quantum Engineering and Systems Science, University of Tokyo.

2) W. Gerhäuser, H.W. Neumüller, W. Schmidt, G. Ries, G. Saemann-Ischenko and S. Klamünyer, Physica C 185-189 (1991) 2339.
3) B. Chenevier, S. Ikeda, H. Kumakura, K. Togano, S. Okayasu and Y. Kazumata, Jpn. J. Appl. Phys. 31 (1992), L777.
4) E.M. Gyorgy, Appl. Phys. Lett. 55 (1989) 283.

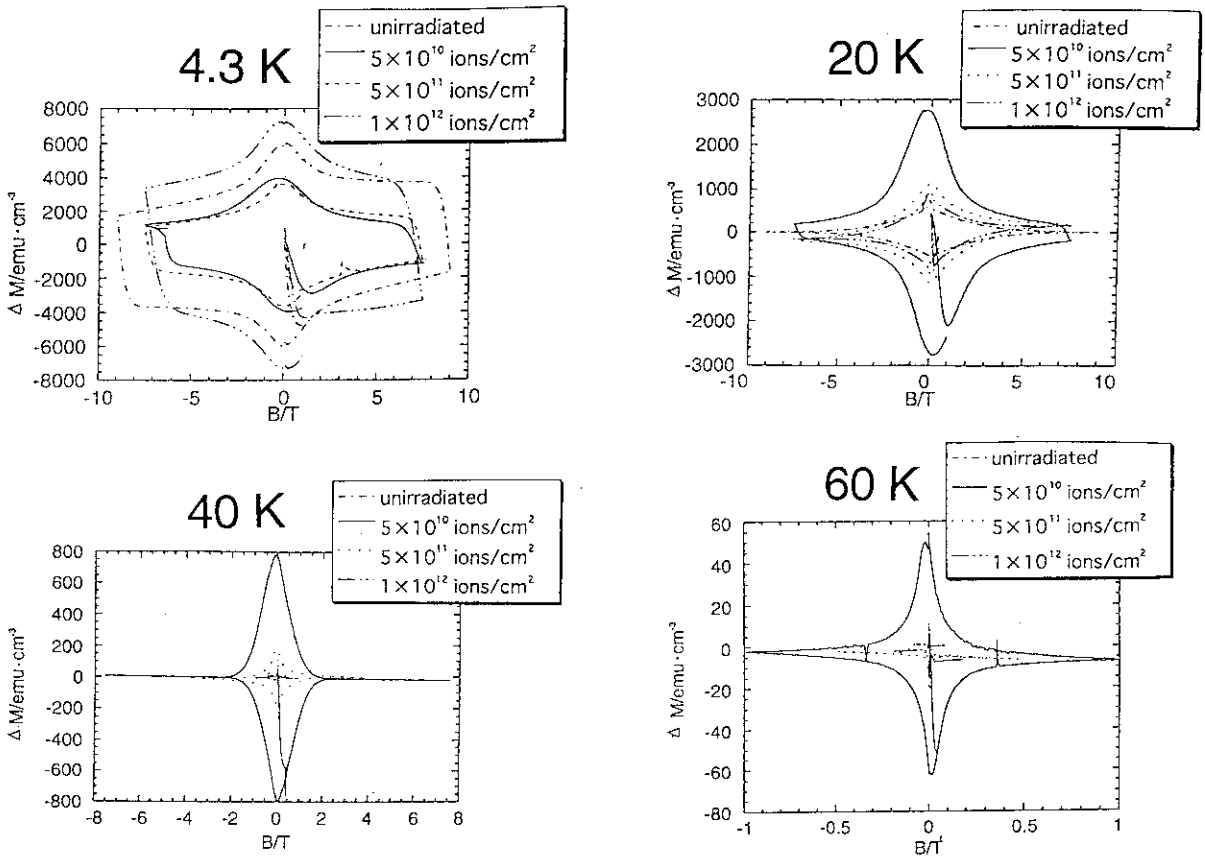

Fig. 1 Magnetization curves of Bi-2212 single crystal specimens at 4.3, 20, 40 and 60 K before and after 240 MeV Au^{14+} ion irradiation.

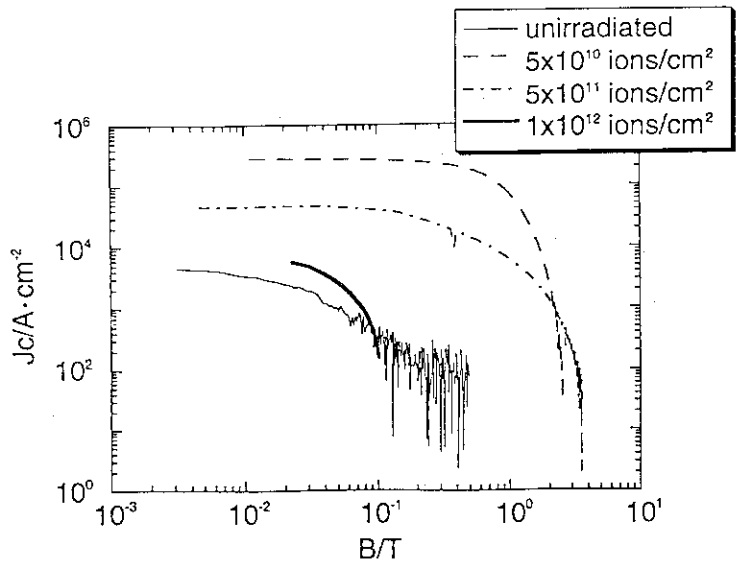

Fig. 2 Magnetic field dependence of Jc at 40 K on Bi-2212 single crystal specimens irradiated with 240 MeV Au^{14+} ions.

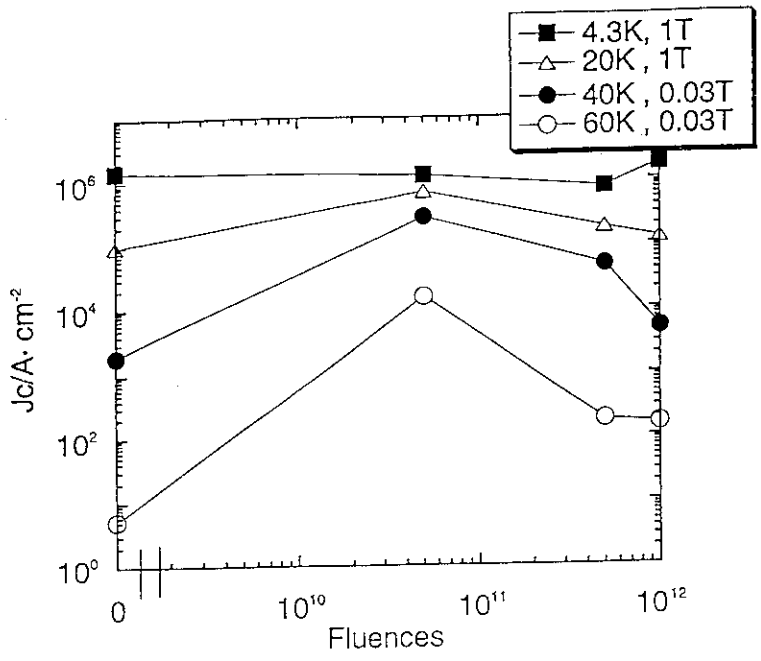

Fig. 3 Dependence of 240 MeV Au^{14+} ion fluence on Jc of Bi-2212 single crystal specimens.

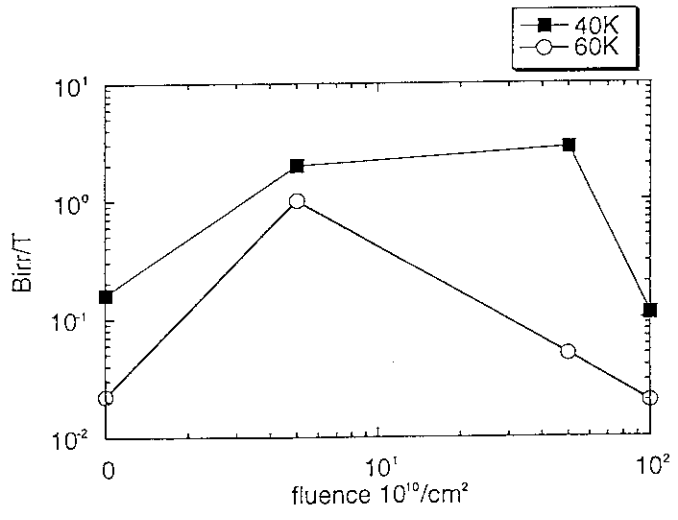

Fig. 4 Dependence of 240 MeV Au^{14+} ion fluence on irreversibility field of Bi-2212 single crystal specimens.

5. 10 Emission of Secondary Ions from the Foil Bombarded with Heavy Ions

T.SEKIOKA[1], M.TERASAWA[1], M.SATAKA and S.KITAZAWA

The electron transport property of high temperature superconductors (HTSC) can be improved remarkably by irradiation of high energy heavy ions at low ion fluence [1,2,3]. This is due to the pinning effect of the created defects which hinder the easy motion of the magnetic flux vortices, so that the critical current density in a high magnetic field is drastically enhanced. High electronic excitations play an important role in the damage process by high energy heavy ions. However, the conversion mechanism of the energy of the excited electrons into kinetic energy for the target atoms is not well understood. The incident ion creates in its wake a cylinder of highly ionized matter. This region is very unstable due to Coulomb repulsion, and a radial kinetic energy is transferred to the highly ionized atoms. If both of adjacent Cu atoms in a high T_C copper oxides are fully ionized, the ions can be accelerated more than 3 keV due to a Coulomb explosion. According to the computer calculation by Averback et al. [4], the cascade collisions can be induced by several keV Cu ions. The columnar defects may be interpreted as the assemblage of such cascades along the incident ion path.

We have been investigating the secondary ions mass spectroscopy from the solid targets by the heavy ion beam from the Tandem accelerator at JAERI, searching for the energetic highly charged target ions produced by Coulomb explosion. Figure 1 shows the Time of Flight (TOF) mass spectra for the secondary ions sputtered from the C-foil (fig.1a) and the Au evaporated C-foil (fig.1b) by the 80 MeV I^{7+} ion beam irradiation. The energy loss of this ion beam is higher than 2 keV/Å above which the electronic energy loss contributes remarkably to the defect production in HTSC [3]. In both fig.1(a) and fig.1(b), we can see C^+ ion peak and the peaks of the ions of hydrogen, sodium and others which might be contained in the foil. The peak around 750 channel in the both figures corresponds to mass to charge ratio of about 55, and may be attributed to C_4 cluster with several hydrogen atoms. In fig.1(b), a broad peak which can be attributed to the sputtered Au^+ ions is observed.

We are planning to investigate the secondary ions mass spectroscopy with more statistical accuracy to identify the energetic highly charged target ions produced by Coulomb explosion.

References

1) M.Terasawa, T.Mitamura, T.Kohara, K.Ueda, H.Tsubakino, A.Yamamoto, Y.Awaya, T.Kambara, Y.Kanai, M.Oura and Y.Nakai, Physica C 235-240 (1994) 2805
2) V.Hardy, J.Provost, D.Groult, Ch.Simon, M.Hervieu, S.Bouffard and B.Raveau, Radiation Effects and Defects in Solids, vol.126, (1993) 137
3) M.Kraus, P.van Haßelt, J.P.Ströbel, S.Peehs, M.Leghissa, G.Kreiselmeyer, B.Holzapfel, W.Gerhäuser, B.Hensel, S.Klaumünzer, S.Bouffard and G.Saemann-Ischenko, Radiation Effects and Defects in Solids, vol.126, (1993) 147
4) R.S.Averback, T.Diaz de la Rubia and R.Benedek, Nucl. Instr. and Meth. B33 (1988) 693

[1]Faculty of Engineering, Himeji Institute of Technology

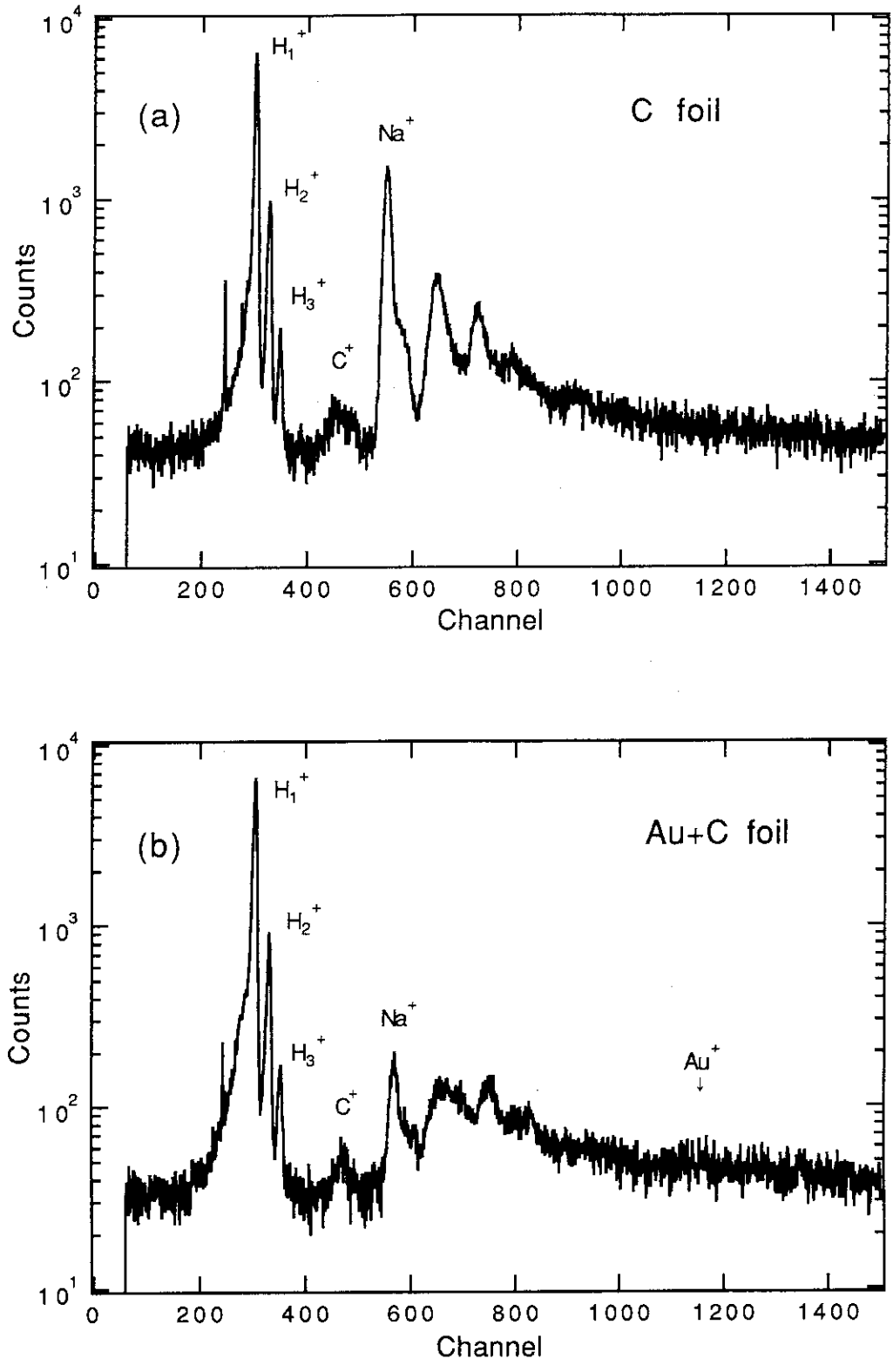

Fig.1. The TOF spectra of the sputtered ions by the 80 MeV I^{7+} ion beam from the C-foil (a) and Au evaporated C-foil (b).

5.11 X-RAY DIFFUSE SCATTERING STUDY OF VACANCY AND INTERSTITIAL LOOPS IN HEAVY ION-IRRADIATED GOLD

H. MAETA, H. OTSUKA, N. MATSUMOTO, H. SUGAI K. HARUNA[1], T. SAOTOME[1], K. OHASHI[1], and F. ONO[2],

Irradiation of materials with energetic ions produces displacement cascades containing high local concentrations of vacancy -interstitial pairs, and at ambient temperature these vacancies and interstitials aggregated to form clusters such as dislocation loops, stacking fault tetrahedra, or voids. Transmission electron microscopy and field ion microscopy investigations of the production and thermal annealing of cascades have provided a considerable amount of information on this process. However, additional quantitative information regarding cascade sizes , morphologies, internal defect densities and thermal evolution is needed for comparison with theoretical calculations and for obtaining a more complete picture of the physics of defect production and defect interaction. Even though scattering techniques do not offer direct imaging of defects as available through micrograpy, x-ray diffuse scattering provides information complementary to that obtained by microscopy imaging in the sense that the defects are studied nondestructively in bulk with inherently good sampling statistics.

In general the diffuse scattering cross-section must be calculated numerically for detailed application [1], but an overall form of the scattering can be identified in the so-called "Huang " and "asymptotic " region for which

$$|A(K)|^2 \sim \left\{\frac{Kb\pi R^2}{q}\right\}^2 \qquad q << 1/R \quad \text{Huang scattering}$$

$$|A(K)|^2 \sim \left\{\frac{Kb\pi R^2}{q^4}\right\} \qquad q > 1/R \quad \text{Asymptotic scattering}$$

where scattering vector $K = h + q$ specifies the measuring position in reciprocal space in terms of the reciprocal vector h and a vector q relative to h. R is radius of dislocation loop and b Burgers vector. The "asymptotic " scattering region falling off as

[1] Faculty of Engineering, Tamagawa University,
[2] Department of Science, Okayama University

the inverse fourth power of q is characterized physically by local Bragg scattering from the highly distorted lattice near the dislocation loop plane. Because the highly distorted region lying near(above and below) interstitial loops is compressed and the corresponding region were expanded for vacancy loops, the local Bragg scattering from interstitial and vacancy loops lies on opposite sides of the Bragg reflection. This separation of the scattering in reciprocal space has made it possible to study vacancy and interstitial loops independently using measurements along the [111] symmetry direction[2].

We have reported an " off-symmetry" x-ray diffuse measurements using the synchrotoron radiation source for the study of dislocation loops in the B ion-irradiated gold. The specimens of the single crystals with <111> orientation were irradiated at 30 K with 70 MeV B ions using 20 MV tandem Accelerator to fluence of 1.8×10^{15} ions/cm^2. Diffuse scattering experiments were performed on a four-circle diffractometer installed at BL-27B at the Photon Factory of the KEK in Tsukuba. The diffuse scattering near the 111 reflection was measured at room temperature. The measured diffuse scattering for B ion irradiated gold is shown in the Fig. 1. These data are scaled by $q^4$and plotted as a function q along the 111 direction in reciprocal space. We note that the scattering magnitudes were found to be relatively comparable for positive and negative q for the irradiation, suggesting the present of substantial numbers of both vacancy and interstitial loops. The average size of the loops was estimated to be about 0.5 nm.

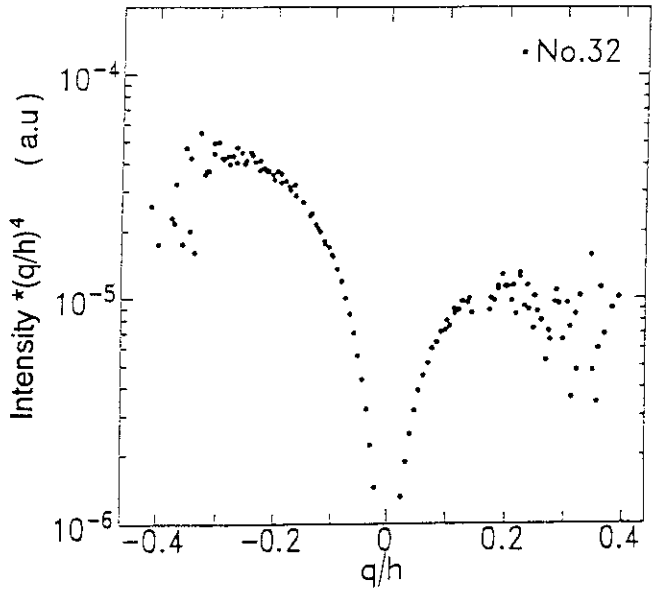

Fig. 1 Measured diffuse scattering for the irradiated gold. Measured intensities scaled by q^4 in order to see the asymptotic region carrying the information on the vacancy-interstitial nature of the loops.

References

1) P.Eherhart, H.Trinkaus and B.C.Larson, Phys. Rev. B25(1982)832.
2) H. Maeta, B.C.Larson ,T.P.Sjoreen, D.K.Thomas, O.S. Oen and J. D. Lewis, Mat. Res. Soc. Symp. Proc. 138(1989) p. 81.

5.12 HEAVY ION IRRADIATION EFFECT ON ELECTRICAL RESISTIVITY OF P-DOPED SILICON AT LOW TEMPERATURE

H. SUGAI, H. MAETA, H. OTSUKA, N. MATUMOTO,
K. HARUNA,[1] and F. ONO[2]

Recently, we can get the synthetic B-doped diamond (p-type semiconductor), but not the diamond of n-type semiconductor [1]. B-doped diamond is destined for use in a number of sensor applications in high radiation environments. In the previous works [2-3], we studied the resistivity and the structual changes of B-doped diamond irradiated with heavy ions at low temperature. In order to make clear the irradiation effects on B-doped diamond, it is important to study the irradiation effects on the materials which has the same crystal structure as diamond. In this report, we present the preliminary result of the resitivity change of P-doped Si irradiated with 180 MeV F^{11+} ions at tempertures below 19 K.

A single crystal wafer of P-doped Si was purchased from the Nilaco Corporation. The wafer is n-type semiconductor, which contains carrier of 0.7 x 10^{15} to 0.1 x 10^{16} cm^{-3}, and the surface parallels the (111) plane. The spcimen (5 mm x 6 mm x 0.5 mm) were cut from the wafer (100 mm in diamter and 0.5 mm in thickness). The specimen were irradiated with 180 MeV F^{11+} ions perpendicular to the surface of spcimen at temperatures below 19 K using the tandem accelerator at JAERI. The total fluence was 0.9 x 10^{14} cm^{-2}. Before and afer irradiation, the resistivity of the irradiated plane of specimen was measured by the van der Pauw method at temperatures between 18 K and 285 K. During irradiation, the temperature of specimen was kept below 19 K and the fluence dependence of the resistivity was measured at 18 K at the time that ion beam was interrupted periodically.

The range of 180 MeV F-ion in Si was estimated to be 30.4 μm using TRIM compuer program. In general, the possible depth to measure the resistivity of semiconductor by the van der Pauw method is shallower than one μm [4]. Therefore, the dominant origin of the resistivity change induced by 180 MeV F-ion irradiation is not the ion implantation, but the damage due to nuclear and electronic energy loss of ion. Figure 1 shows the fluence dependence of the resistivity of P-doped Si irradiated at temperatures below 19 K. The resistivity changes non-monotonicaly with inceasing the ion fluence and the fluence dependence of the resistivity has a maximum around the fluence of

[1]Faculty of Engineering, Tamagawa University
[2]Faculty of Science, Okayama University

0.2×10^{14} cm^{-2}. The non-monotonic fluence dependece of the resistivity is also observed for the B-doped diamond irradiated with 150 MeV P-ion below 30 K [5], and the fluence dependece of resistivity for the diamond has a minimum to the contrary. The possible origins of these non-monotonic behaviors of resistivity are carrier scattering and impurity conduction [6] due to the lattice disorder induced by ion irradiation at low temperature. In the case of Si, many kinds of defects introduced by irradiation at low temperature are reported [7].

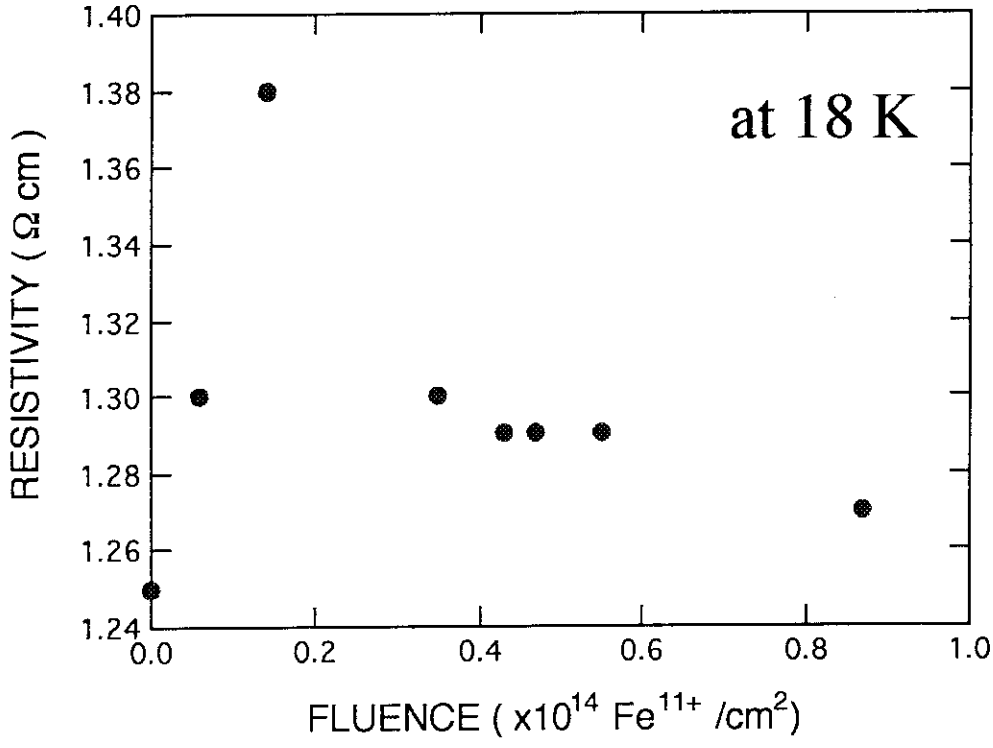

Fig. 1 Fluence dependece of resistivity of Si irradiated with 180 MeV Fe^{11+} ions at temperatures below 19 K.

References

1) M. S. Dresselhaus and R. Kalish, Ion Implantation in Diamond, Graphite and Related Materials (Springer-Verlag, Berlin, Heidelberg and New York, 1922).
2) K. Haruna, H. Maeta, H. Sugai, T. Sato, T. Ootsuki, K. Iwasita, Y. Saito, K. Ohashi, N. Matsumoto, H. Otsuka and F. Ono, to be published in Diamond and Related Materials (1996).
3) H. Maeta, K. Haruna, Lu Bang and F. Ono, Nucl. Instr. and Meth., B80/81 (1993) 1477.
4) For example, H. Ryssel and I. Ruge, Ion Implantation (John Wiley and Sons, New York and Toronto, 1986) p. 188.
5) K. Haruna, private communication.
6) N. F. Mott and W. D. Twose, Adv. Phys. 10 (1961) 107.
7) For example, S. Ishino, Oyo buturi, 46 (1977) 458 [in Japanese].

5.13 X-RAY STUDY OF IRRADIATION DEFECTS CAUSED BY MeV ION IMPLANTATION INTO Si PERFECT CRYSTALS

M.KURIBAYASHI[1)], A.INOUE[1)], K.TAKUMI[1)], T.KANAMARU[1)], H.KATOH[1)], K.ISHIDA[1)], K.AIZAWA, S.OKAYASU, H.TOMIMITU and Y.KAZUMATA

We have studied the nature of the strain layer caused by high energy,over several tens MeV, ion implantation for perfect Si single crystals using the X-ray diffraction [1-3].
So far the following points are studied,
(1) characteristic properties of strain distributions caused by implantations of various ion species.
(2) the observed profile of the lattice strain has a close resemblance to the distribution of the energy loss per unit length [4].
(3) effects of an ion energy and magnitude of dose on the X-ray diffraction profiles.
(4) characteristic properties of X-ray diffraction profiles obtained by various reflection planes.

In this report,we investigate
(5) effects of heat treatments on the strain distribution.

Cu ions were implanted into Si(111) wafers using the tandem Van de Graff accelerator in JAERI at Tokai. The ion energy and the dose were 80MeV and 10^{14} ions/cm^2, respectively. During the implantation the sample holder was cooled with liquid nitrogen.
X-ray rocking curves from distorted crystals were measured by a precise diffractmeter controlled by a computer system with a monochromator system of Si(440) and Si(220) grooved crystals of (+,+)setting.
A series of rocking curves observed before and after heat treatments for the same sample wafer are shown in Fig.1,The heat treatment of each stage was carried out following the previous treatment. Annealing the sample at 325 °C for 30 min.,the rocking curve can not be distinguished from that of the perfect crystal, so that the strain is completely vanished. The strain distributions can be calculated from the rocking curves using the X-ray diffraction theory in distorted crystals [5]. The results are shown in Fig.2. Details of relation between the heat treatment and recovering of the lattice distortion are now in progress.

References

1)H.Tanaka et al., JAERI TANDEM and V.D.G. Report 1992(1993)pp47-50.
2)M.Kuribayashi et al. JAERI TANDEM and V.D.G. Report 1993(1994)pp67-68.
3)M.Kuribayashi et al. JAERI TANDEM and V.D.G. Report 1994(1995)pp73-74.
4)T.Aruga, K.Nakata and S.Takamura: Nuch. Instr. and Meth., **B33**(1988)748.
5)S.Takagi; J.Phys.Soc.Jpn., 26(1969)1239.

---

1)Dept. of Physics, Faculty of Science and Technology, Science Univ. of Tokyo

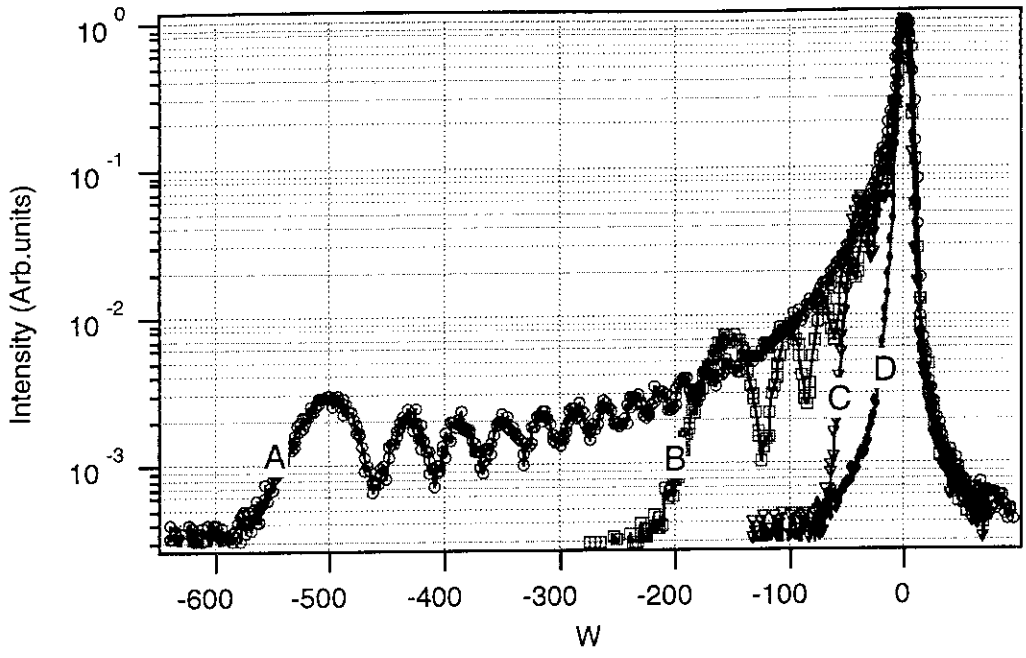

Fig.1. Rocking curves observed in the vicinity of the (333) reflection spot with Cu-Kα_1 radiation for the same sample before and after heat treatments. A; before annealing (just after an ion implantation). B;annealing at 150 °C for 30 min.. C; at 250 °C. D; at 325 °C.

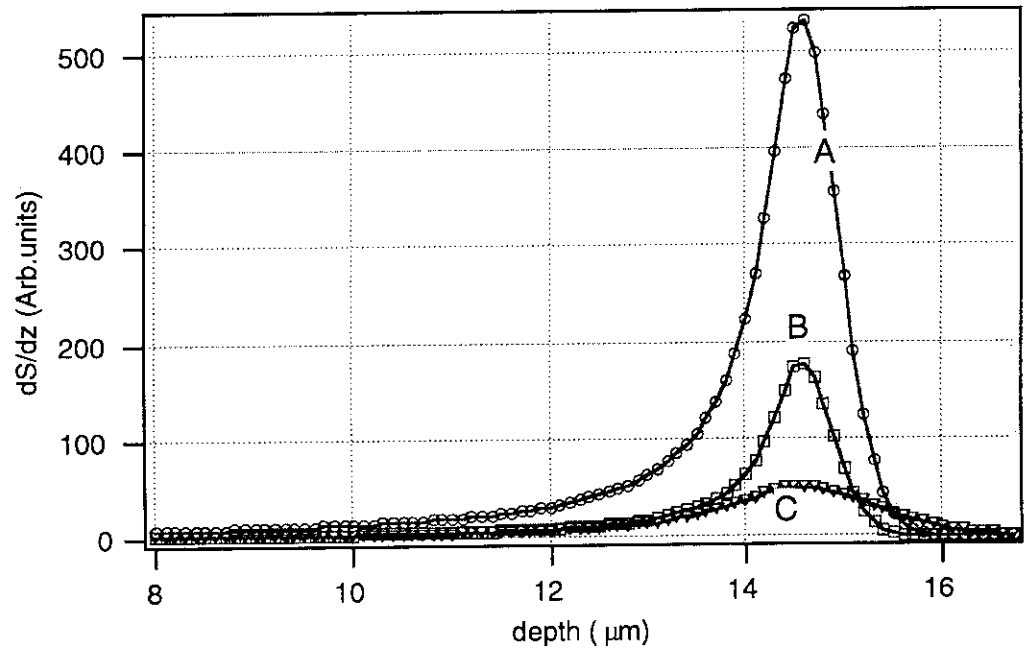

Fif.2. The strain distribution obtained from the rocking curves in Fig.1.

5. 14 ELECTRICAL CONDUCTIVITY OF B-DOPED SYNTHETIC DIAMONDS IRRADIATED BY HEAVY IONS

K.HARUNA[1] ,H.MAETA, H.SUGAI, T.SATO[1],T.OTSUKI[1], F.ONO [2] ,
H.OTSUKA and K.OHASHI [1]

Interesting properties of diamond, such as high thermal conductivity, good thermal and chemical stability make it attractive for use in high temperature semiconductor devices. It is very strong against radiation and fits to the electronic devices in the high temperature region owing to the wide energy gap. In order to make the devices that operate under the circumstances of cosmos and reactor , it is needed to investigate the effects of high energy ion irradiation on the electrical properties of diamond. B-doped diamond is destined for use in a number of sensor applications in high radiation environments. In this study we provide some preliminary data showing that the resistance of a B-doped diamond changes little under 150 MeV P irradiation.

The synthetic B-doped single crystal diamonds which are p-type were purchased from Sumitomo Denki Co.Ltd. The P-ion irradiations were carried out by a tandem accelerator at JAERI. 150 MeV P^{9+} were used in this study. The electrical conductivity before and after the irradiations was measured in a liquid helium-cryostat using the van der Pauw method. The temperature dependence of the specimen during ion-irradiation was kept below about 30 K. Fig.1 shows the conductivity of the irradiated specimen at 20K plotted against irradiation fluence. It shows that the conductivity increases with fluence up to maximum fluence(F_{max}=1.0x10^{14}/cm^2) ,having a maximum at F_{max} , and then decreases with increasing fluence. and the conductivity becomes as same as before irradiation with the further irradiation. The range of 150 MeV P-ion in diamond was estimated to be 26.6 μ m using TRIM computer program. Therefore, the origin of the conductivity change induced by 150 MeV P-ion irradiation is not the damage due to the nuclear energy loss of ion and the implantation itself, but the damage due to the electronic energy loss of ion. Thus, this work is originally the cleanest experiment to examine the effect of radiation damage to the

[1] Faculty of Engineering,Tamagawa University
[2] Faculty of Science,Okayama University

conductivity of diamond. Since our X-ray diffraction study [1] suggests a formation of defects and defect clusters into dislocation loops in the B-doped diamond irradiated by 150 MeV P ion, we suppose the conduction mechanism for the fluence dependence of the conductivity of irradiated specimen as follows. The monotonic increase of conductivity below F_{max} is attributed to the increase of isolated point defects which would be the origin of impurity conduction, on the other hand, the monotonic decrease of conductivity above F_{max} is attributed to a formation of defects and defect clusters into dislocation loops which would be the origin of carrier scattering. The 150 MeV P-ion irradiation introduces the defects in crystals and the conductivity change at very low temperatures (20K) is associated with the quantity and kind of defects. It was found that an introduction of an intermediate number of defects enhances the conduction at low temperatures and too many defects decreases it.

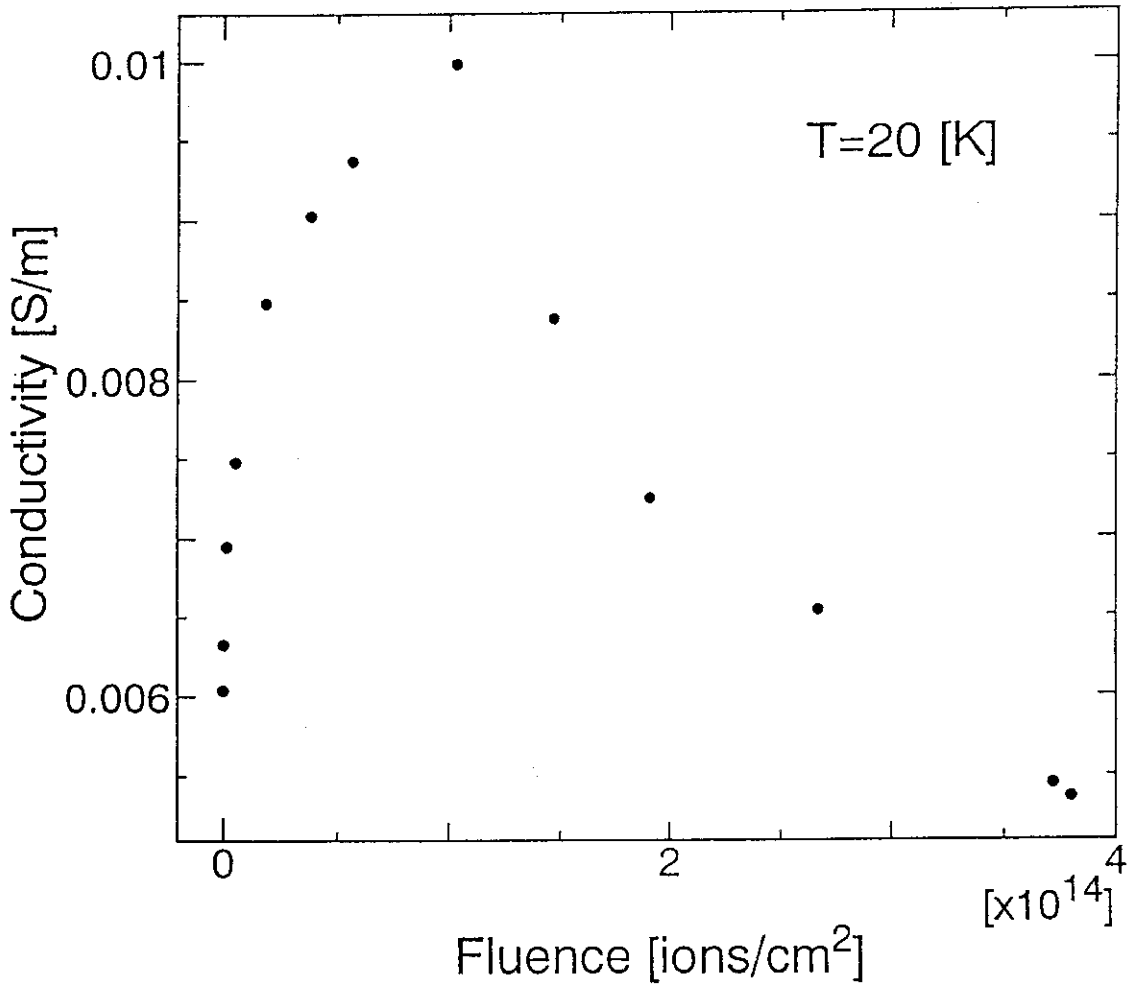

Fig.1 Irradiation effect on the conductivity of B-doped synthetic diamond

References

1 H.Maeta, K.Haruna,Lu Bang and F.Ono,Nucl.Instr.and Meth.,B80/81 (1993)1477.

5. 15 NEW APPARATUS FOR THE RESEARCH OF LOW TEMPERATURE IRRADIATION EFFECTS IN SOLIDS

A. IWASE, N. ISHIKAWA and Y. CHIMI

For the last several years, we have been involved in the research of high-energy ion irradiation effects on FCC metals [1]. In order to extend the research to BCC metals and high-Tc superconductors, we assembled a new apparatus for low temperature irradiation at the H1 beam line of the JAERI tandem accelerator last year. Figure 1 shows the schematic drawing of the apparatus. This apparatus has a lot of functions for the research of irradiation effects. For example, the temperature of the specimen can be varied from 1.5 K to 300 K during irradiation. The cooling power of the cryostat is 1 W at 4.2 K and 100 mW at 1.5 K. This cooling power enables us to irradiate the specimen with the specimen temperature maintained below 4 K. The apparatus has a superconducting magnet which can apply a strong magnetic field at the position of the specimen. The maximum magnetic field is 6 T. To study the irradiation and magnetic field direction dependence, the specimen can be rotated from -30° to +90°. The specimen temperature, rotation of the specimen and the magnetic field can be remote-controlled. Using the apparatus, we can perform the *in-situ* measurements of the irradiation-induced change in electrical resistivity, magnetoresistance and the Hall voltage at low temperatures. We can also measure the annealing behavior of defects in solids by raising the specimen temperature after low temperature irradiation. We are planning to do the following experiments using this low temperature irradiation apparatus; (1) effect of electronic excitation on the defect production and radiation annealing in BCC metals (Fe, Nb and so on), (2) effect of magnetic field on the production and migration of defects in Fe, (3) defect production and annealing in high-Tc superconducting materials, (4) effect of irradiation-produced defects on the superconducting properties of high-Tc and conventional superconductors, and (5) effect of irradiation-induced disorder on the electronic properties of graphite.

[1] A. Iwase and T. Iwata, Nucl. Instr. Meth. B90 (1994) 322. and references therein.

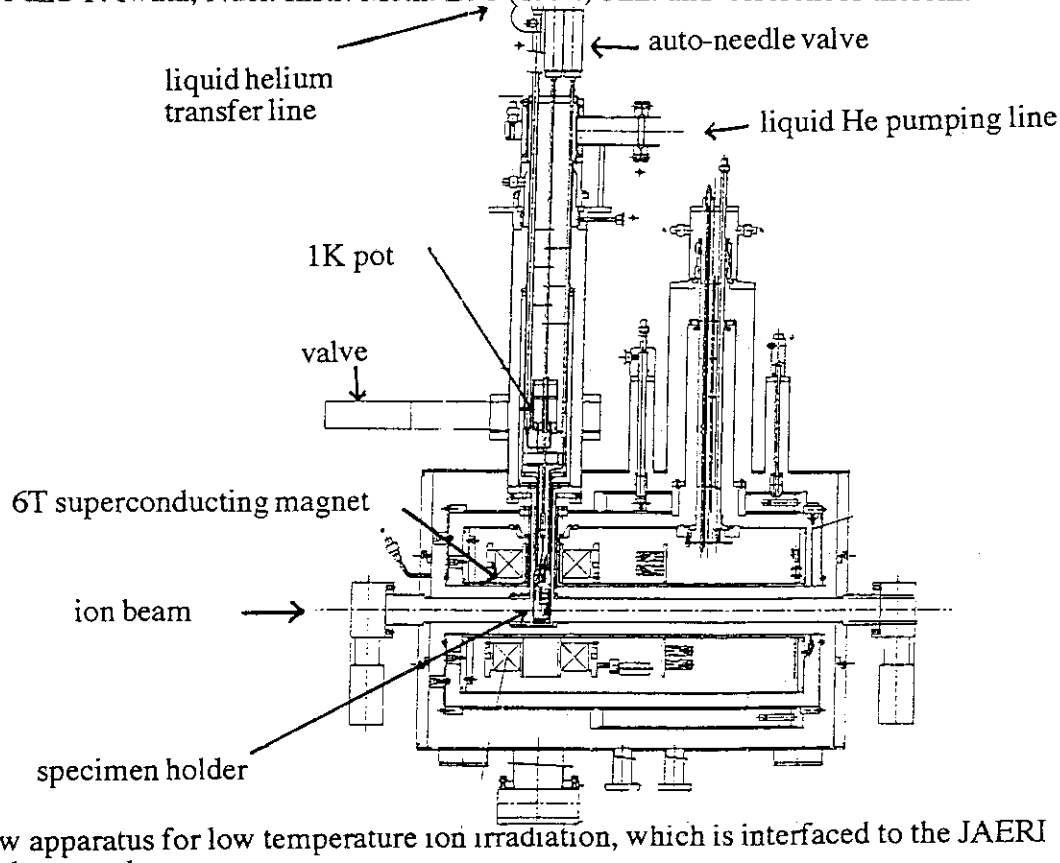

Fig. 1 New apparatus for low temperature ion irradiation, which is interfaced to the JAERI tandem accelerator.

5. 16 ELECTRICAL AND STRUCTURAL PROPERTIES OF Li-ION IRRADIATED β-LiAl

M.YAHAGI[1], NAOTO KUMAGAI[2], K.KURIYAMA[2], H.SUGAI, and H.MAETA

The intermatallic compound β-LiAl has been investigated as one of the useful materials for solid blankets in nuclear fusion [1] as well as a suitable anode material in secondary batteries [2]. β-LiAl is the good mixed conductor with the high electronic conductivity and the high diffusivity of Li ion. This compound crystallizes in the NaTl-type structure over a wide range between about 48 and 56at.%Li. This structure consists of two interpenetrating diamond sublattices each that both the Li and Al atoms are surrounded by four Li atoms and four Al ones. β-LiAl has the interesting properties that Li atoms migrate rapidly even at low temperature since this compound includes the high vacancy concentration at Li sublattice sites, and the ordering or clustering of Li vacancies (V_{Li}) has been observed at about 95K[3].

We have estimated the concentrations[4] of the three kinds of defects (free V_{Li}, free Li_{Al}, and V_{Li}-Li_{Al} complex) in β-phase. The transport properties of β-LiAl are governed by positive carriers [5,6] and considerably affected by these defect structures. On the other hand, radiation effects in β-LiAl make it clear that the Li-vacancy ordering in β-$Li_{0.50}Al_{0.50}$ was destroyed by Li-ion irradiation, while that in β-$Li_{0.48}Al_{0.52}$ did not collapse on irradiation[7]. In the process of Li-ion irradiation, two Frenkel-type defects which consist of a Li interstitial and V_{Li} pair, and an Al interstitial and V_{Al} one are introduced in β-LiAl.

We report the relation between the electrical resistivity and Li-ion fluence in β-LiAl with two different Li contents (C_{Li}).

Samples were prepared using 99.9 % pure Li and 99.999 % pure Al by the same method reported previously[5,6]. $^7Li^{3+}$-ions were irradiated with 60 MeV by a tandem accelerator at JAERI. The dimensions of the samples are about 5x5x1.5 mm^3. The electrical resistivity was measured at about 25K in a helium cryostat using the van der Pauw method after stopping Li-ion irradiation for a time. The specimen during Li-ion irradiation was kept below about 30K.

Figure 1 shows the Li-ion fluence, ϕ, dependences of resistivity of β-LiAl for the specimens with C_{Li} = 48.9 at.% and 49.4 at.%. $\Delta\rho$ is the difference between the resistivity before and after Li-ion irradiation. In the previous report, we have suggested that the increase in the resistivity after the irradiation is due to Frenkel-type defects produced by the knock on of Li-ion irradiation. In the specimen with C_{Li} =48.9 at.%, the values of $\Delta\rho$ increase with Li-ion fluence, and the slope of $\Delta\rho$-ϕ curve becomes a slight increase in the region of above 0.7×10^{15} Li cm^{-2}. On the other hand, the slope of $\Delta\rho$-ϕ curve for β-LiAl with 49.4 at.% Li is smaller than that of specimen with 48.9 at.%Li except the range of lower fluence. The origin of the slight increase of $\Delta\rho$-ϕ curves in the range of high fluence is not clear from this experimental data. The relation between $\Delta\rho$ and ϕ in metal is given by an experimental equation[8],

$$\Delta\rho = A\,(1 - e^{-\beta\phi}) \qquad (1)$$

where A and β are a constant. The solid lines of Fig.1 were calculated using Eq.(1). Then the values of A and β for the specimens with C_{Li} = 48.9at.% and 49.4at.% were determined by the best fit of Eq.(1). Those of A are about 5.1×10^{-7} Ωcm for C_{Li} = 48.9 at.% and about 6.3×10^{-7} Ωcm for C_{Li} = 49.4 at.%, while the values of β are about 1.5×10^{-15} cm^2 for C_{Li} = 48.9 at.% and about 3.7×10^{-16} cm^2 for C_{Li} = 49.4 at.%,respectively. Here, A and β are shown by

$$A = r/\sigma L, \qquad \beta = \sigma_d \nu n_0 L\sigma \qquad (2)$$

[1]Faculty of Engineering, Aomori University.
[2]College of Engineering & Research Center of Ion Beam Technology, Hosei University.

where r is the varying quantity of resistivity due to lattice defect produced by knock on of one atom , σ the cross section when the atom due to knock on is captured in the vacancy, L the mean trajectory of knock-on atom, σ_d the collision cross section on the primary knock-on, ν the mean number of Frenkel defect produced by the primary knock-on atom, n_0 the number of atoms per cm^3, respectively. We assume that the values of parameter r, σ, σ_d, n_0 and L are approximately constant since the difference of C_{Li} for two specimens is small (about 0.5 at.%Li). From Eq.(2), the mean number of Frenkel type defect produced by Li-ion irradiation can be evaluated by

$$\nu = KA\beta \qquad (3)$$

where K is equal to $1/\sigma_d n_0 r$. The ratio of ν for the specimen with 48.9at.%Li to ν for that with 49.4at.%Li was estimated to be about 3.3 from Eq.(3). This result shows that Frenkel type defects are introduced easily in the specimen with lower C_{Li}(48.9at.%) than that of 49.4at.%Li. On the other hand, the concentration of V_{Li}-Li_{Al} complex defects increases over a range from 48.9at.%Li to 49.4at.%Li. Therefore, we deduce that the increase of V_{Li}-Li_{Al} complex defects would cause a decrease of creation of Frenkel type defects by Li-ion irradiation.

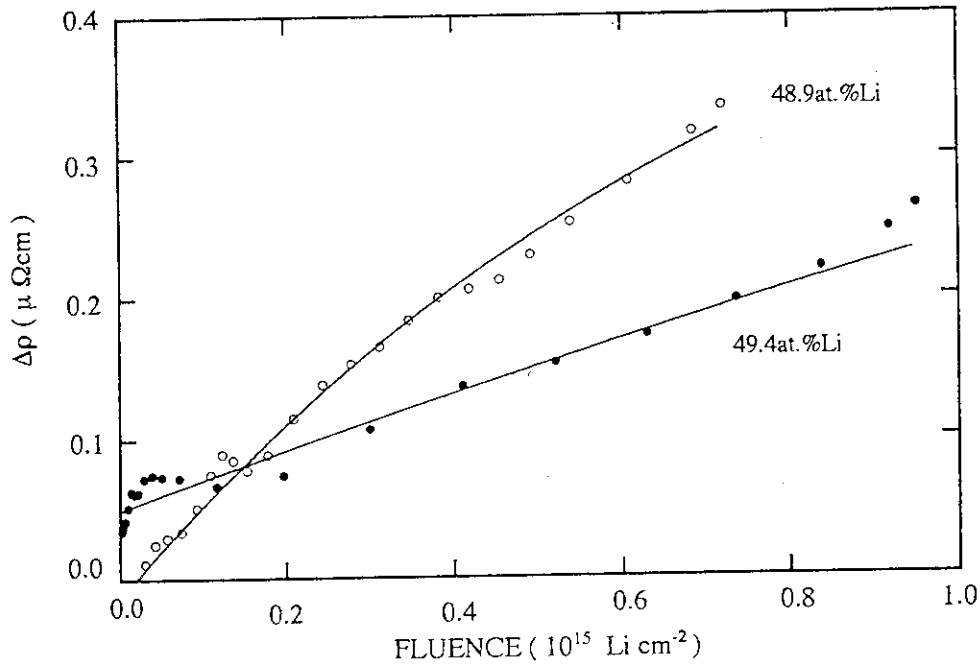

Fig. 1 Li-ion fluence dependence of resistivity for β-LiAl with C_{Li} =48.9at.% and 49.4at.%.

References
1) H. Sugai, Z. Miao, and H. Kudo, Fusion Technol. **21**, (1992) 818.
2) C. H. Wen, B. A. Boukamp, R. A. Huggins, and W. Weppner, J. Electrochem. Soc. **126**, (1979) 2258.
3) K. Kuriyama, S. Yanada, T. Nozaki, and T. Kamijoh, Phys. Rev. B**24**, (1981) 6185.
4) H. Sugai, M. Tanase, M. Yahagi, T. Ashida, H. Hamanaka, K. Kuriyama, and K. Iwamura, Phys. Rev. B**52**, (1995) 4050.
5) M. Yahagi, Phys. Rev. B**24**, (1981) 7401.
6) K. Kuriyama, T. Nozaki, and T. Kamijoh, Phys. Rev. B**26**, (1982) 2235.
7) K. Kuriyama, Takashi Kato, Tomoharu Kato, H. Sugai, M. Maeta, and M. Yahagi, Phys. Rev. B**52**, (1995) 3020.
8) H. G. Cooper, J. S. Koehler, and J. W. Marx, Phys. Rev. **97**, (1955) 599.

5.17 RADIATION DAMAGES IN SYNTHETIC FUSED SILICA INDUCED BY CU IONS IRRADIATION

S.NASU[1], K.NISHIWAKI[1], R.FUJIMORI[1], H.NANTO[1],
R.YAMAMOTO[1],Y.YAMAKI, T.NAKAZAWA, and K.NODA

The $B_2\alpha$ band in fused silicas has been attracting much attention [1,2],because of their importance as materials for various technological applications such as the transmissive and reflective optical materials, the envelops of the special lamps, the high temperature furnace materials for semiconductors, the cores and the claddings of glass fiber waveguides, and the gate, field, and passivation layers of silicon based metal-oxide-semiconductor devices. In the light of the above background, Cu^{+11}ions with 180MeV were irradiated into synthetic fused silica of SK1310 (type IV) in attempt to induce the $B_2\alpha$ band at near surface of this fused silica, so as to simulate in a short time what would occur in many years, and the $B_2\alpha$ band induced were studied by means of optical absorption (OA) and photoluminescence (PL) measurements at room temperature (RT) after Cu^{+11}ions irradiation.

Commercially available synthetic fused silica, SK1310 (type IV, OH content :below 5wppm) were used as samples. These samples were irradiated at RT with 180MeV Cu^{+11}ions at a fluence of 1.1×10^{15}ions/cm^2 using the tandem accelerator in JAERI, Tokai. The nominal irradiation fluences were determined by charge integration. Temperatures of the samples were not monitored during irradiation.

All optical measurements were made at RT. The OA spectra in the visible and ultraviolet region (6.2～1.5eV) were obtained with a Hitachi U-3300 double beam spectrophotometer. The continuous wave PL and PL excitation (PLE) spectra were obtained with a Hitachi F-3010 fluorescence spectrophotometer. After the optical measurements, the samples were subjected to isothermal annealing procedures over the temperature range of 100 to 600℃ in increments of 25 to 50℃ taken each step for 30 minutes in air. Before irradiation, any OA peaks were not observed in the wavelength range of 6.2eV to 1.5eV. After irradiation, a relatively strong OA peak at 5.06eV was clearly observed on the tail of stronger OA above 6.2eV and on the weak OA shoulder around 5.8eV,which seem to be due to the 7.6eV and the E'center respectively . A large PL peak at 4.3eV and a small one at 2.7eV were clearly observed, and the maxima of 4.3eV and 2.7eV PLE have the same peakenergy,indicating that the PL bands at 4.3eV and at 2.7eV are due to the same defect center . It has been known that the $B_2\alpha$ band is intrinsically observed in oxygen

[1]Department of Electrical Engineering, Kanazawa Institute of Technology

deficient fused silicas with the weak OA around 5.1eV and the strong OA around 7.6eV, and the strong and weak PL around 4.3eV and 2.7eV[3,4]. Therefore, the OA peak at 5.06eV and the PL peaks at 4.3eV and 2.7eV obtained can be attributed to the $B_2\alpha$ band due to the oxygen vacancy ($\equiv$ Si—Si $\equiv$), the center of which is located at 26.6μm below the surface with the longitudinal straggling range of 0.74μm, according to the TRIM program. Figure 1 shows annealing behavior of the OA peaks at 5.06eV. The intensities of the OA peaks were determined by the peak heights subtracted from the background intensities. It is clear that thermal bleaching is already significant above 250℃ and is completed at 450℃.This behavior is in marked contrast to that of the intrinsic unrelaxed $B_2\alpha$ band observed in oxygen deficient fused silicas. In hypo-stoichiometic, that is, oxygen deficient fused silicas, it is difficult to pick up oxygens form air because of no extra oxygens in the sample and low network and intenstitial oxygen diffusion processes [5]. On the other hand, in stoichiometric fused silicas it is easy for recoil oxygens to resume the original silicon-oxygen-silicon bond at relatively low temperatures.

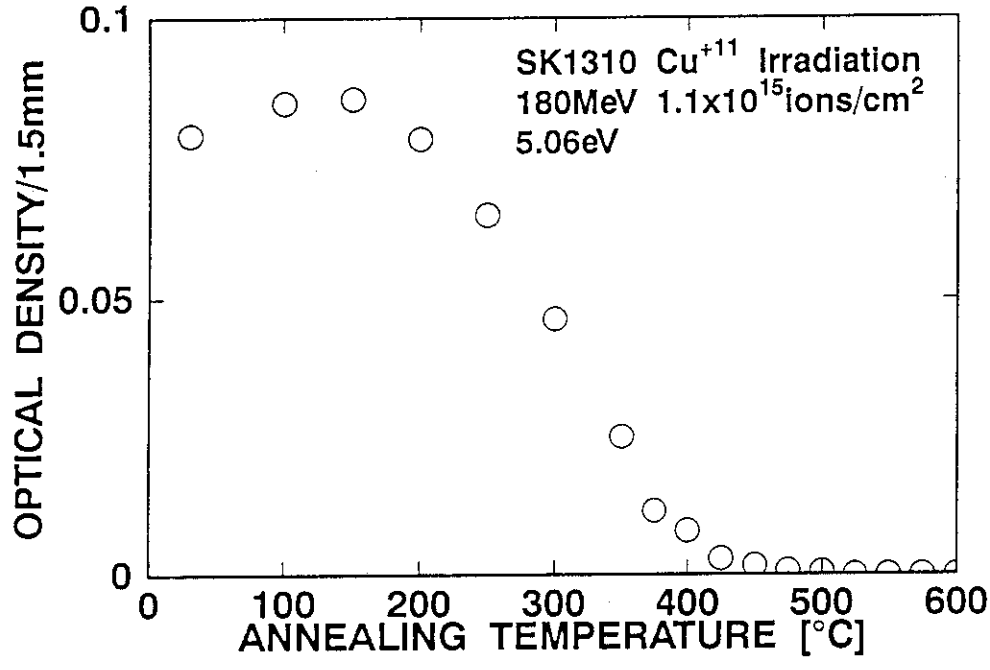

Fig.1. Annealing behavior of optical absorption peaks at 5.06eV for SK1310

References

1)H.Nishikawa, E.Watanabe, D.Ito and Y.Ohki, Phys.Rev.Lett.72(1994)2101.

2)H.Nishikawa, E.Watanabe, D.Ito, M.Takiyama, A.Ieki and Y.Ohki,J.Appl.Phys.78(1995) 842.

3)H.Imai, K.Arai, H.Imagawa, H.Hosono and Y.Abe, Phys.Rev.B38(1988)12772.

4)M.Guzzi, M.Martini, A.Paleari, F.Pio, A.Vedda and C.Azzoni, J.Phys. :Cond.Matter 5(1993)8105.

5)J.D.Kalen, R.S.Boyce and J.D.Cawley, J.Am.Ceram.Soc.74(1991)203.

5.18 RADIATION DAMAGE ON Li_4SiO_4 IRRADIATED WITH HIGH ENERGY IONS

T. NAKAZAWA, D. YAMAKI and K. NODA

Li_4SiO_4 is one of the candidate breeder materials for D-T fusion reactors. The materials in fusion blankets are exposed to severe neutronic environments during the operation of fusion reactors and changes in the properties at high fluence may affect their performance in a fusion blanket application. In this study, radiation damage in Li_4SiO_4 irradiated with high energy ions is investigated by Fourier transform infrared photo-acoustic spectroscopy (FT-IR PAS)[1,2], in order to obtain fundamental information on irradiation defect and decomposition due to high energy neutron irradiation.

The Li_4SiO_4 sintered pellets were irradiated at the ambient temperature with 120MeV oxygen and 60MeV lithium ions by a tandem accelerator at Japan Atomic Energy Research Institute (JAERI). Using the FT-IR PAS, the specimens irradiated to the fluence of 10^{20} ions/m^2 were characterized. The FT-IR PAS is very powerful tool for the nondestructive investigation of the structure changes of ceramics irradiated [3,4]. Especially, information on structural change can be obtained as a function of specimen depth through alteration of the modulation frequency by controlling the optical path difference (OPD) velocity. The instrument of the FT-IR PAS used in this study consists of a Perkin-Elmer model 2000 FT-IR Spectrometer and a MTEC model 200 PAS Detector. In the wave number region 1500 to 450 cm^{-1}, FT-IR PAS spectra for the irradiated samples are measured at room temperature by adjusting sample spectra for a spectral variations which are not due to the sample. FT-IR PAS spectra are obtained at OPD velocity of 0.05cm s^{-1} with resolution of 8cm^{-1}.

The changes of FT-IR PAS spectra of Li_4SiO_4 irradiated with 120MeV oxygen ions and 60MeV lithium ions are shown in fig. 1. The structural information in the region of about 50μm in depth is obtained from the spectra measured with the OPD velocity of 0.05 cm/s. On the spectrum (a) in fig. 1, the characteristic FT-IR PAS peaks associated with the SiO_4 tetrahedron are observed in the wave number range 800 to 1000 cm^{-1}. The three peaks at higher wave numbers correspond to the triply degenerate vibration of the SiO_4 tetrahedron while the one at lower wave numbers correspond to its holosymmetric vibration[5]. The shapes of the FT-IR PAS spectra are varied by irradiation. Spectra (b) and (c) show the FT-IR PAS spectra of Li_4SiO_4 irradiated with 60MeV lithium ions and 120MeV oxygen ions, respectively. Some broad peaks in the wave number 1000 to 1200 cm^{-1} are observed on the spectra (c). The broad peak at about 1040cm^{-1} and shoulder peaks at 1180 and 1230 cm^{-1} appeared owing to irradiation. These broad peaks grown with the fluences are assigned to the vibration associated with bridging oxygen on the basis of the theoretical IR spectra[6]. Thus, by comparing with the theoretical IR spectra the irradiation with 120MeV oxygen ions for Li_4SiO_4 cause the creation of bridging oxygen. This suggests that the polymerization of SiO_4 tetrahedron is caused by the 120MeV oxygen ion irradiation.

On the other hand, the FT-IR PAS spectra of Li_4SiO_4 irradiated with 60MeV lithium ions are shown on spectrum (b). Prominent changes of FT-IR PAS spectra before and after irradiation are not observed. The only slight broadening of peaks due to the SiO_4 tetrahedron is observed.

The depth profiles for displacement damages and ionization energies which are calculated by the TRIM code are shown in fig. 2. The displacement damages due to nuclear collision for 120MeV

oxygen ions and 60MeV lithium ions at 50 μm are 0.15 and 0.002dpa, respectively. The ionization energies are 1.0×10^{10} and 8.7×10^{8}Gy, respectively. The damages and ionization energies calculated for irradiation with oxygen ions are very large compared to those for irradiation with lithium ions. The energy of ions incident to bulk specimens is dissipated by ionization and nuclear collision. The structural changes due to the energy dissipated by the irradiation is observed as the changes of FT-IR spectra of Li_4SiO_4 irradiated(fig. 1). Displacement damage and ionization dose in the oxygen ion irradiation are much higher than those in lithium ion irradiation(fig. 2). It is not clear in this study which contribution to structural change due to irradiation is larger - displacement damage due to elastic collision or ionization. Effects of ionization on structural change will be investigated by irradiation experiment using various kinds of incident ions and energies.

References

1) K. Noda, Y. Ishii, T. Nakazawa, H. Matsui, N. Igawa, D. Vollath, H. Ohno and H. Watanabe, J. Nucl. Mater. 191-194 (1992) 248.
2) T. Nakazawa, K. Noda, Y. Ishii, H. Matsui, N. Igawa, D. Vollath, H. Ohno and H. Watanabe, Proc. 17th Sym. Fusion Technology, Sept. 14-18, 1992 (Rome) p.1444-1448.
3) N.Teramae and S.Tanaka, in:H. Ishida(Ed.), Fourier Transform Infrared Characterization of Polymers, Plenum Publishing Corporation, 1987, pp.315-340.
4) M.J.S. Dewar and W. Thiel, J. Am. Chem. Soc,, 99(1977) 4899.
5)A.N. Lazarev, V.A. Kolesova, L.S. Solntseva, and A.P.Mirgorodskii, Izv. Akad. Nauk SSSR, Neorgan. Mat., 9 (1973) 1969.
6) T.Nakazawa, D.Yamaki and K.Noda, JAERI-Review 95-017 (1995) 81.

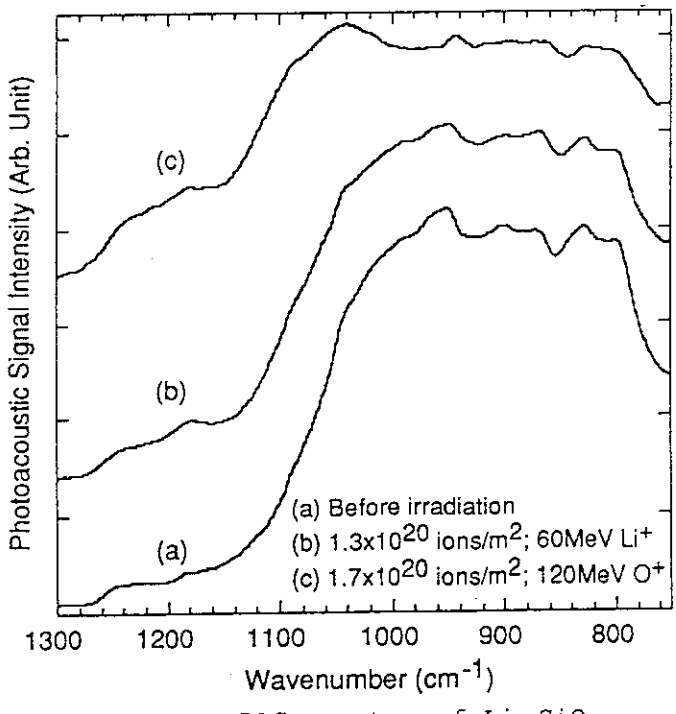

Fig. 1 FT-IR PAS spectra of Li_4SiO_4 irradiated with 120MeV oxygen ions and 60MeV lithium ions.

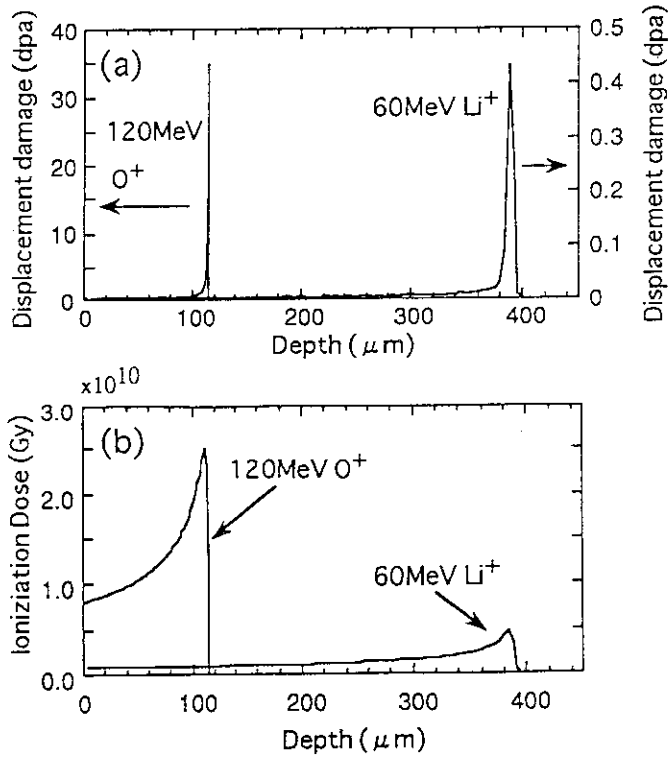

Fig. 2 Calculated depth profiles of displacement damages and ionization energy for Li_4SiO_4 irradiated with 120 MeV oxygen ions and 60MeV lithium ions by TRIM89.

5.19 THE EFFECT OF INCIDENT ION ENERGY ON RADIATION DAMAGE OF UO_2 IN A RANGE OF 100 - 300 MeV

K. HAYASHI, H. KIKUCHI and K. FUKUDA

The present authors have been studying the radiation damage of UO_2 by irradiation of heavy ions, using the Tandem Accelerator in the Tokai Establishment of JAERI. The works are in relevance to the "rim effect" [1], or a microstructural change, in high burnup fuels for light water reactors.

In the previous study [2], depth profiles of lattice parameter changes of UO_2 irradiated with 100 MeV iodine ions were measured by X-ray diffractometry with step-by-step sectioning. The results suggested that the lattice parameter change in the near-surface region may have reflected the defect formation due to the electronic energy deposition as well as the nuclear energy deposition. In the present study, the possibility of defect formation due to the electronic energy deposition was further pursued by changing the incident energy of ions [3].

The experimental procedure was essentially the same as described so far [2,4]. Irradiation was made with 100, 200 and 300 MeV iodine ions at ambient temperatures, and the surface temperature of the specimen was measured to be lower than 200°C. After irradiation, X-ray diffraction analysis was made on the irradiated surface of the UO_2 specimen. The penetration depth of the X-ray (Cu-Kα) was estimated to be about 2 μm.

Figure 1 shows the nuclear and electronic stopping powers, which were calculated by the EDEPJR-87 code [5] as a function of the incident ion energy into UO_2. The electronic energy deposition increases, while the nuclear decreases, with increasing the incident energy in the region around 100 MeV. Considering the X-ray penetration depth of 2 μm and a relatively larger mean projected range of about 7 μm [2] for 100 MeV iodine implantation, the nuclear and electronic energy depositions at the surface region relevant to the surface X-ray diffraction analysis can be approximated by the nuclear and electronic stopping powers, respectively.

Figure 2 shows experimental results obtained so far. The lattice parameter change is considered to reflect the point defect concentration in UO_2. As seen in this figure, the lattice parameter change increases with increasing the incident ion energy in the range of 100 - 300 MeV. The increase in the lattice parameter change with the incident energy is inconsistent with the deceasing tendency of the nuclear energy deposition. This suggest that defect formation cannot be ascribed only to the nuclear energy deposition.

In contrast, the increase in the lattice parameter change is consistent with the increasing tendency of the electronic energy deposition. This suggests that the electronic energy deposition made a larger contribution than the nuclear energy deposition, to the lattice parameter change in the surface region.

In summary, the result described above can be considered as an evidence of formation of lattice defects due to the electronic energy deposition. This follows the first findings of its suggestion in the depth profile measurement [2].

The authors are indebted to Messrs. S. Kashimura, T. Shiratori, K. Tsukada and S. Ichikawa and members of Accelerators Division of JAERI for their experimental assistance in the Tandem Accelerator irradiation.

References

1) e.g. J.O.Barner, M.E.Cunningham, M.D.Freshley and D.D.Lanning, Proc. Intern. Topical Mtg. on LWR Fuel Performance (Avignon, France, April 21-24, 1991) p.538.
2) K. Hayashi, H. Kikuchi and K. Fukuda, JAERI-Review 95-017 (1995) p.79.
3) K. Hayashi, H. Kikuchi and K. Fukuda, presented at Int. Workshop on Inter-facial Effects in Quantum Engineering Systems, IEQES-96, (Aug. 21-23, Mito, Japan) PB-01; submitted to J. Nucl. Mater. (1996).
4) K. Hayashi, H. Kikuchi and K. Fukuda, J. Alloys and Comp. 213/214(1994)351.
5) T. Aruga, K. Nakata, and S. Takamura, Nucl. Instr. Meth. in Phys. Research B33 (1988) 748.

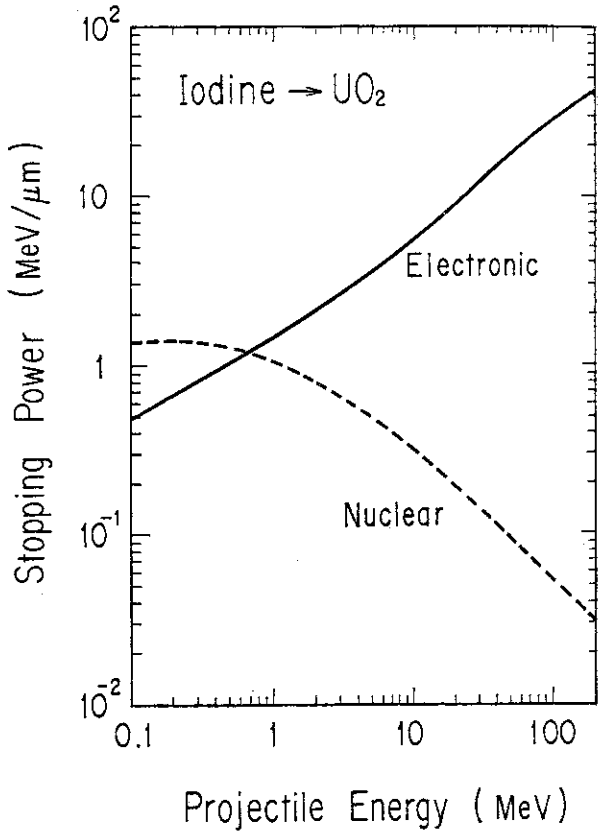

Fig.1 Nuclear and electronic stopping powers calculated by the EDEPJR-87 code [5] as a function of incident energy of ^{127}I ions into UO_2 of 95%TD [3].

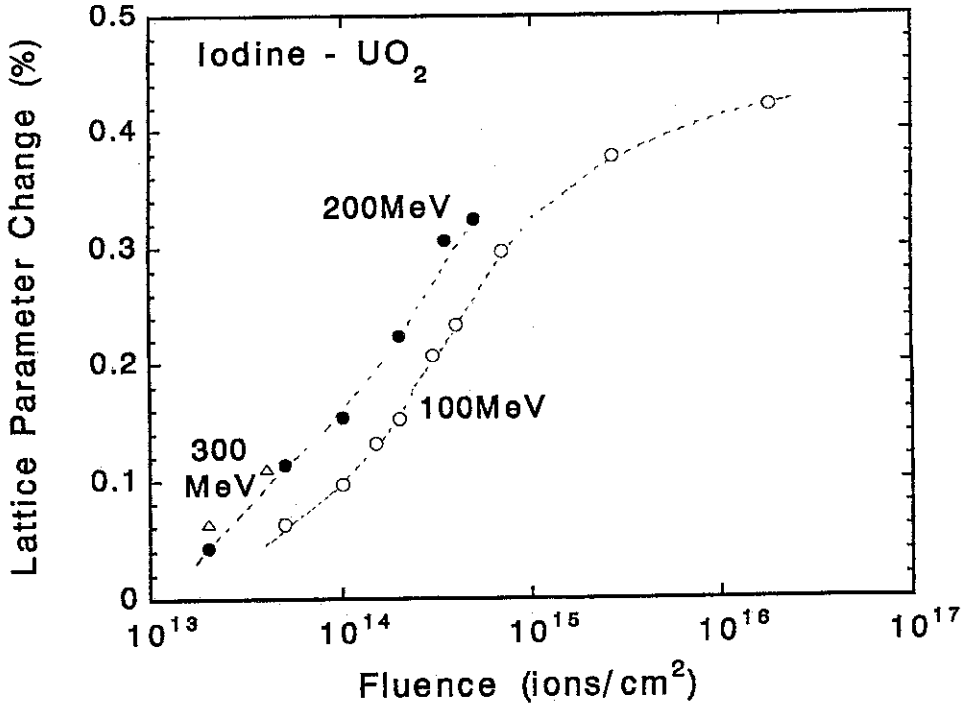

Fig.2 Lattice parameter changes of UO_2 irradiated with 100, 200 and 300 MeV iodine ions as a function of ion fluence.

5. 20 ON AMORPHOUSNESS AND DISORDERING IN OXIDE CERAMICS BY HEAVY-ION BOMBARDMENT

S. KASHIMURA, T. OHMICHI and K.FUKUDA

As a framework of the program for developing the rock-type fuel[1], which is expected to incinerate the excess-plutonium and be disposed without any reprocessing, we have investigated irradiation stability on such several ceramic oxides as alumina(Al_2O_3), spinel($MgAl_2O_4$) and zirconia(ZrO_2), all of which are major components of the fuel. For the study the bombardment of I^{+6} or I^{+7} ions have been carried out on these oxides with ion energy of 70-80 MeV, and fluence ranging from $1.0x10^{15}$ to $5.0x10^{15}$ ions/cm^2. A highlight previously reported in this journal[2] was that the Raman spectroscopy defined clear difference in the spectrum of the bombarded and non-bombarded $MgAl_2O_4$ samples, where one spectra at the wave number of 400 cm^{-1} remained unchanged in the bombarded $MgAl_2O_4$, although other spectrum almost disappeared. Also, all of the spectrum of Al_2O_3 completely disappeared in the bombardment. From the Raman spectroscopy we deduced that bombarded area of $MgAl_2O_4$ is disordered, but not amorphous, meanwhile the area of Al_2O_3 became amorphous.

In order to investigate irradiation-induced disordering of $MgAl_2O_4$ more detail, the trans-electron microscope(TEM) observation and the electron diffraction were performed on the bombarded and non-bombarded samples. For preparation of the TEM samples, the surface area of $MgAl_2O_4$ non-bombarded and bombarded up to $5.0x10^{15}$ ions/cm^2 was filed away with a micro diamond-gimlet, and the powdered samples were used for observation and diffraction in TEM. Fig.1 show typical bright-field images and the electron diffraction patterns of the non-bombarded and bombarded samples. The non-bombarded sample exhibits the Laue spots diffracted by the crystal lattice, meanwhile the bombarded sample showed the broad rings (halo) without any diffraction spots, indicating amorphousness of the samples. In the Raman spectroscopy which takes out information on the atomic arrangement just in the surface of the bombarded area, it clarified disordering of the surface, but not the amorphousness. The TEM diffraction pattern, however, indicated the occurrence of the amorphousness, although the position of the amorphousness is not identified. Thus, it is conceivable that the area from the surface to some extent, probably several micrometers, is under disordering state, and the area beneath the disordering one is under amorphous state.

The above-mentioned structural change in the spinel by the bombardment is verified by the X-ray diffraction. The X-ray penetrates much deeper than the ion-bombarded area in the spinel(approximately 10 μm) so that it is difficult to detect the lattice change induced by the

bombardment. However, if postulating that the diffraction intensity is reduced in proportion to a degree of lattice imperfectness in the bombarded sample, we can evaluate the degree of imperfectness by comparison of the intensity at the individual diffraction angle in the bombarded sample with those of the non-bombarded sample. Fig. 2 depicts the intensity change of the X-ray diffraction which were measured and theoretically evaluated with the degree of disordering in the bombarded area. A large portion of the experimental measurements exist between complete imperfectness(amorphousness) and 70% imperfectness(disordering), indicating that the bombarded area is not amorphous. In this respect alumina evidenced complete imperfectness, i.e., amorphousness. We concluded that spinel is tougher than alumina in the bombardment with heavy ion simulating the fission fragment.

References

[1] H.Akie, et al.,"A new fuel material for once-through weapons plutonium burning", Nucl. Technol., 107(1994) 182-192.

[2] S.Kashimura, et al., "Physical property changes of aluminum constituent oxides by bombardment with 70MeV iodine ions", JAERI-Review 95-017(1995).

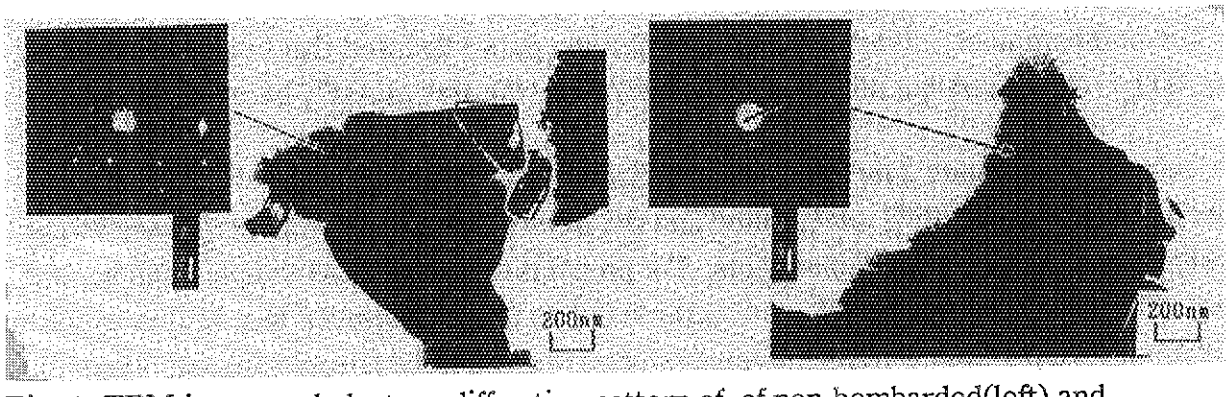

Fig. 1 TEM image and electron-diffraction pattern of of non-bombarded(left) and bombarded(right) spinel.

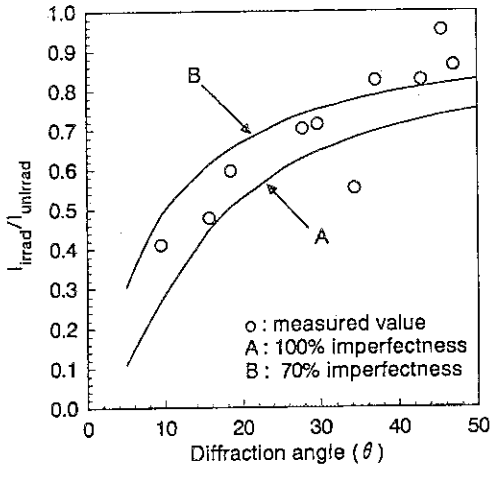

Fig. 2 Comparison of measurement and theoretical evaluation on diffraction intensity change in spinel.

5.21 RESPONSE OF SILICON SURFACE BARRIER DETECTORS TO HEAVY IONS

I.KANNO[1], S.KANAZAWA[1], K.KAMITANI[1], Y.KAJII[1], J.ISHII[1], I.KIMURA[1], H.TAKADA and S.MEIGO

A silicon surface barrier detector (SSBD) is one of the most widely employed charged particle detectors in nuclear physics, nuclear engineering and material science experiments, though the SSBDs have unfavorite properties such as pulse height defect in energy response and plasma delay in timing response.

Both phonomena, the pulse height defect and the plasma delay are caused by a common cause named plasma column. The plasma column is created by an incident charged particle and consists of dense electron-hole pairs, and its effect to the dielectric property causes the two unfavorite properties in the SSBDs. The authors have been studying the energy and the timing responses of the SSBDs experimentally and theoretically. Models of formation and erosion of the plasma column and the resistivity dependence of the plasma delay were reported elsewhere.

Recently, identifying an incident charged particle has become a new subject of interest. As a method of particle identification, we have tried to utilize the rise time of the output pulse. It has been found a possibility of the particle identification based on the rise time analysis in the SSBD.

^{79}Br,^{127}I,^{58}Ni or ^{16}O ions were accelerated by the tandem accelerator of JAERI and scattered by a gold target foil of 100μg/cm^2 in thickness. The scattered ^{79}Br,^{127}I,^{58}Ni or ^{16}O and recoiled ^{197}Au ions were extracted into the flight path of 105cm in length with the angle of 45 degrees.

The SSBDs with resistivities of 362 Ωcm(Det.A), 2.1 kΩcm(Det.B) and 67 kΩcm(Det.C), products of ORTEC, were set at the end of the flight path. The energy and the rise time of incident charged particles were measured with a 2-dimensional pulse height analyzer by changing the bias voltage. Examples of obtained pulse height data are shown in Fig.1. Figure 2 shows the rise time measured for ^{79}Br,^{127}I and ^{197}Au ions as a function of the applied bias voltage. The pulse height and the rise time saturate with increasing applied bias. It seems that the difference of the rise time among the detectors are explained by the difference of electric field strength.

Figure 3 shows the rise time measured for three deterctors(Dets.A,B and C) dependent on the mass number. This result shows that the rise time decreases as the mass number increases. It seems that the decrese of rise times is explained by the difference of plasma column length.

More experiments to investigate the particle identification by the rise time should be carried out in future.

[1]Department of Nuclear Engineering, Kyoto University

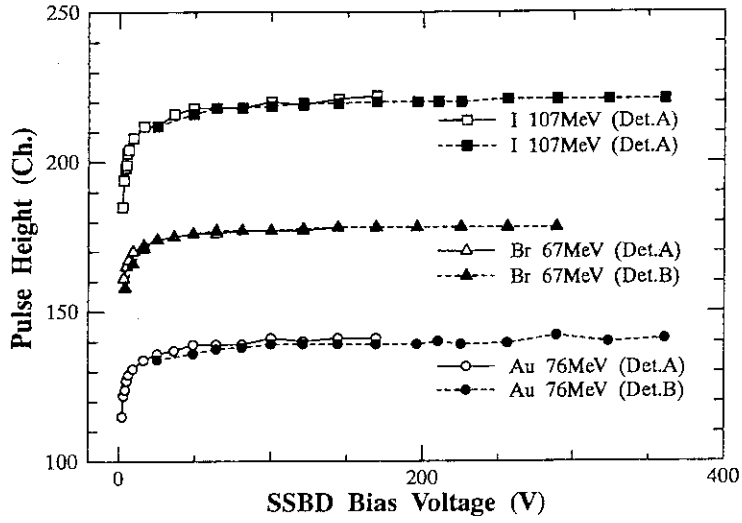

Fig. 1 The pulse height for ^{79}Br,^{127}I and ^{197}Au ions as a function of applied bias.

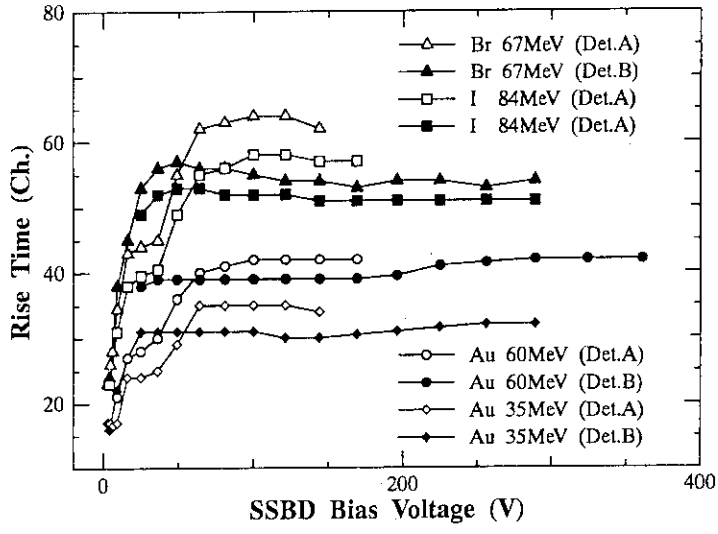

Fig. 2 The rise time for ^{79}Br,^{127}I and ^{197}Au ions as a function of applied bias.

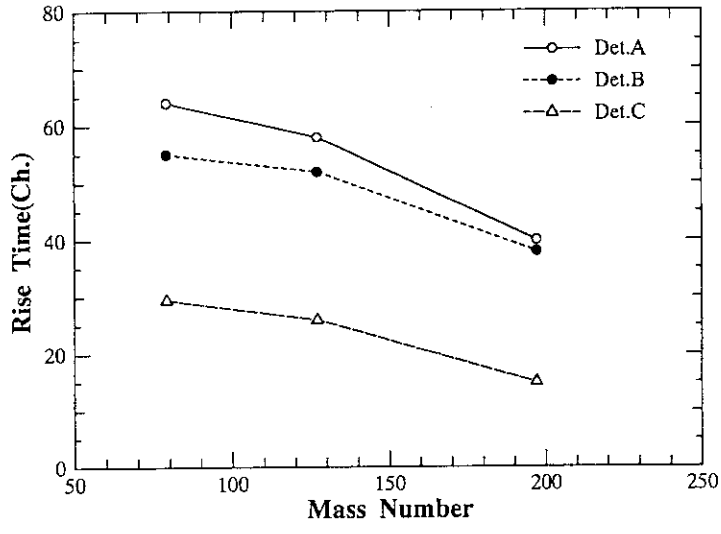

Fig. 3 The rise time as a function of the mass number.

5.22 SINGLE EVENT EFFECT IN POWER MOSFETS BY INCIDENCE OF HIGH-ENERGY IONS

S. T. HADA[1], T. HIRAO, MATSUDA[1], I. NASHIYAMA, J. AOKI[1], M. NAKAMURA[1], T. HIROSE[2], H. OHIRA[2], Y. NAGAI[2]

Power MOSFETs are essential devices for power switching in electric circuits. However, they have a possible catastrophic failure mode known as Single Event Burn-Out(SEB) triggered upon incidence of high-energy ions. When an ion penetrates into the parasitic transistor of Power MOSFET, excess electric current causes of the transistor turn-on and the SEB is occurred. (SEB is an annoying phenomenon to be considered in space electronic systems.) It is necessary to immunize from the SEB when commercial devices are used for space applications. We developed a new Power MOSFET(2SK2271) by reducing the current gain(h_{FE}) of the parasitic transistor in a commercial Power MOSFET(2SK725).

High-energy ions from TANDEM accelerator were utilized this year to analyze the dependence on the parasitic transistor. To observe the SEB, a spectrum of charge collected in the device was measured by a pulse-height analyzer system with a modified charge-sensitive amplifier. Figure 1 shows the SEB cross section(σ) of the Power MOSFETs as a function of source-drain voltage. The data were obtained using 200MeV Nickel ions. The threshold voltage(σ is about 1×10^{-3}) for SEB of 2SK2271 is higher than that of 2SK725 by about 40V. The threshold voltage exceeds 300V which is reqired by the space station project.

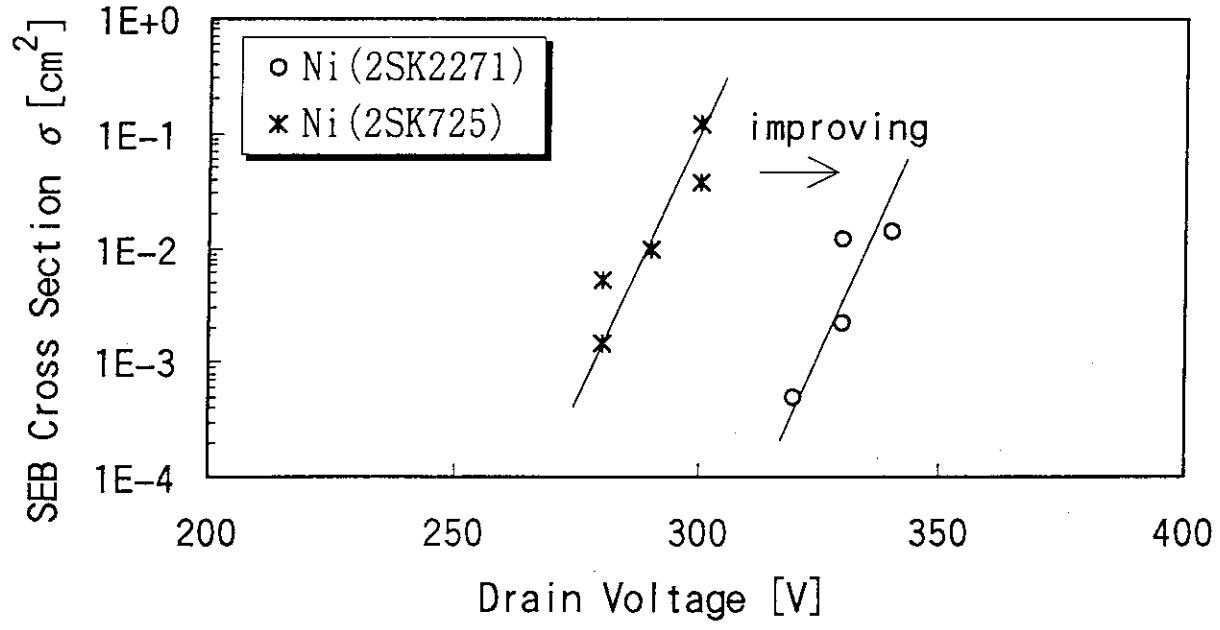

Fig. 1. The SEB cross section of the Power MOSFETs as a function of source-drain voltage.

[1]Electronic Components Technology Laboratory, Components Technology Department, Office of Research and Development, National Space Development Agency of Japan.
[2]Components Engineering Section, Engineering Dept., RYOEI TECHNICA Corporation.

5. 23 LUMINESCENCE CHARACTERISTICS OF PHOTOSTIMULABLE PHOSPHOR WITH HEAVY CHARGED PARTICLES

C. MORI[1], T. SUZUKI[1], H. SAKAI[1], S. KOIDO[1], A. URITANI[1],
M. YOSHIDA, F. TAKAHASHI

Photostimulable phosphor BaFBr:Eu^{2+} is used for two-dimensional position sensitive detectors known as Imaging Plate (IP). The IP can measure extremely low level radioactivity [1], because of its high sensitivity and accumulating effect of the images (F-centers and Eu^{3+} ions) formed by incident particles. Owing to the accumulating effect, however, it is usually impossible to identify the kind and energy of incident particles. We proposed a multiple successive reading method for the identification [2]. In this method, the decrease of PSL (PhotoStimulated Luminescence) intensities as a function of the number of successive readings depends on the kind and energy of incident particles as shown in Fig. 1. The ratio of prompt luminescence intensity to latent image intensity also depends on the kind and energy of incident particles. The purpose of this study is obtaining information to make the PSL mechanism clear by measuring prompt luminescence intensity and PSL intensity as a function of the multiple successive reading for high-energy heavy charged particles which have large stopping power and long ranges. This study may lead to a discovery of new types of phosphors suitable for heavy charged particles.

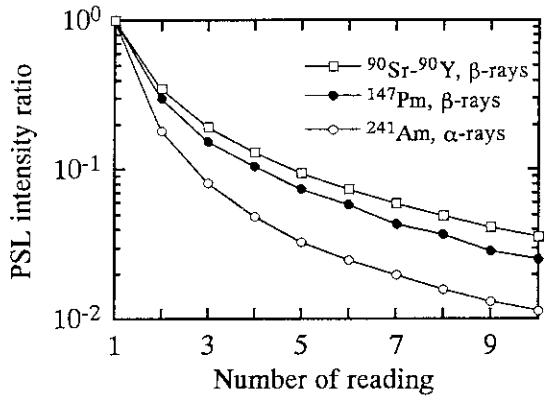

Fig. 1 The multiple successive reading method in the case of α-ray and β-ray incidences.

Figure 2 shows the change of PSL intensity as a function of the number of successive readings for (a) O^{7+} 120 MeV ions and (b) Li^{3+} 50 MeV ions incidences, respectively. Because experimental

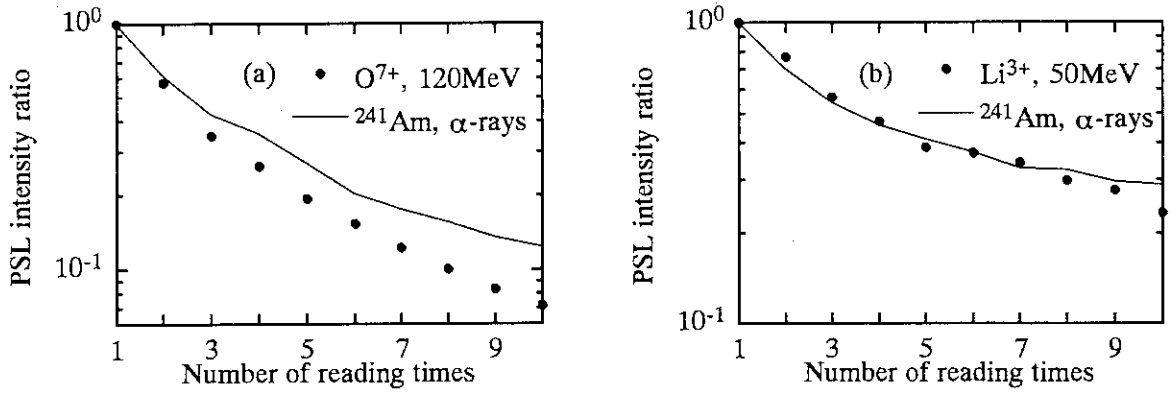

Fig. 2 The multiple successive reading method in the case of α-ray and heavy ion incidences. (a)O^{7+} incidences, (b) Li^{3+} incidences.

[1] School of Engineering, Nagoya University

conditions are different between (a) and (b), these figures cannot be compared with each other. But the results of heavy ion and α-particle incidences in the same figure can be compared. Table 1 shows the average deposited-energy in the phosphor layer, range and stopping power for various kinds of incident particles. For the Li^{3+} ion incidences, which have a stopping power close to that of α-particles, the decrease of PSL intensities with the number of reading was also similar to that for α-rays. For the O^{7+} ion incidences, whose stopping power is larger than that of α-particles, the decrease of PSL intensity is more rapid than that for α-rays. The ratio of latent image intensity to prompt luminescence intensity also depends on the kind and energy of incident particles as shown in Fig. 3. The ratio decreases with increasing the stopping power of incident particles.

An electron excited by an incident particle or a laser photon has a probability that it recombines with a trapped hole and causes luminescence (prompt luminescence or PSL) or it is trapped by an F^+-center and becomes an F-center. The probability of emission depends on the density of trapped holes. If holes distribute densely, the probability of the recombination will be large and many electrons will cause luminescence. Therefore, the ratio of the prompt luminescence intensity is large and PSL intensity decreases rapidly with the number of reading. From these experimental results, it was deduced that the emission characteristics of photostimulable phosphor were caused by the density of the latent images.

Table 1 The average deposited-energy, the range and the stopping power in the phosphor ($BaFBr:Eu^{2+}$) for various kinds of incident particles.

	^{90}Sr-^{90}Y, β-rays	^{147}Pm, β-rays	^{241}Am, α-rays	Li^{3+}, 50MeV	O^{7+}, 120MeV
E(MeV)	0.2	0.03	3.0	18	90
R(μm)	150	6	20	150	100
E/R(MeV/μm)	0.0013	0.005	0.15	0.12	0.9

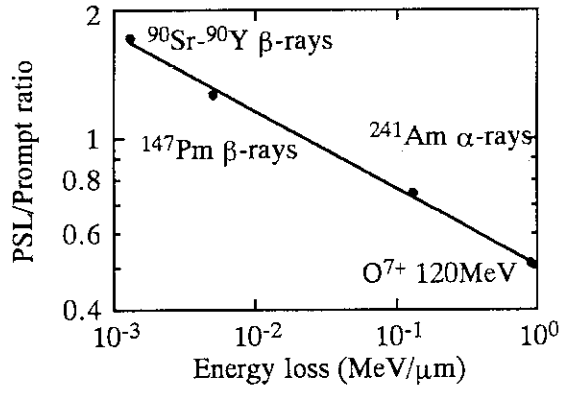

Fig. 3 The ratio of PSL intensity to prompt luminescence intensity.

References

[1] C. Mori, A. Matsumura, T. Suzuki, H. Miyahara, T. Aoyama and K. Nishizawa : Nucl. Instr. and Meth., **A339** (1994) 278.

[2] C. Mori, T. Suzuki, S. Koido, H. Miyahara, A. Uritani and K. Nishizawa : Nucl. Instr. and Meth., **A353** (1994) 371.

5.24 Performance of Light and Heavy Ions Doped Meso-phase Carbon Micro Beads Electrodes for Lithium Battery

S.ISHIYAMA, M. ASANO, H.OMICHI and M.ETO

Recent R&D of new secondary battery of high energy density as a light and miniaturized energy sources for portable equipments are pronounced in the world. In particular, technical advances of lithium secondary battery with carbon negative electrode and lithium positive electrode is manifest, and a lot of noticeable works[1-4] are reported.

However, higher performance have been demanding in these type of battery till now, and inventions of higher density and lower cost materials of electrodes are expected. One of candidate for high performance electrode materials expected its practical use is Meso-phase Carbon Micro Beads(MCMB) and some of those materials are utilized as domestic services.

Table 1 Irradiation conditions of e^-, H^+, B^{+2}, F^{+2}, Au^{+2} and Ag^{+2} on the MCMB targets

Ion	Energy(MeV)	current(micro A)	exposuring time(min)
e^-	0-1.5		0-10
H^+	40	0-1.2	0-30
B^{+2}	50	0-0.2	0-30
F^{+2}	50	0-0.2	0-30
Ag^{+2}	40	0-0.4	0-30
Au^{+2}	40	0-0.35	0-30

Main purpose of present study is to emphasized higher performance of lithium battery electrodes doped with light ion, such as e^-, H^+, B^{+2} and heavy ions such as ,F^{+2} into MCMB material by irradiation techniques. Meso-Carbon Micro Beads(MCMB, Osaka Gas Co. LTD.) powder(grain size >20m), MCMB(Annealing temperature, 2700°C), were prepared to make the electrodes of lithium battery. MCMB powders with polyethylene terephthalate binder are adhered on the nickel mesh electrode targets(200 mesh) of total length and width, 50 mm x 5 mm with 0.5 mm thickness(MCMB attached area;7.5 x 5 x 0.3t) by compressed load. Those electrodes are dried in vacuum at 200 °C for 6 hours prior to irradiation experiments. These MCMB targets have a weight of about 1.3 g. Irradiation experiments of those electrodes were

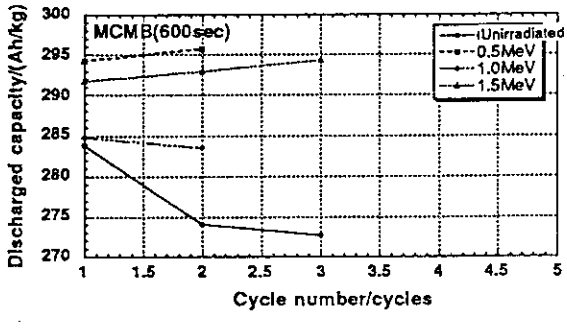

Fig.1 The change in cyclic dischrged capacity of e^- doped MCMB

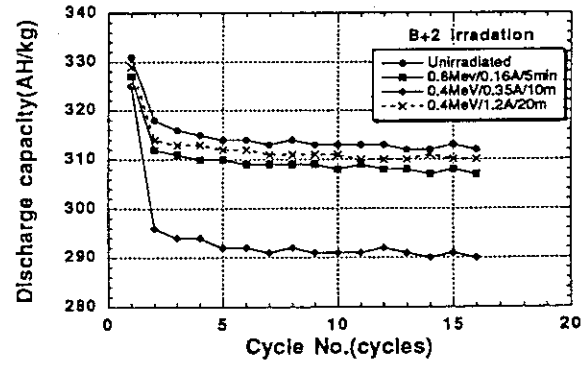

Fig. 2 The change in cyclic discharged capacity of B^{+2} doped MCMB

performed using tandem type accelerator in JAERI. With this apparatus, H^+, B^{+2},F^{+2}, Au^{+2} and Ag^{+2} ions were accelerated up to 50MeV and irradiated on the surface of the electrode targets. Ion beam current was measured by Faraday cup measuring system located in vacuum chamber, which has four stages for irradiation tests and was evacuated up to 10^{-8} torr. During experiments, ion beam can be cut to control ion beam current density doped into the targets by shutter operation. Table 1 shows irradiation conditions for this experiment. The perfoemance of MCMB electrode targets are tested by Galvano-statto(Battery charge-

discharge measurement system, HJ-201B, HOKUTO DENKO Corp.). MCMB and lithium electrode adhered on nickel meshes are settled at negative and positive positions in electrolyte cell poured with lithium perchlorate and ethylene carbonate(1:1) as battery electrolyte. This system are enclosed by argon atmosphere in globe box avoiding oxidation degradation of lithium positive electrode during experiment. In charge and discharged processes, those electrodes are charged cyclically at the currents ranging from 0.1-0.5mA(=0.2-1.0mA/cm^2) with constant voltage of 0-2 V. The battery performance can be evaluated with the charged-discharged capacity obtained in present study.
Fig. 1 shows cyclic discharged performance of e^- irradiated MCMB electrodes obtained in the present study. In the figure, these performance are pronounced as a function of irradiation energy. It is found that the maximum discharged capacity becomes larger than that of unirradiated sample and no degradation, found in unirradiated sample are observed. These facts means that improvement of maximum discharged capacity and cyclical characterization of MCMB can be achieved by the electron irration technique.

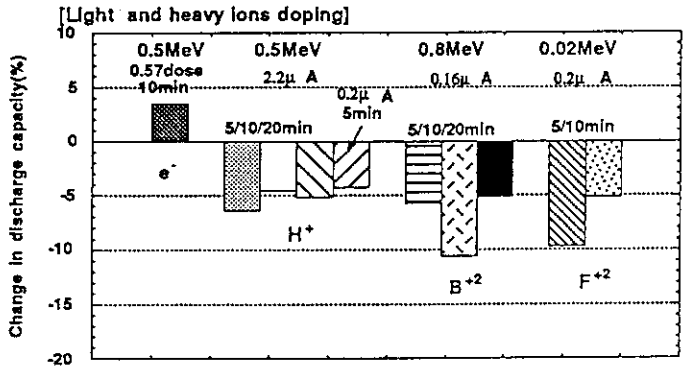

Fig. 3 The change in dischraged capacity of ligh ions doped MCMB

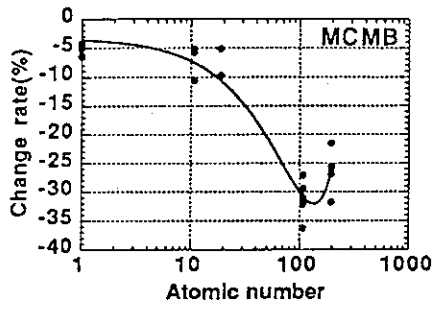

Fig. 4 Degradation rate as a function of atomic number of doped ions

Fig. 2 shows cyclic discharged capacity of B^{+2} doped MCMB samples. There is no remarkable improvement of these characterization after irradiation, but becomes worse at some irradiation conditions. Fig. 3 summarizes the results of discharged capacities of light and heavy ions doped MCMB samples, and Fig. 4 shows the change in discharged capacity of doped MCMB samples by ion doping as a function of atomic number of doped ions. It is clear that degradation rate of maximum discharged capacity is strongly depend on atomic number. These results indicates that doping with such as H^+, B^{+2}, F^{+2}, Au^{+2} and Ag^{+2} ions can not contribute the improvement of MCMB characterizations mainly due to the disturbance of the basal plane structure by ion bombardment. However, recent our results of Li^{+2} doped MCMB exhibits good performance, these detailed results will be reported in next TANDEM report.

References

1) K.A.H.German,C.B.Weare,P.R.Varekamp and et.al., Physical Review Letters,Vol.70(22),pp.3510-3513(1993).
2) S.Yawaguchi, T.Uchida and M.Wakhara, J. of the Electrochemical Soc. V.133(3)pp.677-687(1991).
3) L.W.Shacklette,T.R.Jow,Symp. on Materials and Processes for Lithium Batteries, 9-14 Oct. 1988,Conf-8810205, 408,pp.33-41(1989).
4)K.Inada,D.Ikeda, Y.Sato and et. al., Primary and secondary ambient temperature Li batteries,Hololulu,Hawaii,18-23,Oct. 1987,p530-539(1988).
5) K.M.Abraham, D.M.Pasquariello and G.F.Mcanprews, J. of Electrochem. Soc. V.134(11)P.2661-2676(1987).

6. Publication in Journal and Proceedings, and Contributions to Scientific Meetings

ACCELERATOR OPERATION AND DEVELOPMENT

Journal/Proceedings

Accelerators Division
Development and Construction of the JAERI Tandem-booster
JAERI-Tech 95-034(1995)

Hanashima, S.
Control System for the JAERI Tandem Accelerator
JAERI-Conf 95-021, Proc. of the 10th Symposium on Accelerator Science and Technology, Oct. 25-27, 1995, Hitachinaka, Japan, pp436-438

Takeuchi, S., Shibata, M., Ishii, T., Ikezoe, H. and Yoshida, T.
First Operating Experience with the Superconducting Heavy Ion Tandem-Booster Linac at JAERI
Proc. of the 1994 Int. Linac Conf. Tukuba(1994)pp758-761

Takeuchi, S., Ishii, T., Matsuda, M., Zhang, Y. and Yoshida, T.
Acceleration Tests of the JAERI Tandem Superconducting Booster
Proc. of the 10th Symp. on Accelerator Science and Technology, Hitachinaka Oct. 25-27(1995)pp194-196

Meetings

Takeuchi, S.
The JAERI Tandem Superconducting Booster
The 3rd Symp. on Joint Spectroscopy Experiments Utilizing JAERI Tandem-booster Accelerator, Tokai Sept. 27-28(1995)

Takeuchi, S., Matsuda, M., Zhang, Y. and Yoshida, T.
Acceleration of Heavy Ions by the JAERI Tandem Superconducting Booster
The 7th Int. Conf. on Heavy Ion Accelerator Technology, Camberra Sept. 17-22 (1995)

Yoshida, T.
Status of the JAERI Tandem Accelerator
The 8th Workshop of the Tandem Accelerators and their Associated Technology (Nagoya, July, 6, 1995)

NUCLEAR STRUCTURES

Journal/proceedings

Furutaka, K.
Search for Super Deformed Bands in Ni Region
Proc. 3rd Symposium on Joint Spectroscopy Experimennts Utilizing JAERI Tandem-booster Accelerator (Jul. 27-28, 1995)

Furutaka, K.
Liquid Nitrogen Filling System for Crystal Ball
Proc. 3rd Symposium on Joint Spectroscopy Experiments Utilizing JAERI Tandem-booster Accelerator (Jul. 27-28, 1995)

Hayakawa, T., Furutaka, K., Kidera, M., Hatsukawa, Y., Ishii, T., Oshima, M., Shizuma, T., Mitarai, S., Morikawa, T., Gono, Y., Kusakari, H. and Sugawara, M.
High Spin States of Zn Isotopes
Abstracts of "The Fourth International Conference on Radioactive Nuclear Beams"

Ishii, M., Ishii, T., Makishima, A., Ogawa, M., Momoki, G. and Ogawa, K.
Nuclear Isomerism in ^{100}Sn Neighbors
Physica Scripta 56(1995)89

Kidera, M., Oshima, M., Furutaka, K., Hatsukawa, Y. and Katagiri, M.
Coulomb Excitation of ^{238}U
Proceedings of the Third Symposium on Joint Spectroscopy Experiments Utilizing JAERI Tandem-booster Accelerator. JAERI-Conf, 007(1996)76

Makishima, A., Ishii, T., Ogawa and Ishii, M.
A Graphical Analysis of Decay Curves Measured by the Doppler-shift Recoil distance method
Nucl. Instr. Meth., A363(1995)591

Morikawa, T., Gono, Y., Morita, K., Kishida, T., Murakami, T., Ideguchi, E., Kumagai, H., Lie, G.H., Ferragut, A., Yoshida, A., Zhang, Y.H., Oshima, M., Sugawara, M., Kusakari, H., Ogawa, M., Nakajima, M., Tsuchida, H., Mitarai, S., Odahara, A., Kidera, M., Shibata, M., Kim J.C., Cahe, S.J., Hatsukawa, Y. and Ishihara, M.
Coulomb Excitation of ^{174}Hf K-Isomer
Phys. Lett. B350(1995)169.

Ogawa, M., Tsuchida, H., Makishima, A., Ishii, T., Ishii, M., Momoki, G. and Ogawa, K.
Subnanosecond Isomers in ^{105,107}Sn
Physica Scripta 56(1995)289

Oshima, M., Morikawa T., Hatsukawa, Y., Iimura, H., Hamada, S., Ishii, T., Kusakari H., Kobayashi, N., Taki, M., Sugawara, M., Ideguchi, E. and Gono, Y.
Two-Phonon γ-Vibrational States in Deformed Nuclei
Proc. of Intern. Sympo. on Frontiers of Nuclear Structure Physics (March, 1994) 95.

Oshima, M., Morikawa T., Hatsukawa, Y., Ichikawa, S., Shinohara, S., Matsuo, M., Kusakari, H., Kobayashi, N., Sugawara M. and Inamura, T.
Two-Phonon γ-Vibrational State in ^{168}Er
Phys. Rev. C52(1995)3492

Oshima, M.
On the Three-phonon γ-Vibratinal State
JAERI-Conf 96-007(1996)p.79.

Oshima, M.
Present Status of Joint Spectroscopy Experiments
JAERI-Conf 96-007(1996)p.101.

Meetings

Furutaka, K.
In-beam γ-ray Spectroscopy in A$\sim$60 Region
INS Symposium on "Short-lived nuclear beams '96"(Jan. 6-8, 1996)

Furutaka, K.
Liquid Nitrogen Filling System for JBC Mini-Crystal Ball
Riken Symposium "In-beam γ-ray spectroscopy and Exotic Beam"(Feb. 28, 1996)

Furutaka, K., Kidera, M., Matsuda, M., Hayakawa, T., Hatsukawa, Y., Ishii, T., Oshima, M., Mitarai, S., Shizuma, T., Shibata, M., Watanabe, H., Morikawa T., Komatsubara, T., Saitoh, T., Hashimoto, N., Kusakari, H. and Sugawara, M.
High Spin States of Nulei in Mass 60 Region (Even Nuclei)
Spring Meeting of Physical Society of Japan in Kanazawa (Apr. 3, 1996)

Hayakawa, T.
Japan Ball Project
Riken Symposium of "Gamma Ray Spectroscopy and Exotic Beam"(Feb. 28, 1996)

Hayakawa, T., Furutaka, K., Kidera, M., Hatsukawa, Y., Ishii, T., Oshima, M., Shizuma, T., Mitarai, Shibata, M., Watanabe, H., S., Morikawa T., Gono, Y., Komatsubara, T., Saitou, T., Hashimoto, N., Kusakari, H. and Sugawara, M.
High Spin States of Odd Zn Isotopes
Spring Meeting of Physical Society of Japan in Kanazawa (Apr. 3, 1996)

Ishida, Y., Iimura, H., Ichikawa, S. and Horiguchi, T.
Development of Frequency-reference for Collinear Laser-Ion-Beam Spectroscopy
Spring Meeting of the Physical Society of Japan in Kanazawa (Apr. 2, 1996)

Ishii, T., Makishima, A., Itoh M., Ogawa, M. and Ishii, M.
A g-Factor Measurement of the 6^+ State of $^{106,108}Sn$
Spring Meeting of the Physical Society of Japan in Kanazawa (Apr. 3, 1995)

Kidera, M., Oshima, M., Furutaka, K., Hatsukawa, Y. and Katagiri, M.
Coulomb Excitation of ^{238}U
Proceedings of the Third Symposium on Joint Spectroscopy Experiments Utilizing JAERI Tandem-booster Accelerator in JAERI (Jul. 28, 1995)

Kidera, M., Oshima, M., Hatsukawa, Y. and Morikawa, T.
Multi Coulomb Excitation of ^{238}U
Fall Meeting of the Physical Society of Japan in Nagoya (Sep. 29, 1995)

Komatsubara, T., Jun Lu, Hayakawa, T., Saitoh, T., Hashimoto, N., Takahashi, H., Uchiyama, K., Mukai, J., Furuno, K., Oshima, M., Hatsukawa, Y., Furutaka, K., Kidera, M., Matsuda, M., Ishii, T. and Mitarai, S.
Nuclear Structure of the Odd-Odd ^{122}Cs
Spring Meeting of the Physical society of Japan in Kanazawa (April 3, 1996)

Mukai, J., Tsuchida, H., Mitarai, S., Gono, Y., Morikawa, T., Odahara, A., Shibata, T., Kidera, M., Watanabe, H., Oshima, M., Ishi, T., Hatsukawa, Y., Furutaka, K., Hayakawa, T., Matsuda, M., Komatsubara, T., Ideguchi, E. and Shizuma, T.
Study of High Spin States Following the (^{40}Ca + ^{32}S) Reaction
Spring Meeting of the Physical Society of Japan in Kanazawa (Mar. 31, 1996)

Oshima, M.
On the Three-phonon γ-Vibrational State
3rd Sympo. on Joint Spectroscopy Experiments Utilizing JAERI Tandem-booster Accelerator (Tokai, July 27,28, 1995)

Oshima, M.
Present Status of Joint Spectroscopy Experiments
3rd Sympo. on Joint Spectroscopy Experiments Utilizing JAERI Tandem-booster Accelerator (Tokai, July 27-28, 1995)

Oshima, M., Furono, K., Komatsubara, T., Hayakawa, T., Furutaka, K., Kidera, M., Mitarai, S., Shizuma, T., Hatsukawa, Y., Ishii, T. and Japan Ball collaboration
High-spin States in Nuclei at A=60 Region -Preliminary Results from Joint Program of γ-ray Spectroscopy Experiments at JAERI Tandem Booster Facility-
RIKEN sympo. on Structures of Medium-mass Nuclei (Saitama, December 26-27, 1995)

Oshima, M. and Japan Ball collaboration
Joint Spectroscopy Experiments Utilizing Mini Crystal Ball at JAERI Tandem Booster Accelerator
Spring Meeting of Japan Physical Society of Japan (Kanazawa, April 3, 1996)

Saitoh, T., Hashimoto, N., Uchiyama, K., Takahashi, H., Mukai, J., Jun Lu, Komatsubara, T., Ishii, T., Kidera, M., Hatsukawa, Y., Furutaka, K., Hayakawa, T., Matsuda, M., Oshima, M. and Furuno, K.
Measurement of Internal Conversion Electrons and the Investigation of Shape Coexistence in ^{193}Tl
Spring Meeting of the Physical society of Japan in Kanazawa (April 3, 1996)

NUCLEAR REACTIONS
Journal/Proceedings

Konashi, K., Teshigawara, M., Noro, H., Kayano, H., Aratono Y. and Furukawa, K.
D+D Reactions Induced by Heavy-ion Bombardment
Genshikaku Kenkyu 40, 5, 85(1995)

Kondo, Y., Sugiyama, Y., Tomita, Y., Yamanouchi, Y., Ikezoe, H., Ideno, K., Hamada, S., Sugimutsu, T., Hijiya, M. and Fujita, H.
Airy Minimum Crossing θ_{cm}=90° at E_{lab}=124MeV for the $^{16}O+^{16}O$ System
Phys. Lett. B365(1996)17.

Nagame, Y.
Bimodal Fission
Radioisotopes, 44(1995)677

Pu, Y.H., Lee, S.M., Jeong, S.C., Fujiwara, H., Mizota, T., Futami, Y., Nakagawa, T., Ikezoe, H. and Nagame, Y.
The Competition between Fusion-Fission and Deeply Inelastic Reactions in the Medium Mass Systems.
Z. Phys. A353(1996)387

Sugiyama, Y.
Elastic and Qausi-Elastic Scattering in Heavy-Ion Collisions around the Coulomb Barrier
Proccedings to XV Nuclear Physics Division Conference of European Physical Society on "Low Energy Nuclear Dynamics", St. Petersburg, Russia, 1995, p384-391

Watanabe, Y., Aoto, A., Kashimoto, H., Chiba, S., Fukahori, T., Hasegawa, K., Mizumoto, M., Sugimoto, M., Yamanouti, Y., Koori, N., Chadwick, M.B. and Hodgson, P.E.
Feshbach-Kerman-Koonin Model Analysis of Preequilibrium (p,p') and (p,n) Reactions at 12 to 26 MeV.
Phys. Rev. C51(1995)189

Watanabe, Y.
Applications of the Feshbach-Kerman-Koonin Model to (p,p') Reactions at Low Incident Energies
Proc. of Int. Symp. on Pre-Equilibrium Reactions, Smolenice, Ocober 1995, acta physica slovaca 45(1995)749

Meetings

Fujita, H.
Magnetic Substate Populations and Spin Assignments of Intermediate Structures in $^{12}C(^{16}O,^{12}C(2^{+}))^{16}O$
Oral contribution to 2nd Kyushu-Korea Joint Symposium on Nuclear Physics, Fukuoka (November, 1995)

Hatsukawa, Y., Hata, K., Tsukada, K., Shinohara, N., Oura, Y., Nagame, Y., Nishinaka, I. and Ichikawa, S.
Study of the Excitation Functions of $^{238}U(^{6,7}Li,xn)^{245,244-x}Am$ Reactions.
The 39th symposium on radiochemistry in Niigata (Oct. 2, 1995)

Ikezoe, H., Nagame, Y., Ikuta, T., Hamada, S., Nishinaka I. and Ohtsuki, T.
JAERI Recoil Mass Separator,
IN2P3-RIKEN symposium, 1995

Nagame, Y., Nishinaka, I., Tsukada, K., Oura, Y., Ichikawa, S., Ikezoe, H., Zhao, Y.L., Sueki, K., Nakahara, H., Ohtsuki, T., Tanikawa, M., Kudo, H., Hamajima, Y., Takamiya, K. and Chung, Y.H.
Bimodal Nature of Actinide Fission
1995 International Chemical Congress of Pacific Basin Society in Honolulu (Dec. 19, 1995)

Nagame, Y., Nishinaka, I., Tsukada, K., Oura, Y., Ichikawa, S., Ikezoe, H., Zhao, Y.L., Sueki, K., Nakahara, H., Ohtsuki, T., Tanikawa, M., Kudo, H., Hamajima, Y., Takamiya, K. and Chung, Y.H.
Two Independent Deformation Paths in Low Energy Fission of Actinide
Spring Meeting of the Physical Society of Jpan in Kanazawa (Mar. 31, 1996)

Nakanishi, K., Inoue, T., Takamiya, K., Yokoyoma, A., Saito, T., Baba, H., Nagame, Y., Nishinaka, I, Tsukada, K. and Shinohara, N.
The Proton Induced Fission of ^{238}U
Spring Annual Meeting of the Chemical Society of Japan, Tokyo (March, 28-31, 1996)

Nakanishi, K., Inoue, T., Takamiya, K., Yokoyoma, A., Saito, T., Baba, H., Nagame, Y., Nishinaka, I, Tsukada, K. and Shinohara, N.
The Proton Induced Fission of ^{238}U
Spring Annual Meeting of the Chemical Society of Japan, Tokyo (March, 28-31, 1996)

Nishinaka, I., Nagame, Y., Oura, Y., Tsukada, K., Ichikawa, S., Ikezoe, H., Zhao, Y., Sueki, K., Nakahara, H., Kudo, H., Hamajima, Y., Ohtsuki, T., Tanikawa, M., Takamiya, K. and Chung, Y.
Fission of p + ^{232}Th System Ⅱ-Neutron Emission from Fission Fragments.
The 39th Symposium on Radiochemistry, Niigata (Oct., 2-4, 1995).

Nishinaka, I., Nagame, Y., Oura, Y., Tsukada, K., Ichikawa, S., Ikezoe, H., Zhao, Y., Sueki, K., Nakahara, H., Kudo, H., Hamajima, Y., Ohtsuki, T., Tanikawa, M., Takamiya, K. and Chung, Y.
Correlation between Mass Division Modes and Neutron Multiplicity in Fission.
Spring Annual Meeting of the Chemical Society of Japan, Tokyo (March, 28-31, 1996)

Oura, Y., Tsukada K., Nishinaka, I., Hatsukawa, Y., Shinohara, N., Ichikawa, S., Hata, K. and Nagame Y.
Search for ^{236}Am(2)
The 39th Symposium on Radiochemistry (Oct. 2, 1995)

Sueki, K., Zhao, Y.L., Nakahara, H. Nagame, Y., Nishinaka, I., Tsukada, K., Oura, Y., Ichikawa, S., Ikezoe, H., Tanikawa, M., Ohtsuki, T., Kudo, H., Hamajima, Y., Takamiya, K. and Chung, Y.H.
Energy Dependence on Two Mode of Mass Divisions in the Actinoid Fission
Spring Meeting of the Chemical Society of Japan in Tokyo (Mar. 31, 1996)

Sugiyama, Y.
New Approach to Resonance Spin Determinations
Joint Japan-US Seminer on Clustering Phenomena in Nuclear and Mesoscopic Systems, Dec. 14-16, 1995, Honolulu, Hawai

Sugiyama, Y.
Elastic Two-Neutron Transfer Reactions Around the Coulomb Barrier
INS Symposium of Experimental and Theoretical Study on Unified description for Neuclear Reaction Mechanism, INS, University of Tokyo (Mar. 25, 1996)

Tanikawa, M., Nishinaka, I., Oura, Y., Nagame, Y., Tsukada, K., Ichikawa, S., Ikezoe, H., Zhao, Y.L., Sueki, K., Nakahara, H., Kudo, H., Hamajima, Y., Ohtsuki, T., Takamiya, K. and Chung, Y.H.
Fission of p+^{232}Th System -Fragment Mass and Kinetic Energy Distributions-
The 39th Symposium on Radiochemistry in Niigata (Oct. 2, 1995)

Teshigawara, M., Konashi, K., Yamamoto, T., Kayano, H., Aratono, Y., Furukawa, K. and Tachikawa, E.
D+D Reaction Induced by Heavy-ion Bombardment
Fourth International Conference on Cold Fusion in Hawaii (December 6-9. 1993)

Teshigawara, M., Konashi, K., Yamamoto, T., Kayano, H., Aratono, Y., Furukawa, K. and Tachikawa, E.
D+D Reaction Induced by Heavy-ion Bombardment
Spring Meeting of the Physical Society of Japan in Fukuoka (March 28-31. 1994)

Uno, Y., Meigo, S., Chiba, S., Fukahori, T., Ikeda, Y., Kasugai, Y. and Iwamoto, O.
Measurements of Activation Cross Sections at 17.5-30 MeV by Using the $^{7}Li(p,n)$ Quasi Monoenergetic Neutron Source at JAERI-tandem II
Spring Meeting of Japan Atomic Energy Society of Japan in Osaka (Mar. 27-29, 1996)

Yamanouti, Y., Sugiyama, Y., Tomita, Y. and Ideno, K.
Elastic and Inelastic Scattering of 115MeV ^{12}C from ^{54}Fe
Fall Meeting of the Physical Society of Japan in Nagoya (Sept. 27, 1995)

Yamanouti, Y., Sugiyama, Y., Tomita, Y. and Ideno, K.
$^{50}Ti(^{12}C,^{12}C')^{50}Ti^{*}$ Reaction at E=115MeV
Spring Meeting of the Physical Society of Japan in Kanazawa (Apr. 1, 1996)

NUCREAR TEHORY
Journal/Proceedings

Angel, A., Tanaka, E., Maruyama, Tomoyuki., Ono, A. and Horiuchi, H.
Delta Degree of Freedom in Antisymmetrized Molecular Dynamics and (p,p') Reactions in the Delta Region
Phys. Rev. C52(1995)3231.

Chadwick, M.B., Chiba, S., Niita, K., Maruyama, Toshiki. and Iwamoto, A.
Quantum Molecular Dynamics and Multistep-Direct Analysis of Multiple Preequilibrium Emission
Phys. Rev. C52(1995)2800.

Chadwick, M.B., Young, P.G. and Chiba, S.
Photonuclear Angular Distribution Systematics in the Quasideuteron Regime
J. Nucl. Sci. & Tech. 32(1995)1154.

Chiba, S., Fukahori, T., Takada, H., Maruyama, Toshiki., Niita, K. and Iwamoto, A.
Applicability of the Quantum Molecular Dynamics to Nucleon-Nucleus Collisions
Proc. Int. Conf. Nuclear Data for Science and Technology, World Scientific, p505(1995)

Fujii, H., Maruyama, Tomoyuki., Mutoh, T. and Tatsumi, T.
Equation of State with Kaon Condensation and Neutron Stars
Nucl. Phys. A597(1966)645.

Ishibashi, K., Yoshizawa, N., Takada, H. and Nakahara, Y.
High-Energy Transport Code HETC-3Step Applicable to Incident Energies Below 100MeV
Proc. Int. Conf. Nuclear Data for Science and Technology, World Scientific, p571(1995)

Iwamoto, A., Möller, P., Nix, J.R. and Sagawa H.
Collision of Deformed Nuclei: A Path to the Far Side of the Superheavy Island
Nucl. Phys. A596(1996)329.

Iwamoto, A.
Summary of the VHE Ⅲ Section
Proc. Tours Symp. on Nuclear Physics Ⅱ, World Scientific, p414.

Maruyama, Tomoyuki., Cassing, W., Mosel, U. and Teis, S.
High Energy Heavy-Ion Collisions in a RBUU-Approach with Momentum-Dependent Mean-Fields
Proc. Theor. Phys. Supplement No.120(1995)283.

Maruyama, Tomoyuki., Maruyama, Toshiki. and Niita K.
Relativistic Effects in Sumulations of the Fragmentation Process with the Microscopic Framework
Phys. Lett. B358(1995)34.

Maruyama, Tomoyuki., Niita, K. and Iwamoto, A.
Extension of Quantum Molecular Dynamics and Its Application to Heavy-Ion Collisions
Phys. Rev. C53(1996)297.

Niita, K., Chiba, S., Maruyama, Toshiki., Maruyama Tomoyuki., Takada, H., Fukahori, T., Nakahara Y. and Iwamoto, A.
Analysis of the (N,$_x$N') Reactions by Quantum Molecular Dynamics Plus Statistical Decay Model
Phys. Rev. C52(1995)2620.

Tanaka, E.I., Ono, A., Horiuchi, H., Maruyama, Tomoyuki. and Engel, A.
Proton Inelastic Scattering to Continuum Studied with Antisymmetrized Molecular Dynamics
Phys. Rev. C52(1995)316.

Yoshizawa, N., Ishibashi, K. and Takada, H.
Development of High Energy Transport Code HETC-3STEP Applicable to the Nuclear Reaction with Incident Energies above 20 MeV
J. Nucl. Sci. & Tech. 32(1995)601.

Meetings

Chiba, S., Niita, K., Maruyama, Toshiki., Takada, H., Fukahori, T. and Iwamoto, A.
The Quantum Molecular Dynamics Approach to Nucleon-Nucleus Reaction at Intermediate Energy Region
3rd Int. Seminar on Interaction of Neutrons with Nuclei, Dubna (Apr. 26, 1995)

Iwamoto, A.
Extended QMD and Low Energy Heavy-Ion Reactions
Int. Symp. on Heavy Ion Physics and Its Applications, Ransyu (Aug. 31, 1995)

Iwamoto, A., Möller, P., Nix, J.R. and Sagawa, Y.
Sper-Heavy-Element Productin using the Fusion of Deformed Nuclei
Fall Meeting of the Physical Society of Japan, Nagoya (Sep. 30, 1995)

Iwamoto, O., Chiba, S., Niita, K. and Iwamoto, A.
Calculation of the Isotope-Production Cross Sections with QMD
Spring Meeting of the Atomic Energy Society of Japan, Osaka (Mar. 28, 1996)

Maruyama, Tomoyuki.
Multifragmentation in α(5GeV/u)+Au Reactions
2nd RIKEN/INFN Joint Symposium (May 22, 1995)

Maruyama, Tomoyuki.
Intermediate Energy Heavy-Ion Collisions with Neutron Rich Nuclei
Int. Nuclear Physics Conf., Beijing, Poster (Aug. 22, 1995)

Maruyama, Tomoyuki.
Second Order Effects on Kaon Condensation in Relativistic Mean-Field Theory
Int. Nuclear Physics Conf., Beijing, Poster (Aug. 22, 1995)

Maruyama, Tomoyuki.
Multifragmentation in α(5 GeV/u)+Au Reactions
The 3rd Symposium on Simulation study of Hadronic Many-body System in JAERI
(December, 1995)

Maruyama, Tomoyuki.
Properties of Nuclear Matter using the Relativistic Mean Field Approximation with K-N Interaction
Fall Meeting of the Physical Society of Japan, Nagoya (Sep. 28, 1995)

Maruyama, Tomoyuki.
Multifragmentation in α(5GeV/u)+Au Reactions
Fall Meeting of the Physical Society of Japan, Nagoya (Sep. 30, 1995)

Maruyama, Tomoyuki.
Influence of the Momentum-Dependent Mean Field on Measurable Quantitiy
RCNP Meeting on Relativistic Approach to Nuclear Structure and Reactions,
Osaka (Nov. 9, 1995)

Maruyama, Tomoyuki.
The Isovector Optical Potential and the Symmetry Energy at High Density in the Relativistic Approach — Application to the Neutron Star —
Mini-Winter-School on Unified Neutron Optical Potential, Hakata (Jan. 12, 1996)

Maruyama, Tomoyuki.
Multifragmentation in α+Au Collision at E_{lab}=5 GeV/u
International Nuclear Physics Conference in Beijing (August, 21-26, 1995)

Maruyama, Tomoyuki., Niita, K. and Maruyama, Toshiki.
Heavy-Ion Reactions and Relativistic Effect
Fall Meeting of the Physical Society of Japan, Nagoya (Sep. 30, 1995)

Möller, P. and Iwamoto, A.
Nuclear Deformation and SUb-Barrier Fusion Cross Sectins
Int. Nuclear Physics Conf., Beijing, Poster (Aug. 22, 1995)

Maruyama, Toshiki., Niita, K. and Iwamoto, A.
Low-Energy Nuclear Reactions Calculated by QMD Model
Fall Meeting of the Physical Society of Japan, Nagoya (Sep. 30, 1995)

Maruyama, Toshiki., Niita, K. and Iwamoto, A.
Extention of Quantum Molecular Dynamics and Its Application to Heavy-Ion Collisions
Int. Nuclear Physics Conf., Beijing, Poster (Aug. 22, 1995)

Maruyama, Tomoyuki., Teis, S., Cassing, W. and Mosel, U.
High Energy Heavy-Ion Reactions in the RBUU Approach
Int. Nuclear Physics Conf., Beijing, Poster (Aug. 22, 1995)

Niita, K., Chiba, S., Takada, H., Fukahori, T., Maruyama, Toshiki. and Iwamoto, A.
Quantum Molecular Dynamics Calculations for Nucleus-Nucleus Reactions
Int. Nuclear Physics Conf., Beijing, Poster (Aug. 22, 1995)

ATOMIC PHYSICS, SOLID STATE PHYSICS AND RADIATION EFFECTS OF MATERIALS
Journal/Proceedings

Gao, X., Kazumata, Y., Kumakura, H and Togano, K.
Effects of 230 MeV Au^{14+} Irradiation on $Bi_2Sr_2CaCu_2O_x$
Physica C250(1995)325

Harada, K., Kasai, H., Kamimura, O., Matsuda, T., Tonomura, A., Okayasu, S. and Kazumata, Y.
Observation of Dynamics of Flux-Line Relaxation in Ion Irradiated $Bi_2Sr_{1.8}CaCu_2O_x$ by Lorentz Microscopy
Phys. Rev. B53(1996)9400.

Ishikawa, N., Iwase, A., Iwata, T., Maeta, H., Tsuru, K. and Michikami, O.
Ion Irradiation Effects in $EuBa_2Cu_3O_y$ Thin Film
J. of Supercond., 7(1994)241.

Ishikawa, N., Iwase, A., Chimi, Y., Maeta, H., Tsuru, K. and Michikami, O.
Lattice Expansion in $EuBa_2Cu_3O_y$ Irradiated with Energetic Ions
Physica C259(1996)54.

Kanno, I., Nishio, K., Mikawa, T., Nakagome, Y., Kobayashi, K. and Kimura, I.
Resistivity Estimation of Irradiated Silicon Surface Barrier Detector
Nucl. Instrum. and Meth., A348(1994)479.

Kanno, I., Inbe, T., Kanazawa, S. and Kimura, I.
Improved Model of Plasma Column Erosion in a Silicon Surface Barrier Detector
Rev. Sci. Instrum., 65(1994)3040.

Kanno, I.
Electric Field Stregth in a Silicon Surface Barrier Detector with the Presence of a Dielectric Plasma Column
Nucl. Instrum. and Meth., A353(1994)93.

Kazumata, Y., Gao, X., Kumakura, H. and Togano, K.
Irradiation Effects of High-T_c Superconductors
Proc. US-Japan Workshop on High-T_c Superconductors (Oct., 24-25, 1995)291

Kumakura, H., Togano, K., Tomita, N., Yanagisawa, E., Okayasu, S. and Kazumata, Y.
Comparative study on 180MeV Cu^{11+} Irradiation Effect on Textured $YBa_2Cu_3O_x$ and $Bi_2Sr_2CaCu_2O_y$
Physica C251(1995)231

Kuriyama, K., Kato, Takashi., Kato, Tomoharu., Sugai, H., Maeta, H. and Yahagi, M.
Radiation Effects on Li-vacancy Ordering in β-LiAl
Phys. Rev. B52(1995)3020

Ono, F., Matsumoto, N., Maeta, H., Jakubovics, J.P., Hruna, H. and Kato, T.
Induced Magnetic Anisotropy in Amorphous Ferromagnetic Alloys by Ion Beam Irradiation
Ion Beam Modiafication of Metals (eds by J.S. Willians, R.G. Elliman and M.C. Ridgway)(1996)p1020.

Sasaki, Y., Zhou, W.L., Ikuhara, Y. and Saka, H.
Cascade Defects as Flux Pinning Centers in Bi2212 Single Crystal Generated by Ion Irradiation.
Proc. The JIM '95 Fall Annual Meeting in Hawaii (Dec. 13-15, 1995)

Zhou, W.L., Sasaki, Y. and Ikuhara, Y.
Microstructure characterization of $Bi_2Sr_2CaCu_2O_x$ single crystal irradiation with 18 MeV Fe^{8+}ions
Physica C234(1994)323

Meetings

Furukawa, K., Ohno, S., Namba, H., Taguchi, M. and Watanabe, R.
Radial Dose Distribution around an Energetic Heavy Ion's Path and an Ion Track Structure Model
The 7th International Symposium on Advanced Nuclear Energy Research in Takasaki (Mar. 19, 1995)

Haruna, K., Maeta, H., Sugai, H., Iwasita, K., Saito, Y., Matsumoto, N., Ono, F., Otsuka, H. and Ohashi, K.
Electrical Conductivity of B-doped Synthetic Diamonds Irradiated by Heavy Ions
Diamond Films'95 Barcelona, Spain (11 Sept. 1995)

Haruna, K., Maeta, H., Sugai, H., Sato, T., Ootsuki, T., Iwasita, K., Saito, Y., Matsumoto, N., Ono, F., Otsuka, H. and Ohashi, K.
Electrical Conductivity of B-doped Diamonds Irradiated by Heavy Ions
9th Diamond Symposium in Tokyo (Nov. 21, 1995)

Hayashi, K., Kikuchi, H., Fukuda, K., Nogita, K. and Une, K.
Radiation Damage of UO_2 and Gd_2O_3-doped UO_2 by High Energy Ions
(I) Changes in Surface Structure and Lattice Parameter
1996 Annual Meeting of Atomic Energy Soc. Japan (March 28, 1996, Osaka Univ.)

Ishikawa, N., Iwase, A., Chimi, Y., Maeta, H., Tsuru, K. and Michikami, O.
Lattice Parameter Change in $EuBa_2Cu_3O_y$ Illadiated with Heavy Ions
Fall meeting of the Physical Society of Japan in Osaka (Sep. 30, 1995)

Ishikawa, N., Iwase, A., Chimi, Y., Maeta, H., Tsuru, K. and Michikami, O.
Unusual Lattice Expansion in $EuBa_2Cu_3O_y$ Illadiated with Heavy Ions
1995 Materials Research Society Fall Meeting in Boston (Nov. 27, 1995)

Iwase, A.
Defect Production and Annihilation in Metals through Electonic Excitation by Energeric Heavy Ion Bombardment
The 7th International Symposium on Advanced Nuclear Energy Reserch in Takasaki (March 19, 1996).

Kanno, I., Kanazawa, S., Takada, H. and Meigo S.
Simultaneous Measurement of Pulse Height and Rise Time in Si Surface Barrier Detector
1995 Fall Meeting of the Atomic Energy Society of Japan in Tokai (Oct. 18, 1995)

Kasai, H., Harada, K., Kamimura, O., Matsuda, T., Tonomura, A., Okayasu, S. and Kazumata, Y.
Observation of Dynamics of Flux-Line Relaxation in Ion Irradiated $Bi_2Sr_{1.8}CaCu_2O_x$ by Lorentz Microscopy.
The 52nd Annual Meeting of the Japanese Society of Electron Microscopy in Tokyo (May 23, 1996)

Kazumata, Y., Gao, X., Kumakura, H. and Togano, K.
Effects of 230 MeV Au^{14+} Irradiation in $Bi_2Sr_2CaCu_2O_x$
Int. Conf. Surface Modification by Ion Beam (INASMET, '95) at San Sebastian in Spain (Sept. 2. 1995)

Kazumata, Y., Gao, X., Kumakura, H. and Togano, K.
Irradiation Effects of High-T_c Superconductors
US-Japan workshop on high-T_c Superconductors at Tsukuba (Oct., 25, 1995)

Kuribayashi, M., Inoue, A., Katoh, H., Ishida, K., Tomimitu, H. and Kazumata, Y.
Diffraction Plane Dependence of X-ray Diffraction Patterns from Distorted Crystals.
Annu. Meeting of the Physical Society of Japan in Osaka (Sept. 29, 1995)

Kuribayashi, M., Inoue, A., Katoh, H., Ishida, K., Tomimitu, H. and Kazumata, Y.
X-ray Study of Defects Produced By MeV Ion Implantation into Si Perfect Crystals.
AsCA'95 Conference in Bangkok (Nov. 23, 1995)

Maeta, H., Haruna, K., Matsumoto, N., Saotome, T., Ono, F., Otsuka, H. and Ohashi, K.
A Characterization of Synthetic and Natural Single Crystal Diamonds by X-ray Diffraction
DIAMOND FILMS'95 Barcelona, Spain (11 Sept. 1995)

Maeta, H., Haruna, K., Matsumoto, N., Saotome, T., Ono, F., Otsuka, H., Kato, T. and Ohashi, K.
A Characterization of Synthetic and Natural Single Crystal Diamonds by X-ray Diffuse Scattering
9th Diamond Symposium in Tokyo (Nov. 21, 1995)

Matsumoto, N. and Maeta, H.
A Study of Defect Structure in Diamond by X-ray Diffuse Scattering Method
Spring Meeting of the Physical Society of Japan in Kanazawa (March 30, 1996).

Nakazawa, T., Yamaki, D. and Noda, K.
Structural Changes of Li_4SiO_4 Irradiated with Ion Beam
Annual Meeting of Atomic Energy Soc. Japan in Kyoto (March, 27, 1996)

Nogita, K., Une, K., Masuda, H., Hayashi, K. and Fukuda, K.
Radiation Damage of UO_2 and Gd_2O_3-doped UO_2 by High Energy Ions
(II) Depth Profiles of Damage

1996 Annual Meeting of Atomic Energy Soc. Japan (March 28, 1996, Osaka Univ.) K32

Ohtsuka H., Maeta, H., Matsumoto, N., Yamakawa, K., Kato, T., Sasase, M., Saotome, T., Yuya, H., Arita, Y. and Motohashi, H.
X-ray Diffuse Scattering from Defect Clusters in FCC Metals
Spring Meeting of the Phsical Society of Japan in Kanazawa (Apr, 1, 1996).

Okayasu, S. and Kazumata, Y.
Proton Irradiation Effects on QMG-YBCO(Ⅱ)
Fall Meeting of the Japan Physics Society in Osaka (Sept. 30, 1995)

Sataka, M., Kitazawa, S., Komaki, K., Yamazaki, Azuma, T., Y., Shibata, H., Kawatsura, K. and Tawara, H.
Electron Capture Differential Cross Sections for 5 MeV Proton -Rare Gas Collisions.
Spring Meeting of Physical Society of Japan in Kanazawa (Mar. 31 1996).

Sasaki, Y., Zhou, W.L. and Ikuhara, Y.
Effect of Ion Irradiation on Superconductivity and Microstructure of $Bi_2Sr_2CaCu_2O_x$ Superconductor
Spring Meeting of the Ceramic Society of Japan in Yokohama (Apr. 2, 1995)

Sasaki, Y., Zhou, W.L. and Ikuhara, Y.
Qualitative Determination of Relationship between Flux Pinning Effect and Irradiation Defects in Bi2212 Single Crystal.
International Symposium on Superconductivity '95 in Hamamatsu (Oct. 30. 1995)

Sugai, H., Yahagi, M., Kuriyama, K., Tanase, M. and Maeta, H.
Radiation Effects on Electrical Resistivity in Intermetallic Compound β-LiAl
Fall Meeting of the Atomic Energy Society of Japan in Tokai (Oct. 17, 1996)

Suzuki, T., Sakai, H., Uritani, A., Mori, C., Yoshida, M., Takahashi, F. and Takahashi, K.
Luminescence Characteristics of Imaging Plate with Heavy Charged Particle
The 33rd Annual Meeting on Radioisotopes in the Physical Sciences and Industries in Tokyo (Jul. 2, 1996)

7. Personnel and Committees

(1) Personeel (FY 1995)

Department of Reactor Engineering

	Yoshio Murao	Director
	Yasuo Suzuki	
	Hiroshi Maekawa	Deputy Director
	Takashi Okabe	Administrative Manager

Accelerators Division

Scientific Staff	Chiaki Kobayashi*
	Suehiro Takeuchi
	Susumu Hanashima
	Makoto Matsuda
Technical Staff	Tadashi Yoshida
	Isao Ohuchi
	Tokio Shoji
	Susumu Kanda
	Katsuzo Horie
	Yoshihiro Tsukihashi
	Shinichi Abe
	Shuhei Kanazawa
	Nobuhiro Ishizaki
	Hidekazu Tayama

Nuclear Data Center

	Yasuyuki Kikuchi*
	Satoshi Chiba
	Tokio Fukahori
	Osamu Iwamoto

Thermal Reactor Physics Laboratory

	Tsuyoshi Yamane
	Hiroshi Takada
	Shin-ichiro Meigo

Fusion Neutronics Laboratory

Yujiro Ikeda*

Yoshitomo Uno

Yoshimi Kasugai

* Head

Advanced Science Research Center
Mitsuhiko Ishii

Research Group for Exotic Heavy Nuclei
Hiroshi Ikezoe*
Yasuharu Sugiyama
Masumi Ohshima
Yoshiaki Tomita
Kazumi Ideno
Yoshimaro Yamanouti
Michiaki Sugita
Tetsuro Ishii
Shingo Hamada
Tomohiko Ikuta
Kazuyoshi Furutaka
Takehito Hayakawa

Research Group for Hadron Transport Theory
Akira Iwamoto*
Yasuaki Nakahara
Toshiki Maruyama
Tomoyuki Maruyama

Research Group for Low-Temperature Radiation Effects
Akihiro Iwase*
Norito Ishikawa
Yasuhiro Chimi

Department of Health Physics
Radiation Control Division II
Masayuki Ueno
Katsuya Kawasaki
Tohru Tayama

Radiation Dosimetry Laboratory
Makoto Yoshida
Fumiaki Takahashi

* Head or Leader

Department of Materials Science and Engineering
Material Innovation Laboratory
Kenji Noda*
Tetsuya Nakazawa
Daijyu Yamaki

Solid State Physics Laboratory
Yukio Kazumata*
Masao Sataka
Satoru Okayasu
Sin-iti Kitazawa

Neutron Scattering Laboratory
Hiroshi Tomimitsu
Kazuya Aizawa

Synchrotron Radiation and Solid States Laboratory
Hiroshi Maeta*
Hideo Ohtsuka
Norimasa Matsumoto
Teruo Kato

Department of Chemistry and Fuel Research
Physical Chemistry Laboratory
Yoshihide Komaki
Jiro Ishikawa

Laser Chemistry Laboratory
Koji Shiraishi*
Katsutoshi Furukawa
Yasuyuki Aratono

Fuel Irradiation and Analysis Laboratory
Kousaku Fukuda*
Satoru Kashimura
Kimio Hayashi
Hironobu Kikuchi
Toshiko Ohmichi

* Head

Department of Radioisotopes
Isotope Research and Development Division
Nobuo Shinohara
Yuichiro Nagame
Shin-ichi Ichikawa
Yuichi Hatsukawa
Kazuaki Tsukada
Hideki Iimura
Hiroyuki Sugai
Ichiro Nishinaka
Kentaro Hata
Yasuji Oura

Department of High Temperature Engineering
Energy Materials Development Laboratory
Motokuni Eto*
Shintaro Ishiyama
Shin-ichi Baba
Hirokazu Ugachi
Masahiro Ishihara

Applied Radiation Laboratory
Shinichiro Meigo
Hiroshi Takada

Functional Materials Laboratory
Masaharu Asano
Hideki Omichi

* Head

(2) Tandem Steering Committee

(Chirman)	Shinzo	Saito	(Deputy Director General, Tokai Research Establishment)
	Muneyuki	Date	(Director, Advanced Science Research Center)
	Satoru	Funahashi	(Director, Department of Materials Science and Engineering)
	Yoshio	Murao	(Director, Department of Reactor Engineering)
	Muneo	Handa	(Director, Department of Chemistry and Fuel Research)
	Michio	Hoshi	(Director, Department of Chemistry and Fuel Research)
	Hisamichi	Yamabayashi	(Director, Department of Radioisotopes)
(Secretary)	Chiaki	Kobayashi	(Head, Accelerator Division)
(Secretary)	Tadashi	Yoshida	(Head, Accelerator Division)
(Secretary)	Tadashi	Okabe	(Administrative Manager, Department of Reactor Engineering)

(3) Tandem Consultative Committee

(Chairman)	Michio	Ichikawa	(Director General, Tokai Research Establishment)
(Vice Chairman)	Shinzo	Saito	(Deputy Director General, Tokai Research Establishment)
(Vice Chairman)	Yoshio	Murao	(Director, Department of Reactor Engineering)
	Mamoru	Akiyama	(Professor, University of Tokyo)
	Hiroyasu	Ejiri	(Professor, Osaka University)
	Naohiro	Hirakawa	(Professor, Tohoku University)
	Nobutsugu	Imanishi	(Professor, Kyoto University)
	Jun	Imasato	(Professor, National Laboratory for High Energy Physics)
	Masayasu	Ishihara	(Professor, University of Tokyo, Research Scientist, Institute of Physical and Chemical Research)
	Yasuo	Ito	(Associate professor, University of Tokyo)
	Hisaaki	Kudo	(Associate professor, Niigata University)
	Kohzoh	Masuda	(Professor, University of Tsukuba)
	Shunpei	Morinobu	(Professor, Kyushu University)
	Hiromichi	Nakahara	(Professor, Tokyo Metropolitan University)

	Naoto	Sekimura	(Associate professor, The University of Tokyo)
	Akito	Takahashi	(Professor, Osaka University)
	Hiroyuki	Tawara	(Associate Professor, Institute of Plasma Physics, Nagoya University)
	Hirosuke	Yagi	(Professor, University of Tsukuba)
	Sadae	Yomaguchi	(Professor, The Research Institute for Iron Steel and Other Metals, Tohoku University)
	Kenji	Morita	(Professor, Nagoya University)
(Secretary)	Yasuo	Suzuki	(Department of Reactor Engineering)
(Secretary)	Hiroshi	Maekawa	(Deputy Director, Deportment of Reactor Engineering)
(Secretary)	Hiroshi	Ikezoe	(Head, Research Group for Exotic Heavy Nuclei, Advanced Science Research Center)
(Secretary)	Akira	Iwamoto	(Head, Research Group for Hadron Transport Theory)
(Secretary)	Akihiro	Iwase	(Head, Research Group for Low-Temperature Radiation Effects, Advanced Science Research Center)
(Secretary)	Hiroshi	Maeta	(Head, Synchrotron Radiation and Solid State Labratory)
(Secretary)	Kenji	Noda	(Head, Material Innovation Laboratory, Department of Materials Science and Engineering)

(Secretary)	Takashi	Okabe	(Adiministrative Manager, Depertment of Reactor Engineering)
(Secretary)	Toshiaki	Sekine	(Department of Radioisotopes)
(Secretary)	Suehiro	Takeuchi	(Department of Reactor Engineering)
(Secretary)	Tadashi	Yoshida	(Head, Accelerators Division)

8. Cooperative Researches

	Title	Contact person Organization
		H8-4-1
1.	Study of Unstable Nuclei Produced by Multi-Nucleon Transfer Reactions	Toru NOMURA Institute for Nuclear Study, University of Tokyo
2.	Atomic Collision Research Using Highly Charged Ions	Ken-Ichiro KOMAKI Institute of Physics, College of Arts and Sciences, University of Tokyo
3.	Electromagnetic Properties of Proton-rich Nuclei	Masao OGAWA Tokyo Institute of Technology
4.	Radiation Effects of High T_c Materials	Hiroaki KUMAKURA National Research Institute for Metals
5.	X-Ray Study of Irradiation Defects Caused by MeV Ion Implatation in Si Perfect Crystals.	Kohtaro ISHIDA Faculty of Science, Science University of Tokyo
6.	Study of Multipole Deformed State in Heavy Nuclei II	Hideshige KUSAKARI Faculty of Education, Chiba University
7.	Dependence of Bimodal Fission on Excitation Energy	Hiromichi NAKAHARA Faculty of Science, Tokyo Metropolitan University
8.	Study on Decay Properties of Heavy Nuclei Using JAERI Recoil Mass Separator	Jirota KASAGI Laboratory of Nuclear Science, Tohoku University

9.	Study of Molecular Resonance in Heavy-Ion Reaction	Takao NAKAJIMA Department of Physics, Kyushu University
10.	Search for Large Nuclear Deformation near N=Z Region	Yasuyuki GONO Faculty of Science, Kyushu University
11.	Responce of Semiconductor Detectors to Heavy Ions	Itsuro KIMURA Division of Nuclear Engineering, Kyoto University
12.	Radiation Damage of Materials for Environment Resistance Devices	Kazutoshi OHASHI Faculty of Engineering, Tamagawa University
13.	Irradiation Effect on Electrical Property of LiAl with Li and Other Heavy Ions	Kazuo KURIYAMA Research Center of Ion Beam Technology, Hosei University
14.	Radiation Effects of Li_2O	Shoichi NASU Kanazawa Institute of Technology
15.	Study of Luminescence Charactoristics of Photostimulable Phoser with Heavy Charged Particles	Chizuo MORI School of Engineering, Nagoya University
16.	Study of Phase Trnasition on Nuclear Fission Phenomenon	Hiroshi BABA Faculty of Science, Osaka University
17.	Study of D-D Fusion in Solid Using Heavy-Ion	Hideo KAYANO Institute for Material Research, Tohoku University

18.	Study of Electromagnetic Properties of Nuclear High-Spin State through Crystal Ball	Kohei FURUNO Tandem Accelerator Center, Tsukuba University
19.	Study of Single-Events Induced by High Energy Ions(I)	Sumio MATUDA NASDA
20.	Study of Preequibrium Particle Emission in Proton-Induced Reactions	Yukinobu WATANABE Department of Energy Converion Engineering, Graduate School of Engineering Sciences, Kyushu University
21.	Research of Coulomb Explosion by Heavy Ions Irradiation	Mititaka TERASAWA Faculty of Engineering, Himeji Institute of Technology
22.	Study of the Property and Microstructure on the Oxide Superconductors Irradiated with High Energy Ions	Yukichi SASAKI Japan Fine Ceramics Center
23.	Study on Dynamic Interaction between Columnar Defects and Flux Lines	Akira TONOMURA Advanced Research Laboratory, Hitachi, Ltd
24.	Irradiation Effects of Oxide Superconductors	Takayuki TERAI Faculty of Engineering, University of Tokyo

FACSIMILE FORM
(for the JAERI tandem & V.d.G annual report)

TO: Dr. S. TAKEUCHI FAX. +81 29 282 6321

Accelerators Division
Department of
Reactor Engineering
Phone: 029 282 5860

JAPAN ATOMIC ENERGY RESEARCH INSTITUTE
TOKAI RESEARCH ESTABLISHMENT
TOKAI, NAKA, IBARAKI 319-11 JAPAN

I would like to ask you;

☐ **to keep my name in the mailing list.**
☐ **to remove my name from the mailing list.**
☐ **to renew my mailing address.**

NAME:_____

INSTITUTION:_____

_____

ADDRESS:_____

_____

_____

PHONE NO.:_____

FAX NO.: _____